

We sincerely thank the Referee for the valuable comments. Our manuscript has been revised according to the comments from the Referee and our responses to the comments are as follows. For clarity, the comments are reproduced in blue, authors' responses are in black and changes in the manuscript are in red.

5

Responses to Anonymous Referee #1

This smog chamber study investigated the effects of NH₃, SO₂, and NO_x on SOA formation under UV irradiation from 1,2,4-trimethylbenzene (TMB) over a period of 5-6 hours. The smog chamber was monitored in real time using a scanning mobility particle sizer; gas analyzers for SO₂, NO_x, NH₃, and O₃; and gas chromatography-flame ionization for TMB. Offline analysis used infrared spectrophotometry, ion chromatography, and liquid chromatography-mass spectrometry. The study found that the presence of NH₃ and SO₂ both individually and synergetically increase SOA yield, and that SO₂ speeds nucleation, possibly through uptake onto H₂SO₄ surfaces. New organosulfates were identified and reaction schemes and structures were proposed for some; some organosulfates had molecular weights consistent with TMB-derived aerosol components found in the atmosphere. NH₃ was found to react to form organic nitrogen compounds in the aerosol phase, but only in the presence of SO₂, attributed to formation of ammonium sulfate. Aerosol components had a wide range of volatility almost nine orders of magnitude, as predicted by elemental composition from mass spectrometry.

This study is a good match for the scope and aims of ACP, and it does an excellent job conveying its own novelty even if the reader is not well versed in aromatic aerosol chemistry. It represents a necessary contribution to the aerosol research community's understanding of SO₂ and NH₃ dynamics, and has implications for reactions of a large number of aromatic VOCs as well as human health in the findings regarding enhanced UFP fraction.

Major Comments

This article is solid, if not concise, and all sections contribute to the main point as a

cohesive whole. The introduction, methods section, and discussion of limitations are excellent, and while there is far more description of results than there is analysis of results I believe that both the analysis and discussion of atmospheric implications are sufficient. All of my suggestions for improvement are minor, relating to clarity and readability.

Minor Comments

line 13: Consider a brief explanation of the atmospheric relevance of TMB in the abstract.

40 **Author Reply:**

Aromatic hydrocarbons can dominate the VOC budget in certain urban areas with TMB being one of the most significant species (Ran et al., 2009). TMB is mostly emitted from anthropogenic sources such as solvent use (Mo et al., 2021). Recent studies have recognized TMB as an important species in SOA formation in the atmosphere (Wang et al., 2020; Zaytsev et al., 2019; Mehra et al., 2020). Hence, the following text has been added in the abstract to explain the relevance of TMB in the atmosphere.

Aromatic hydrocarbons can dominate the volatile organic compounds budget in the urban atmosphere. Among them, 1,2,4-trimethylbenzene (TMB), mainly emitted from solvent use, is one of the most important secondary organic aerosols (SOA) precursors.

line 69-70: "Equivocally not originated from biogenic VOCs" is a little unclear. Possibly change to "unidentified OSs with C₂-C₂₅ skeletons that may not have originated from biogenic VOCs" or similar.

55 **Author Reply:**

We have modified the sentence in the revised manuscript as: Recent field studies reported that some unidentified OSs with C₂-C₂₅ skeletons may not be originated from biogenic VOCs.

60 line 254-55: Make it clear whether ammonium sulfate particles were introduced during

experiments or as an independent wall loss experiment.

Author Reply:

Ammonium sulfate (AS) particles were not introduced into the chamber over the course of particle formation experiments. We used inert AS particles only in independent wall loss experiments in order to characterize the wall loss rate of AS particles, which was adopted to correct aerosol particle concentrations. This particle wall-loss correction method has been commonly used in previous studies (Chen et al., 2019; Charan et al., 2020). For clarity, we have included the following sentences in the revised manuscript.

70 Page 5, lines 166–167

Seed particles were not introduced into the chamber over the course of particle formation experiments.

Page 10, line 273–274

75 In order to determine the particles wall loss rates, we carried out independent wall loss experiments using ammonium sulfate particles.

Is this dependent on humidity or hygroscopicity of the particles? Not VERY important, but may be a limitation worth discussing.

Author Reply:

80 We agree with the Referee that particle wall depositions are affected by the physicochemical properties of particles to some extent. It should be noted that the description of an important step of the wall loss experiments was missing in our original manuscript. Indeed, the AS solution was added to a TSI atomizer (Model 3076) to produce droplets, which passed simultaneously through a silica gel diffusion dryer to produce dry AS particles. Although the hygroscopicity of AS particles is not totally similar to aerosol particles generated, the wall-losses of particles are commonly evaluated by independent seed experiments where inert AS particles are used (Chen et al., 2019; Charan et al., 2020).

90 Aerosol particles can deposit onto the chamber walls due to gravitational settling, Brownian diffusion, convection, and electrostatic effects (Crump and Seinfeld, 1981).

The wall-loss rate of particles depends mainly on the smog chamber design parameters (Charan et al., 2019). Previous studies showed that elevating RH inside the chamber did not remarkably influence the particle wall loss rates (Yu et al., 2011; Ge et al., 2017). Ge et al. (2017) used a same wall loss constant for the particle wall-loss corrections in experiments with RH ranged from 11% to 90%. Although the changes in RH can also influence the hygroscopicity, density, size, and chemical composition of particles (Hinks et al., 2018; Yu et al., 2011), almost identical humidity ((25 ± 1) %) condition was achieved among each experiment in the current work. Therefore, we believe that the particle wall depositions are not basically influenced by humidity or hygroscopicity of the particles. The description about the wall loss experiments has been included in the revised manuscript as follow.

Page 10, lines 274–280

An aqueous solution of ammonium sulfate was fed to a constant output atomizer (Model 3706, TSI, USA) to produce droplets, which passed simultaneously through a silica gel diffusion dryer to introduce dry particles into the chamber. The size distributions of ammonium sulfate particles were measured by SMPS for 480 min. Almost identical humidity ((25 ± 1) %) condition was achieved among each experiment. The wall losses of particles are size-dependent and, thus, we used a size-dependent particle wall-loss correction approach, which is described in detail in the Supplement.

110

line 284: Were these from two single experiments? If so, include experiment numbers. Otherwise I want to know the standard deviations for these values.

Author Reply:

Yes, the reported particle number concentrations were obtained in independent SO₂-free experiments with different initial NO_x levels. We have highlighted the experiment numbers in the revised manuscript as:

After 300 min UV irradiation without SO₂ introduction, the total maximum number concentration of aerosol particles was only $2.7 \times 10^4 \text{ cm}^{-3}$ and $2.9 \times 10^4 \text{ cm}^{-3}$ under low-NO_x (Exp. 1) and high-NO_x (Exp. 5) experiments, respectively.

120

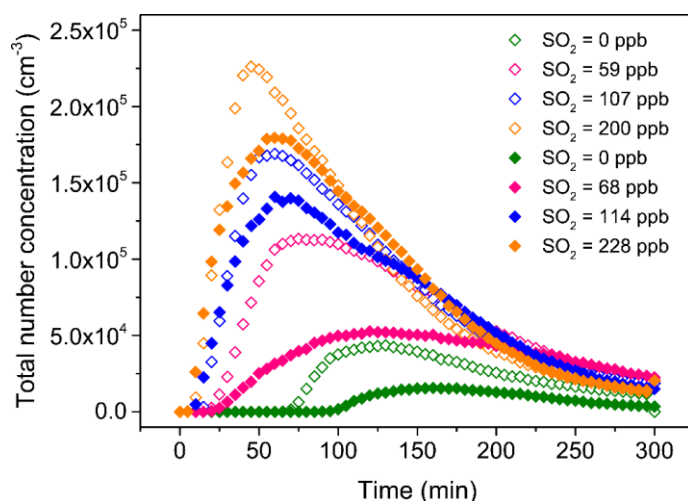
line 291-95: Before noting that UFP are more harmful to human health, you may want to make it explicit in the text analysis of figure 1 that increased SO₂ concentration increases the fraction of UFP in the aerosol size distribution.

Author Reply:

125 The SMPS instrument could measure particles larger than 4.50 nm in this work. In order to more clearly analyze the effects of SO₂ on the ultrafine particle formation, the number concentrations of ultrafine particles in the range of 4.50–100 nm were summed up and they are shown in Fig. R1, where it can be seen that the total number concentration of ultrafine particles is significantly enhanced with increasing SO₂ levels.
130 Therefore, the following text was added in the revised manuscript and Fig. R1 was added as Fig. S2 in the revised supplement.

Page 11, lines 309–314

135 Interestingly, the particle maximum number concentration considerably increased with increasing SO₂ levels, regardless of low- or high-NO_x conditions (Table 1). As shown in Fig. 1, although the unimodal particle size distribution in the presence of SO₂ was similar to that in its absence, particles with mobility diameter ranging from 10 to 80 nm, especially, dominated particle number concentrations with SO₂ addition. The time series of total ultrafine particles (diameter < 100 nm) number concentration are shown in Fig. S2, where it is seen that SO₂ considerably enhanced ultrafine particle formation.



140

Figure R1. The total number concentrations of ultrafine particles (< 100 nm) as a function of reaction time (Exps. 1–8). The open symbols and solid symbols represent low- and high-NO_x experiments, respectively.

145 line 323: I would be interested in more detail about the mechanics of H₂SO₄ as a
"condensed surface for key compounds." I take this to mean reactive uptake or
heterogeneous reactions of VOCs with H₂SO₄. However, you don't justify this assertion;
I might recommend citing Wang et al. 2010 (doi.org/10.1021/es9036868) and/or Zhang
et al. 2019 (doi.org/10.1021/acsearthspacechem.9b00209) for VOC heterogeneous
150 reaction with sulfuric acid surfaces.

Author Reply:

The oxidation of SO₂ can contribute to the formation of H₂SO₄ in SO₂-involved
experiments. The formed H₂SO₄ plays a key role in nucleation and can contribute to the
increase in nucleation rate (Sipila et al., 2010; Lehtipalo et al., 2018; Yao et al., 2018),
155 which are responsible for the short nucleation time observed in the TMB/NO_x/SO₂
regime (Wyche et al., 2009). Several H₂SO₄ nucleation mechanisms have been
suggested, including binary nucleation, ternary nucleation, ion-induced nucleation, and
so on (Sipila et al., 2010; Lehtipalo et al., 2018; Yao et al., 2018). SOA-forming
compounds can be produced in the gas-phase via photooxidation of TMB, and the
160 chamber walls and particle surfaces are competitive condensation sinks for these
compounds (Charan et al., 2020). Seed particles were not introduced into the chamber
during particle production experiments in this work. In the original sentence, we meant
that the H₂SO₄-induced new particles are an attractive condensation sinks for SOA-
forming compounds and can subsequently provide surfaces like seed particles onto
165 which the compound can condense.

We have carefully read the two recommended papers. Wang et al. (2010) found that
H₂SO₄ can effectively uptake gas-phase alkylamines, hence contributing to the growth
of aerosol particles. Zhang et al. (2019) highlighted the significance of uptake of
isoprene-derived epoxydiols onto sulfate aerosol particles. This process can influence
170 the phase state, morphology, and acidity of aerosol particles. Reactive uptake or
heterogeneous reactions of organic vapors with H₂SO₄ are important, which can
promote the growth of particle and the increase in particle mass (Deng et al., 2017;
Wang et al., 2010). However, it should be noted that we focused on analyzing SO₂

effects on the particle nucleation time in line 323 of the original text. The heterogenous
175 reactions promote mainly the formation of the accumulation mode particles instead of
the nucleation mode particles (Lu et al., 2019). The original sentence has been revised
as: **The formed H₂SO₄ could induce nucleation and increase the nucleation rate (Zhao
et al., 2018; Blair et al., 2017), and these processes are responsible for the short
nucleation time observed in the TMB/NO_x/SO₂ regime (Wyche et al., 2009).**

180

We fully agree with the Referee that acidic surfaces on aerosol particles can
promote the reactive uptake of organic vapors (Zhang et al., 2019; Wang et al., 2010).
The acid-catalyzed heterogenous reactions were already discussed in Sect. 3.1.2 in the
original manuscript as follows.

185 “The increase in aerosol acidity could be largely responsible for the observed
enhancements in SOA formation in SO₂-involved experiments. The OH oxidation of
TMB can result in the formation of multifunctional carbonyl compounds (Liu et al.,
2012; Zaytsev et al., 2019), which could promote SOA formation via acid-catalyzed
heterogeneous reactions.”

190

line 329-30: **As neither this work nor that of Julin et al. attempts to explain the
"nonlinear dynamics of aerosol populations," rather than attributing your results to these
dynamics it might be more effective to say something like "The nonlinear response of
the mean particle diameter to SO₂ initial concentration is similar to results found by
195 Julin et al. (2018) in a modelling study."**

Author Reply:

We have carefully read the study of Julin et al. (2018) again, who suggested
nonlinear response of particle size distributions to ammonia emissions. In the revised
manuscript, the sentence has been revised as follows:

200 **The nonlinear response of the particle mean diameter to SO₂ initial level is similar to
the findings of Julin et al. (2018), who found the response of particle size distribution
to NH₃ emissions to be also nonlinear.**

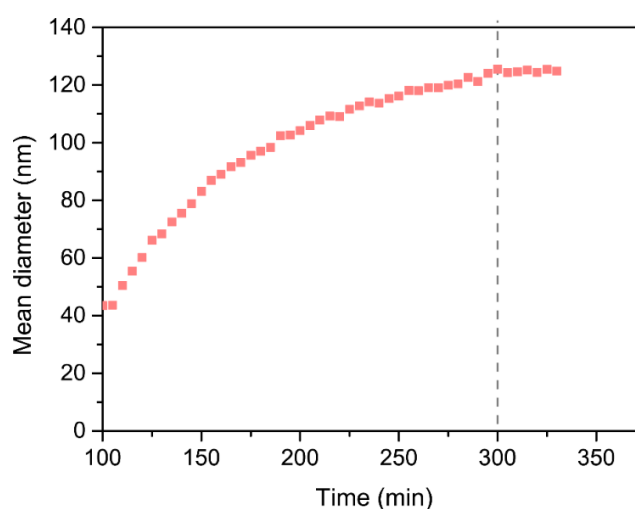
line 336: Is this the mean particle diameter after 30 minutes? Be explicit. You defined
205 initial growth rate as average for 0-30 minutes, but did not define a timeframe for mean
diameter.

Author reply:

Figure R2 shows the mean diameter of aerosol particles at different reaction times,
which was measured with SMPS. The particle mean diameter can stabilize after about
210 300 min photooxidation. Therefore, the particle mean diameter measured at 300 min in
each experiment are compared in Fig. 2 in the main manuscript. The related text and
Fig. 2 have been updated in the revised manuscript as follows.

Page 11, lines 330–334

The particle size rapidly increased within 30 min after nucleation, and gradually reached
215 a stable level within 300 min photooxidation (Fig. 1). Consequently, the initial growth
rate (GR_{initial}), calculated based on the method of Kulmala et al. (2012), is defined as the
particle growth rate within 30 min after nucleation (Li et al., 2018). **The mean diameter
reported in this work represents the particle mean diameter measured at 300 min in each
experiment.**



220

Figure R2. The mean diameter of aerosol particles generated as a function of reaction time.

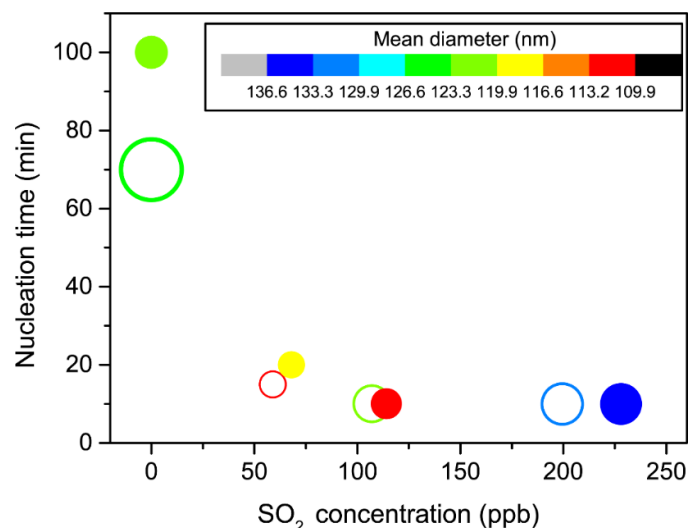


Figure 2. Particle nucleation time as a function of initial SO₂ concentration under low-
 225 NO_x (open circles) and high-NO_x (solid circles) conditions (Exps. 1–8). The symbol
 color indicates the particle mean diameter and symbol size represents the particle initial
 growth rate. Values of the particle parameters are listed in Table S1.

line 383-84: If you believe you have not sufficiently justified the necessity of chemical
 230 composition studies, I recommend you do so in the introduction instead.

Author Reply:

In the Introduction, we initially highlighted the necessity to analyze the chemical
 composition of particles as follows:

235 “To better understand TMB-SOA formation and growth, detailed laboratory
 characterization of TMB-SOA composition and TMB oxidation mechanisms with
 inorganic perturbation are required.”

“The mechanisms leading to secondary aerosol formation in the urban environment
 remain highly elusive and controversial, particularly for the processes related to
 changes in secondary aerosol mass and chemical composition.”

240 However, based on the Referee’s suggestion, we moved the original sentence to the
 Introduction to further supplement the necessity of studying particle chemical
 composition.

Page 2, lines 55–62

High levels of SO₂, NH₃, and VOCs have been reported in certain regions such as

245 Guangzhou (Zou et al., 2015), Beijing (Meng et al., 2020), Handan (Li et al., 2017) in
China. During haze pollution episodes, Li et al. (2017) observed that SO₂ levels can be
up to 200 ppb in Handan, China. A recent study also showed significant increasing NH₃
levels in the atmosphere over the United States and the European Union (Warner et al.,
2017). However, less focus has been placed on the SO₂ and NH₃ perturbations on SOA
250 formation and chemical composition. Aerosol particles contain a multitude of
compounds with different physicochemical properties.

line 589: Figure 9 may belong in the supplement, because it has only a brief mention in
the text that is limited to the observation that positive mode MS spectra skew toward
255 lower m/z's.

Author Reply:

Figure 9 has been moved to the supplement.

line 594, 600: The contents of Figure 10 are also not discussed in the text, so it could
260 be moved to the supplement as well.

Author Reply:

Figure 10 presents the predicted saturation mass concentrations of detected
products, which is an important part of our discussion. Therefore, we keep Fig. 10 (now
labeled as Fig. 9) in the revised manuscript.

265
line 509-10: use comparable measures to compare the SO₂-involved and SO₂ free
conditions. I would recommend including the multiplicative factor of the change for
both.

Author Reply:

270 We have modified the original sentence following the Referee's suggestion as:
Increasing the NH₃ level to 200 ppb enhanced the particle maximum number
concentration by factors of 2.0 and 1.7 under SO₂-free and SO₂-involved conditions,
respectively.

275 line 524-26: The sentence "Initial growth rate... as shown in Fig. S6" is redundant, and
to the next sentence "In SO₂-free experiments... initial growth rate of aerosol particles"
I would add something like "compared to the SO₂-involved condition."

Author Reply:

We have deleted the sentence "Initial growth rate... as shown in Fig. S6" in the
280 revised manuscript. In addition, we already compared the initial growth rate of particles
in SO₂-free and SO₂-involved experiments in the original manuscript as: "**In SO₂-free
experiments**, the increase in NH₃ initial concentrations led to remarkable increase of
the initial growth rate of aerosol particles. High initial growth rates were also found in
the photooxidation of other aromatics such as toluene and o/m/p-xylene with NH₃
285 addition (Li et al., 2018). This result may be explained by the fact that under SO₂-free
condition, NH₃ mainly reacts with acids to produce ammonium salts. Previous studies
have reported that ammonium salts could partition into the initial growth process of
new secondary aerosol particles and thus increase the particle initial growth rate (Li et
al., 2018; Zhu et al., 2014). More interestingly, NH₃ level did not substantially affect
290 the initial growth rate of particles **in the presence of SO₂** (Fig. S9)."

References

- Blair, S. L., MacMillan, A. C., Drozd, G. T., Goldstein, A. H., Chu, R. K., Pasa-Tolic,
295 L., Shaw, J. B., Tolic, N., Lin, P., Laskin, J., Laskin, A., and Nizkorodov, S. A.:
Molecular characterization of organosulfur compounds in biodiesel and diesel fuel
secondary organic aerosol, *Environ. Sci. Technol.*, 51, 119-127,
10.1021/acs.est.6b03304, 2017.
- Charan, S. M., Huang, Y., and Seinfeld, J. H.: Computational Simulation of Secondary
300 Organic Aerosol Formation in Laboratory Chambers, *Chem. Rev.*, 119, 11912-11944,
10.1021/acs.chemrev.9b00358, 2019.
- Charan, S. M., Buenconsejo, R. S., and Seinfeld, J. H.: Secondary organic aerosol yields
from the oxidation of benzyl alcohol, *Atmos. Chem. Phys.*, 20, 13167-13190,
10.5194/acp-20-13167-2020, 2020.

- 305 Chen, T., Liu, Y., Ma, Q., Chu, B., Zhang, P., Liu, C., Liu, J., and He, H.: Significant source of secondary aerosol: formation from gasoline evaporative emissions in the presence of SO₂ and NH₃, *Atmos. Chem. Phys.*, 19, 8063-8081, 10.5194/acp-19-8063-2019, 2019.
- Crump, J. G., and Seinfeld, J. H.: turbulent deposition and gravitational sedimentation
310 of an aerosol in a vessel of arbitrary shape, *Journal of Aerosol Science*, 12, 405-415, 10.1016/0021-8502(81)90036-7, 1981.
- Deng, W., Liu, T., Zhang, Y., Situ, S., Hu, Q., He, Q., Zhang, Z., Lu, S., Bi, X., Wang, X., Boreave, A., George, C., Ding, X., and Wang, X.: Secondary organic aerosol formation from photooxidation of toluene with NO_x and SO₂: chamber simulation with
315 purified air versus urban ambient air as matrix, *Atmos. Environ.*, 150, 67-76, 10.1016/j.atmosenv.2016.11.047, 2017.
- Ge, S., Xu, Y., and Jia, L.: Secondary organic aerosol formation from ethylene ozonolysis in the presence of sodium chloride, *Journal of Aerosol Science*, 106, 120-131, 10.1016/j.jaerosci.2017.01.009, 2017.
- 320 Hinks, M. L., Montoya-Aguilera, J., Ellison, L., Lin, P., Laskin, A., Laskin, J., Shiraiwa, M., Dabdub, D., and Nizkorodov, S. A.: Effect of relative humidity on the composition of secondary organic aerosol from the oxidation of toluene, *Atmos. Chem. Phys.*, 18, 1643-1652, 10.5194/acp-18-1643-2018, 2018.
- Julin, J., Murphy, B. N., Patoulias, D., Fountoukis, C., Olenius, T., Pandis, S. N., and
325 Riipinen, I.: Impacts of Future European Emission Reductions on Aerosol Particle Number Concentrations Accounting for Effects of Ammonia, Amines, and Organic Species, *Environ. Sci. Technol.*, 52, 692-700, 10.1021/acs.est.7b05122, 2018.
- Kulmala, M., Petaja, T., Nieminen, T., Sipila, M., Manninen, H. E., Lehtipalo, K., Dal Maso, M., Aalto, P. P., Junninen, H., Paasonen, P., Riipinen, I., Lehtinen, K. E.,
330 Laaksonen, A., and Kerminen, V. M.: Measurement of the nucleation of atmospheric aerosol particles, *Nat. Protoc.*, 7, 1651-1667, 10.1038/nprot.2012.091, 2012.
- Lehtipalo, K., Yan, C., Dada, L., Bianchi, F., Xiao, M., Wagner, R., Stolzenburg, D., Ahonen, L. R., Amorim, A., Baccarini, A., Bauer, P. S., Baumgartner, B., Bergen, A., Bernhammer, A.-K., Breitenlechner, M., Brilke, S., Buchholz, A., Mazon, S. B., Chen,

- 335 D., Chen, X., Dias, A., Dommen, J., Draper, D. C., Duplissy, J., Ehn, M., Finkenzeller, H., Fischer, L., Frege, C., Fuchs, C., Garmash, O., Gordon, H., Hakala, J., He, X., Heikkinen, L., Heinritzi, M., Helm, J. C., Hofbauer, V., Hoyle, C. R., Jokinen, T., Kangasluoma, J., Kerminen, V.-M., Kim, C., Kirkby, J., Kontkanen, J., Kuerten, A., Lawler, M. J., Mai, H., Mathot, S., Mauldin, R. L., III, Molteni, U., Nichman, L., Nie,
340 W., Nieminen, T., Ojdanic, A., Onnela, A., Passananti, M., Petaja, T., Piel, F., Pospisilova, V., Quelever, L. L. J., Rissanen, M. P., Rose, C., Sarnela, N., Schallhart, S., Schuchmann, S., Sengupta, K., Simon, M., Sipila, M., Tauber, C., Tome, A., Trostl, J., Vaisanen, O., Vogel, A. L., Volkamer, R., Wagner, A. C., Wang, M., Weitz, L., Wimmer, D., Ye, P., Ylisirnio, A., Zha, Q., Carslaw, K. S., Curtius, J., Donahue, N. M., Flagan, R.
345 C., Hansel, A., Riipinen, I., Virtanen, A., Winkler, P. M., Baltensperger, U., Kulmala, M., and Worsnop, D. R.: Multicomponent new particle formation from sulfuric acid, ammonia, and biogenic vapors, *Sci. Adv.*, 4, 10.1126/sciadv.aau5363, 2018.
- Li, H., Zhang, Q., Zhang, Q., Chen, C., Wang, L., Wei, Z., Zhou, S., Parworth, C., Zheng, B., Canonaco, F., Prevot, A. S. H., Chen, P., Zhang, H., Wallington, T. J., and He, K.:
350 Wintertime aerosol chemistry and haze evolution in an extremely polluted city of the North China Plain: significant contribution from coal and biomass combustion, *Atmos. Chem. Phys.*, 17, 4751-4768, 10.5194/acp-17-4751-2017, 2017.
- Li, K., Chen, L., White, S. J., Yu, H., Wu, X., Gao, X., Azzi, M., and Cen, K.: Smog chamber study of the role of NH₃ in new particle formation from photo-oxidation of
355 aromatic hydrocarbons, *Sci. Total Environ.*, 619-620, 927-937, 10.1016/j.scitotenv.2017.11.180, 2018.
- Liu, S., Shilling, J. E., Song, C., Hiranuma, N., Zaveri, R. A., and Russell, L. M.: Hydrolysis of Organonitrate Functional Groups in Aerosol Particles, *Aerosol Sci. Technol.*, 46, 1359-1369, 10.1080/02786826.2012.716175, 2012.
- 360 Lu, K., Guo, S., Tan, Z., Wang, H., Shang, D., Liu, Y., Li, X., Wu, Z., Hu, M., and Zhang, Y.: Exploring atmospheric free-radical chemistry in China: the self-cleansing capacity and the formation of secondary air pollution, *National Science Review*, 6, 579-594, 10.1093/nsr/nwy073, 2019.
- Mehra, A., Wang, Y., Krechmer, J. E., Lambe, A., Majluf, F., Morris, M. A., Priestley,

- 365 M., Bannan, T. J., Bryant, D. J., Pereira, K. L., Hamilton, J. F., Rickard, A. R., Newland, M. J., Stark, H., Croteau, P., Jayne, J. T., Worsnop, D. R., Canagaratna, M. R., Wang, L., and Coe, H.: Evaluation of the chemical composition of gas- and particle-phase products of aromatic oxidation, *Atmos. Chem. Phys.*, 20, 9783-9803, 10.5194/acp-20-9783-2020, 2020.
- 370 Meng, Z., Wu, L., Xu, X., Xu, W., Zhang, R., Jia, X., Liang, L., Miao, Y., Cheng, H., Xie, Y., He, J., and Zhong, J.: Changes in ammonia and its effects on PM_{2.5} chemical property in three winter seasons in Beijing, China, *Sci. Total Environ.*, 749, 142208, 10.1016/j.scitotenv.2020.142208, 2020.
- Mo, Z., Lu, S., and Shao, M.: Volatile organic compound (VOC) emissions and health
375 risk assessment in paint and coatings industry in the Yangtze River Delta, China, *Environ. Pollut.*, 269, 115740, 10.1016/j.envpol.2020.115740, 2021.
- Ran, L., Zhao, C., Geng, F., Tie, X., Tang, X., Peng, L., Zhou, G., Yu, Q., Xu, J., and Guenther, A.: Ozone photochemical production in urban Shanghai, China: Analysis based on ground level observations, *J. Geophys. Res. Atmos.*, 114,
380 10.1029/2008jd010752, 2009.
- Sipila, M., Berndt, T., Petaja, T., Brus, D., Vanhanen, J., Stratmann, F., Patokoski, J., Mauldin, R. L., III, Hyvarinen, A.-P., Lihavainen, H., and Kulmala, M.: The role of sulfuric acid in atmospheric nucleation, *Science*, 327, 1243-1246, 10.1126/science.1180315, 2010.
- 385 Wang, L., Lal, V., Khalizov, A. F., and Zhang, R.: Heterogeneous Chemistry of Alkylamines with Sulfuric Acid: Implications for Atmospheric Formation of Alkylammonium Sulfates, *Environ. Sci. Technol.*, 44, 2461-2465, 10.1021/es9036868, 2010.
- Wang, Y., Mehra, A., Krechmer, J. E., Yang, G., Hu, X., Lu, Y., Lambe, A., Canagaratna,
390 M., Chen, J., Worsnop, D., Coe, H., and Wang, L.: Oxygenated products formed from OH-initiated reactions of trimethylbenzene: autoxidation and accretion, *Atmos. Chem. Phys.*, 20, 9563-9579, 10.5194/acp-20-9563-2020, 2020.
- Warner, J. X., Dickerson, R. R., Wei, Z., Strow, L. L., Wang, Y., and Liang, Q.: Increased atmospheric ammonia over the world's major agricultural areas detected from space,

- 395 Geophys. Res. Lett., 44, 2875-2884, 10.1002/2016gl072305, 2017.
- Wyche, K. P., Monks, P. S., Ellis, A. M., Cordell, R. L., Parker, A. E., Whyte, C., Metzger, A., Dommen, J., Duplissy, J., Prevot, A. S. H., Baltensperger, U., Rickard, A. R., and Wulfert, F.: Gas phase precursors to anthropogenic secondary organic aerosol: detailed observations of 1,3,5-trimethylbenzene photooxidation, *Atmos. Chem. Phys.*, 400 9, 635-665, 10.5194/acp-9-635-2009, 2009.
- Yao, L., Garmash, O., Bianchi, F., Zheng, J., Yan, C., Kontkanen, J., Junninen, H., Mazon, S. B., Ehn, M., Paasonen, P., Sipila, M., Wang, M., Wang, X., Xiao, S., Chen, H., Lu, Y., Zhang, B., Wang, D., Fu, Q., Geng, F., Li, L., Wang, H., Qiao, L., Yang, X., Chen, J., Kerminen, V.-M., Petaja, T., Worsnop, D. R., Kulmala, M., and Wang, L.: 405 Atmospheric new particle formation from sulfuric acid and amines in a Chinese megacity, *Science*, 361, 278-281, 10.1126/science.aao4839, 2018.
- Yu, K. P., Lin, C. C., Yang, S. C., and Zhao, P.: Enhancement effect of relative humidity on the formation and regional respiratory deposition of secondary organic aerosol, *J Hazard Mater*, 191, 94-102, 10.1016/j.jhazmat.2011.04.042, 2011.
- 410 Zaytsev, A., Koss, A. R., Breitenlechner, M., Krechmer, J. E., Nihill, K. J., Lim, C. Y., Rowe, J. C., Cox, J. L., Moss, J., Roscioli, J. R., Canagaratna, M. R., Worsnop, D., Kroll, J. H., and Keutsch, F. N.: Mechanistic study of the formation of ring-retaining and ring-opening products from the oxidation of aromatic compounds under urban atmospheric conditions, *Atmos. Chem. Phys.*, 19, 15117-15129, 10.5194/acp-19- 415 15117-2019, 2019.
- Zhang, Y., Chen, Y., Lei, Z., Olson, N. E., Riva, M., Koss, A. R., Zhang, Z., Gold, A., Jayne, J. T., Worsnop, D. R., Onasch, T. B., Kroll, J. H., Turpin, B. J., Ault, A. P., and Surratt, J. D.: Joint Impacts of Acidity and Viscosity on the Formation of Secondary Organic Aerosol from Isoprene Epoxydiols (IEPOX) in Phase Separated Particles, *ACS Earth Space Chem.*, 3, 2646-2658, 10.1021/acsearthspacechem.9b00209, 2019.
- 420 Zhao, D., Schmitt, S. H., Wang, M., Acir, I.-H., Tillmann, R., Tan, Z., Novelli, A., Fuchs, H., Pullinen, I., Wegener, R., Rohrer, F., Wildt, J., Kiendler-Scharr, A., Wahner, A., and Mentel, T. F.: Effects of NO_x and SO₂ on the secondary organic aerosol formation from photooxidation of α -pinene and limonene, *Atmos. Chem. Phys.*, 18, 1611-1628,

- 425 10.5194/acp-18-1611-2018, 2018.
- Zhu, Y., Sabaliauskas, K., Liu, X., Meng, H., Gao, H., Jeong, C.-H., Evans, G. J., and Yao, X.: Comparative analysis of new particle formation events in less and severely polluted urban atmosphere, *Atmos. Environ.*, 98, 655-664, 10.1016/j.atmosenv.2014.09.043, 2014.
- 430 Zou, Y., Deng, X. J., Zhu, D., Gong, D. C., Wang, H., Li, F., Tan, H. B., Deng, T., Mai, B. R., Liu, X. T., and Wang, B. G.: Characteristics of 1 year of observational data of VOCs, NO_x and O₃ at a suburban site in Guangzhou, China, *Atmos. Chem. Phys.*, 15, 6625-6636, 10.5194/acp-15-6625-2015, 2015.

We sincerely thank the Referee for the valuable comments. Our manuscript has been revised according to the comments from the Referee and our responses to the comments are as follows. For clarity, the comments are reproduced in blue, authors' responses are in black and changes in the manuscript are in red.

5

Responses to Anonymous Referee #2

General comments

The authors have studied SOA formation from photo-oxidation of 1,2,4-trimethylbenzene under different concentrations of NO_x, SO₂ and NH₃ in an indoor smog chamber. The reactants and the particle generation and growth were monitored using a series of standard instrumentations. The chemical functional groups were characterized by ATR-FTIR in each experiment and inorganic constituents were analyzed using ion chromatography. The molecular level information is provided using UPLC-HRMS and dd-MS² scans. Ten new organosulfates are identified in the presence of SO₂, including 3 in which the origin was previously unknown and some previously reported to be originated from biogenic precursors. Formation mechanisms for 8 of the newly identified organosulfates are proposed based on previous literature. Their results indicate that SO₂ is a key parameter for ultrafine particle formation. A synergistic effect of NH₃ and SO₂ in particle formation is also shown, indicating the importance of reducing both SO₂ and NH₃ emissions to improve lowering PM. Their results also suggest that ammonium sulfate form by the reaction of NH₃ with H₂SO₄ facilitate aerosol formation and growth through condensation of organic vapors.

This article advances the current knowledge of aerosol formation from photo-oxidation of a typical aromatic hydrocarbon in the presence of NO_x, SO₂ and NH₃, therefore is of interest to the scientific community of ACP. The manuscript is well written and organized. The experiments are well executed, methods are explained adequately, results are discussed thoroughly, and conclusions are well supported. I have some minor comments to improve the quality of this manuscript that are listed below. I recommend accepting this manuscript for publication in ACP with minor revisions.

30

Specific comments

Line 13 Indicate the major emission sources of TMB.

Author Reply:

Aromatic hydrocarbons can dominate the VOC budget in certain urban areas with
35 TMB being one of the most significant species (Ran et al., 2009). TMB is mostly
emitted from anthropogenic sources such as solvent use (Mo et al., 2021). Recent
studies have recognized TMB as an important species in SOA formation in the
atmosphere (Wang et al., 2020; Zaytsev et al., 2019; Mehra et al., 2020). Hence, the
following text has been added in the abstract.

40 Aromatic hydrocarbons can dominate the volatile organic compounds budget in the
urban atmosphere. Among them, 1,2,4-trimethylbenzene (TMB), mainly emitted from
solvent use, is one of the most important secondary organic aerosols (SOA) precursors.

Line 45 Define 'certain regions.

45 Author Reply:

The original text has been supplemented as follows: High levels of SO₂, NH₃, and
VOCs have been reported in certain regions such as Guangzhou (Zou et al., 2015),
Beijing (Meng et al., 2020), Handan (Li et al., 2017) in China. During haze pollution
episodes, Li et al. (2017) observed that SO₂ levels can be up to 200 ppb in Handan,
50 China. A recent study also showed significant increasing NH₃ levels in the atmosphere
over the United States and the European Union (Warner et al., 2017).

Line 54-56 Add reference/s.

Author Reply:

55 The following studies have been added to the references list.

1. Estillore, A. D., Hettiyadura, A. P. S., Qin, Z., Leckrone, E., Wombacher, B.,
Humphry, T., Stone, E. A., and Grassian, V. H.: Water Uptake and Hygroscopic Growth
of Organosulfate Aerosol, Environ. Sci. Technol., 50, 4259-4268,
10.1021/acs.est.5b05014, 2016.
- 60 2. Fleming, L. T., Ali, N. N., Blair, S. L., Roveretto, M., George, C., and Nizkorodov,

S. A.: Formation of Light-Absorbing Organosulfates during Evaporation of Secondary Organic Material Extracts in the Presence of Sulfuric Acid, *ACS Earth Space Chem.*, 3, 947-957, 10.1021/acsearthspacechem.9b00036, 2019

3. Hansen, A. M. K., Hong, J., Raatikainen, T., Kristensen, K., Ylisirniö, A., Virtanen, A., Petäjä, T., Glasius, M., and Prisle, N. L.: Hygroscopic properties and cloud condensation nuclei activation of limonene-derived organosulfates and their mixtures with ammonium sulfate, *Atmos. Chem. Phys.*, 15, 14071-14089, 10.5194/acp-15-14071-2015, 2015.

4. Riva, M., Chen, Y., Zhang, Y., Lei, Z., Olson, N. E., Boyer, H. C., Narayan, S., Yee, L. D., Green, H. S., Cui, T., Zhang, Z., Baumann, K., Fort, M., Edgerton, E., Budisulistiorini, S. H., Rose, C. A., Ribeiro, I. O., RL, E. O., Dos Santos, E. O., Machado, C. M. D., Szopa, S., Zhao, Y., Alves, E. G., de Sa, S. S., Hu, W., Knipping, E. M., Shaw, S. L., Duvoisin Junior, S., de Souza, R. A. F., Palm, B. B., Jimenez, J. L., Glasius, M., Goldstein, A. H., Pye, H. O. T., Gold, A., Turpin, B. J., Vizuete, W., Martin, S. T., Thornton, J. A., Dutcher, C. S., Ault, A. P., and Surratt, J. D.: Increasing Isoprene Epoxydiol-to-Inorganic Sulfate Aerosol Ratio Results in Extensive Conversion of Inorganic Sulfate to Organosulfur Forms: Implications for Aerosol Physicochemical Properties, *Environ. Sci. Technol.*, 53, 8682-8694, 10.1021/acs.est.9b01019, 2019.

5. Zhang, Y., Chen, Y., Lei, Z., Olson, N. E., Riva, M., Koss, A. R., Zhang, Z., Gold, A., Jayne, J. T., Worsnop, D. R., Onasch, T. B., Kroll, J. H., Turpin, B. J., Ault, A. P., and Surratt, J. D.: Joint Impacts of Acidity and Viscosity on the Formation of Secondary Organic Aerosol from Isoprene Epoxydiols (IEPOX) in Phase Separated Particles, *ACS Earth Space Chem.*, 3, 2646-2658, 10.1021/acsearthspacechem.9b00209, 2019.

85 They are cited in the revised manuscript as follows:

The presence of OSs could alter aerosol morphology (Riva et al., 2019), viscosity (Riva et al., 2019; Zhang et al., 2019), particle acidity (Riva et al., 2019), phase state (Zhang et al., 2019), hygroscopicity (Estillore et al., 2016; Hansen et al., 2015), and optical properties (Fleming et al., 2019), thereby resulting in large climate effects.

Line 98-99 Briefly indicate what MCM is and add a link to the version.

Author Reply:

The Master Chemical Mechanism (MCM, <http://mcm.leeds.ac.uk/MCMv3.2/>, last access: 23 February 2021) is a near-explicit chemical mechanism that can describe, in detail, the tropospheric degradation of numerous VOCs. The oxidation processes of VOCs are highly complex. Explicit chemical mechanisms might cause missing oxidation pathways and products, thus leading to large gaps between the modeled and measured SOA mass. Wang et al. (2020) suggested that recently identified autoxidation pathways for OH oxidation of TMB are not included in the current MCM and the detected products are more diverse than the products shown in MCM. The updates for the OH-initiated oxidation mechanism of TMB can be achieved only when the rate, branching ratios and product distributions can be explicitly obtained. Therefore, more investigations are needed to further explore the detailed chemical processes for OH oxidation of TMB. According to the suggestion of the Referee, the following text was added in the revised manuscript.

Page 4, lines 122–131

In addition, the Master Chemical Mechanism (MCM, <http://mcm.leeds.ac.uk/MCMv3.2/>, last access: 23 February 2021) is a near-explicit chemical mechanism that can describe, in detail, the tropospheric degradation of TMB. A recent study reported that identified autoxidation pathways during OH oxidation of TMB are not included in the current MCM and the detected TMB products are more diverse than the products shown in MCM (Wang et al., 2020b). The updates for the OH-initiated oxidation mechanism of TMB can be achieved only when the rate constants, branching ratios and product distributions can be explicitly obtained. However, TMB photooxidation is highly complex and sensitive to environmental conditions. To better understand TMB SOA formation and growth, investigating chemical processes of TMB photooxidation with inorganic perturbation is required.

Line 210 Indicate how the mass calibration was performed.

Author Reply:

125 We used standard calibration solutions provided by the manufacturer to calibrate the MS instrument every five days. The following text was added in the revised manuscript.

Page 9, lines 257–258

The MS instrument was calibrated every five days with standard calibration solutions provided by the manufacturer.

130 Line 200 Indicate the mass resolution in full MS, top N in dd-MS², isolation width (mass window) etc

Author Reply:

In the revised manuscript, detailed parameters are indicated as follows:

Page 9, lines 251–257

135 MS spectra were recorded in the range of m/z 50 to 750 in full MS scan with a mass resolving power of 70000 (FWHM at m/z 200). The full MS scan was followed by data-dependent MS/MS (dd-MS²) scans using stepped collision energies of 20, 40, and 60 eV via high-energy collisional dissociation. The resolution was 17500 and an isolation width of 2 m/z units was applied for the dd-MS² scan. The other parameters for MS²
140 experiments were as follow: AGC target, 2×10^5 ; maximum IT, 50 ms; loop count, 3; minimum AGC target, 1×10^5 ; apex trigger, 2–6 s; dynamic exclusion, 6 s.

Line 277 Add initial growth rates to Table 1 or SI.

Author Reply:

145 The aim of depicting Fig. 2 in the original manuscript was to clearly reflect the changes of the particle nucleation time, initial growth rate, and mean diameter with the initial SO₂ concentration. The specific particle parameters including the particle initial growth rate have been summarized in the table below.

150 **Table R1.** Particle parameters for experiments 1–8.

Exp.	Nucleation time (min)	Particle mean diameter (nm)	Initial particle growth rate (nm h ⁻¹)
1	70	125.5	46.53
2	15	109.9	20.09
3	10	121.2	27.42
4	10	130.6	31.09
5	100	123.1	23.51
6	20	118.5	19.30
7	10	112.4	22.14
8	10	136.5	29.82

Table R1 has been added in the revised supplement as Table S1 and the caption of Fig. 2 has been also updated as follows.

155 **Figure 2.** Particle nucleation time as a function of initial SO₂ concentration under low-NO_x (open circles) and high-NO_x (solid circles) conditions (Exps. 1–8). The symbol color indicates the particle mean diameter and symbol size represents the particle initial growth rate. Values of the particle parameters are listed in Table S1.

160 Line 277-280 Can the authors elaborate the reasons for the observed non-linear response of the particle diameter with initial SO₂ concentrations?

Author Reply:

OH-initiated oxidation of VOCs can yield a number of products with different degrees of volatility (Xu et al., 2014). The growth of aerosol particles is related to the coagulation, the condensation of non-volatility oxidation products, and gas-particle partitioning of semi-volatility organic compounds (SVOCs). For SVOCs, the evaporation is important after partitioning to the particle phase. Therefore, the rate at which SVOCs participate in the particle growth is lower than their condensation rate. Interestingly, recent studies showed that the particle-phase chemistry such as heterogeneous reactions of SVOCs are substantially pronounced for particle growth (Shiraiwa et al., 2013; Paasonen et al., 2018; Apsokardu and Johnston, 2018). Apsokardu and Johnston (2018) explored the influences of particle-phase chemistry on the growth rate of aerosol particles with a kinetic growth model and found that some

SVOCs can undergo accretion reactions in the particle-phase to further accelerate the particle growth. Paasonen et al. (2018) also showed that the increase in particle growth rate is related to particle-phase reactions. The study of Shiraiwa et al. (2013) highlighted the importance of particle-phase chemistry in the changes of SOA size distribution and suggested that particle-phase chemistry depends to some extent on particle acidity. Organosulfates can be produced by particle-phase reactions involving interactions between organics and inorganics. In this work, we measured organosulfates only in SO₂-involved photooxidation, indicating that additional particle-phase reactions can occur under SO₂-involved conditions. Increasing initial SO₂ levels could induce the formation of more sulfate (Fig. S4) and the enhancement in the particle acidity during photooxidation (Liu et al., 2016; Kroll et al., 2006). The elevated particle acidity can promote more SVOCs to transform into non-volatile products in the particle phase (Lin et al., 2014; Lal et al., 2012). Additional SVOCs could be moved from the gas phase to particle phase to increase the particle size and the evaporation of SVOCs can be inhibited, thereby promoting the particle growth.

It is somewhat interesting that the particle mean diameter in low-SO₂ ($[\text{SO}_2]_0 < 100$ ppb) experiments is smaller than that in SO₂-free experiments. Our result is in line with the study of Wyche et al. (2009), who attributed this phenomenon to the larger number of particles produced under SO₂-involved condition. In this work, the presence of 59 ppb SO₂ caused the maximum number concentration of particles to increase by $8.5 \times 10^4 \text{ cm}^{-3}$ under low-NO_x condition. When the SO₂ level increased from 0 to 68 ppb in high-NO_x experiments, the corresponding particle number concentration increased from 2.9×10^4 to $9.3 \times 10^4 \text{ cm}^{-3}$. Therefore, the amounts of products that condensed onto each aerosol particles may significantly decrease in low-SO₂ experiments, which can result in the decrease in particle diameter (Liu et al., 2015). The promoting effect of particle-phase chemistry on the particle size growth may not offset the inhibiting effect of the emergence of large number of particles on the particle size growth, thereby leading to the low particle diameter in low-SO₂ experiments. We have added the following text to explain the reasons for the observed non-linear response of the particle diameter with initial SO₂ level.

Aerosol particles can grow in different ways such as gas-particle partitioning of semi-volatility organic compounds (SVOCs). Since the evaporation of SVOCs is important after partitioning to the particle phase, the rate at which SVOCs participate in the particle growth is lower than their condensation rate. However, recent advances give an insight that the particle-phase chemistry such as heterogeneous reactions of SVOCs are substantially pronounced for the particle growth (Shiraiwa et al., 2013; Paasonen et al., 2018; Apsokardu and Johnston, 2018). Organosulfates can be produced by particle-phase reactions involving interactions between organics and inorganics. In this work, organosulfates were only detected in SO₂-involved photooxidation, indicating that additional particle-phase reactions can occur under SO₂-involved conditions. Increasing the initial SO₂ level could induce the formation of more sulfate (Fig. S4) and the enhancement in the particle acidity during photooxidation (Liu et al., 2016; Kroll et al., 2006). The elevated particle acidity can promote more SVOCs to transform into low-volatile products such as organosulfates in the particle phase, thereby promoting the particle growth (Lin et al., 2014; Lal et al., 2012). Then, additional SVOCs could be further transferred from the gas phase to the particle phase to increase the particle size. However, the particle mean diameter in low-SO₂ ([SO₂]₀ < 100 ppb) experiments is smaller than that in SO₂-free experiments. Our result is in line with the study of Wyche et al. (2009), who attributed this phenomenon to the larger number of particles produced under SO₂-involved condition. The presence of 59 ppb SO₂ caused the maximum number concentration of particles to increase by 8.5×10^4 cm⁻³ under low-NO_x condition. When the SO₂ level increased from 0 to 68 ppb in high-NO_x experiments, the corresponding particle number concentration increased from 2.9×10^4 to 9.3×10^4 cm⁻³. Therefore, the amounts of products that condensed onto each aerosol particles significantly decreased in low-SO₂ experiments, which could result in the decrease in particle diameter (Liu et al., 2015). The promoting effect of particle-phase chemistry on the particle size growth may not offset the inhibiting effect of the emergence of large number of particles on the particle size growth, thereby leading to the low particle diameter in low-SO₂ experiments.

Figure 4 – Indicate what error bars represent.

235 **Author Reply:**

The error bars represent errors in the SOA yield results. The errors were calculated from error propagation using the sum of the uncertainties in TMB data and the systematic error of SMPS. The following note was included in the caption of Fig. 4.

240 The error bars represent errors in the SOA yield results and the errors were calculated from error propagation using the sum of the uncertainties in TMB data and the systematic error of SMPS.

Figure 5 – Indicate the experiment numbers relevant to a) to f)

Author Reply:

245 The experimental numbers have been added in the caption of Fig. 5 as:

Figure 5. ATR-FTIR spectra of aerosol particles generated from TMB/NO_x (a, Exp. 1; b, Exp. 5), TMB/NO_x/SO₂ (c, Exp. 4; d, Exp. 8), TMB/NO_x/NH₃/SO₂ (e, Exp. 12), and TMB/NO_x/NH₃ (f, Exp. 10) photooxidation.

250 Lines 346-348 – Add detailed information of the common products observed in SO₂ free and SO₂ involved experiments to the SI.

Author Reply:

The detailed information of representative products mentioned in the original manuscript were provided in Table S3 in the revised supplement.

255

Table S3 – Indicate clearly whether this table shows the compounds that are detected in both SO₂ free and SO₂ involved experiments with NH₃ or the products only formed from the experiments involved both NH₃ and SO₂.

Author Reply:

260 The major products shown in Table S3 are the products detected in both SO₂-free and SO₂-involved experiments with NH₃ addition. The revised table in the supplement is now labeled as Table S4 and the caption was revised as: **Observed products in both**

SO₂-free and SO₂-involved experiments with NH₃ addition.

265 Tables S2 and S3 – Add UPLC retention times.

Author Reply:

The retention times have been added in the indicated tables, which are now labeled as Table S3 and S4.

270 Technical corrections

Line 105 – Add ‘in the atmosphere’ to the end of “Given the ubiquity of SO₂, NH₃, and TMB...

Author Reply:

275 According to the suggestion of the Referee, we have added “in the atmosphere” at the indicated place in the revised manuscript.

Line 200 – It is better to write it as data-dependent MS/MS (dd-MS²) scans

Author Reply:

We have modified it in the text.

280

Line 206 – Add B after 3%.

Author Reply:

We have added “B” in the revised manuscript.

285 Figure 6 – Label the red structures as OS-226, OS-228...etc. (Authors may replace the chemical formula with their abbreviated names as the structures are shown.)

Author Reply:

The red structures in Fig. 6 have been marked with OS-266, OS-228...etc.

290

Figure 10 – Match the color of the TMB on the figure with carbon number (should be light blue as it has 9 carbons)

295 **Author Reply:**

We have corrected it in the revised manuscript.

References

- 300 Apsokardu, M. J., and Johnston, M. V.: Nanoparticle growth by particle-phase chemistry, *Atmos. Chem. Phys.*, 18, 1895-1907, 10.5194/acp-18-1895-2018, 2018.
- Estillore, A. D., Hettiyadura, A. P. S., Qin, Z., Leckrone, E., Wombacher, B., Humphry, T., Stone, E. A., and Grassian, V. H.: Water Uptake and Hygroscopic Growth of Organosulfate Aerosol, *Environ. Sci. Technol.*, 50, 4259-4268, 10.1021/acs.est.5b05014, 2016.
- 305 Fleming, L. T., Ali, N. N., Blair, S. L., Roveretto, M., George, C., and Nizkorodov, S. A.: Formation of Light-Absorbing Organosulfates during Evaporation of Secondary Organic Material Extracts in the Presence of Sulfuric Acid, *ACS Earth Space Chem.*, 3, 947-957, 10.1021/acsearthspacechem.9b00036, 2019.
- 310 Hansen, A. M. K., Hong, J., Raatikainen, T., Kristensen, K., Ylisirniö, A., Virtanen, A., Petäjä, T., Glasius, M., and Prisle, N. L.: Hygroscopic properties and cloud condensation nuclei activation of limonene-derived organosulfates and their mixtures with ammonium sulfate, *Atmos. Chem. Phys.*, 15, 14071-14089, 10.5194/acp-15-14071-2015, 2015.
- 315 Kroll, J. H., Ng, N. L., Murphy, S. M., Flagan, R. C., and Seinfeld, J. H.: Secondary organic aerosol formation from isoprene photooxidation, *Environ. Sci. Technol.*, 40, 1869-1877, 10.1021/es0524301, 2006.
- Lal, V., Khalizov, A. F., Lin, Y., Galvan, M. D., Connell, B. T., and Zhang, R.: Heterogeneous reactions of epoxides in acidic media, *J. Phys. Chem. A*, 116, 6078-6090, 10.1021/jp2112704, 2012.
- 320 Li, H., Zhang, Q., Zhang, Q., Chen, C., Wang, L., Wei, Z., Zhou, S., Parworth, C., Zheng, B., Canonaco, F., Prevot, A. S. H., Chen, P., Zhang, H., Wallington, T. J., and He, K.:

- Wintertime aerosol chemistry and haze evolution in an extremely polluted city of the North China Plain: significant contribution from coal and biomass combustion, *Atmos. Chem. Phys.*, 17, 4751-4768, 10.5194/acp-17-4751-2017, 2017.
- 325 Lin, Y. H., Budisulistiorini, H., Chu, K., Siejack, R. A., Zhang, H. F., Riva, M., Zhang, Z. F., Gold, A., Kautzman, K. E., and Surratt, J. D.: Light-Absorbing Oligomer Formation in Secondary Organic Aerosol from Reactive Uptake of Isoprene Epoxydiols, *Environ. Sci. Technol.*, 48, 12012-12021, 10.1021/es503142b, 2014.
- 330 Liu, C., Ma, Q., Chu, B., Liu, Y., He, H., Zhang, X., Li, J., and Hao, J.: Effect of aluminium dust on secondary organic aerosol formation in m-xylene/NO_x photo-oxidation, *Science China-Earth Sciences*, 58, 245-254, 10.1007/s11430-014-5023-0, 2015.
- Liu, T., Wang, X., Hu, Q., Deng, W., Zhang, Y., Ding, X., Fu, X., Bernard, F., Zhang, 335 Z., Lu, S., He, Q., Bi, X., Chen, J., Sun, Y., Yu, J., Peng, P., Sheng, G., and Fu, J.: Formation of secondary aerosols from gasoline vehicle exhaust when mixing with SO₂, *Atmos. Chem. Phys.*, 16, 675-689, 10.5194/acp-16-675-2016, 2016.
- Mehra, A., Wang, Y., Krechmer, J. E., Lambe, A., Majluf, F., Morris, M. A., Priestley, M., Bannan, T. J., Bryant, D. J., Pereira, K. L., Hamilton, J. F., Rickard, A. R., Newland, 340 M. J., Stark, H., Croteau, P., Jayne, J. T., Worsnop, D. R., Canagaratna, M. R., Wang, L., and Coe, H.: Evaluation of the chemical composition of gas- and particle-phase products of aromatic oxidation, *Atmos. Chem. Phys.*, 20, 9783-9803, 10.5194/acp-20-9783-2020, 2020.
- Meng, Z., Wu, L., Xu, X., Xu, W., Zhang, R., Jia, X., Liang, L., Miao, Y., Cheng, H., 345 Xie, Y., He, J., and Zhong, J.: Changes in ammonia and its effects on PM_{2.5} chemical property in three winter seasons in Beijing, China, *Sci. Total Environ.*, 749, 142208, 10.1016/j.scitotenv.2020.142208, 2020.
- Mo, Z., Lu, S., and Shao, M.: Volatile organic compound (VOC) emissions and health risk assessment in paint and coatings industry in the Yangtze River Delta, China, 350 *Environ. Pollut.*, 269, 115740, 10.1016/j.envpol.2020.115740, 2021.
- Paasonen, P., Peltola, M., Kontkanen, J., Junninen, H., Kerminen, V.-M., and Kulmala, M.: Comprehensive analysis of particle growth rates from nucleation mode to cloud

- condensation nuclei in boreal forest, *Atmos. Chem. Phys.*, 18, 12085-12103, 10.5194/acp-18-12085-2018, 2018.
- 355 Ran, L., Zhao, C., Geng, F., Tie, X., Tang, X., Peng, L., Zhou, G., Yu, Q., Xu, J., and Guenther, A.: Ozone photochemical production in urban Shanghai, China: Analysis based on ground level observations, *J. Geophys. Res. Atmos.*, 114, 10.1029/2008jd010752, 2009.
- Riva, M., Chen, Y., Zhang, Y., Lei, Z., Olson, N. E., Boyer, H. C., Narayan, S., Yee, L.
- 360 D., Green, H. S., Cui, T., Zhang, Z., Baumann, K., Fort, M., Edgerton, E., Budisulistiorini, S. H., Rose, C. A., Ribeiro, I. O., RL, E. O., Dos Santos, E. O., Machado, C. M. D., Szopa, S., Zhao, Y., Alves, E. G., de Sa, S. S., Hu, W., Knipping, E. M., Shaw, S. L., Duvoisin Junior, S., de Souza, R. A. F., Palm, B. B., Jimenez, J. L., Glasius, M., Goldstein, A. H., Pye, H. O. T., Gold, A., Turpin, B. J., Vizuete, W., Martin,
- 365 S. T., Thornton, J. A., Dutcher, C. S., Ault, A. P., and Surratt, J. D.: Increasing Isoprene Epoxydiol-to-Inorganic Sulfate Aerosol Ratio Results in Extensive Conversion of Inorganic Sulfate to Organosulfur Forms: Implications for Aerosol Physicochemical Properties, *Environ. Sci. Technol.*, 53, 8682-8694, 10.1021/acs.est.9b01019, 2019.
- Shiraiwa, M., Yee, L. D., Schilling, K. A., Loza, C. L., Craven, J. S., Zuend, A.,
- 370 Ziemann, P. J., and Seinfeld, J. H.: Size distribution dynamics reveal particle-phase chemistry in organic aerosol formation, *P. Natl Acad. Sci. U. S. A.*, 110, 11746-11750, 10.1073/pnas.1307501110, 2013.
- Wang, Y., Mehra, A., Krechmer, J. E., Yang, G., Hu, X., Lu, Y., Lambe, A., Canagaratna, M., Chen, J., Worsnop, D., Coe, H., and Wang, L.: Oxygenated products formed from
- 375 OH-initiated reactions of trimethylbenzene: autoxidation and accretion, *Atmos. Chem. Phys.*, 20, 9563-9579, 10.5194/acp-20-9563-2020, 2020.
- Warner, J. X., Dickerson, R. R., Wei, Z., Strow, L. L., Wang, Y., and Liang, Q.: Increased atmospheric ammonia over the world's major agricultural areas detected from space, *Geophys. Res. Lett.*, 44, 2875-2884, 10.1002/2016gl072305, 2017.
- 380 Wyche, K. P., Monks, P. S., Ellis, A. M., Cordell, R. L., Parker, A. E., Whyte, C., Metzger, A., Dommen, J., Duplissy, J., Prevot, A. S. H., Baltensperger, U., Rickard, A. R., and Wulfert, F.: Gas phase precursors to anthropogenic secondary organic aerosol:

detailed observations of 1,3,5-trimethylbenzene photooxidation, *Atmos. Chem. Phys.*, 9, 635-665, 10.5194/acp-9-635-2009, 2009.

385 Xu, L., Kollman, M. S., Song, C., Shilling, J. E., and Ng, N. L.: Effects of NO_x on the volatility of secondary organic aerosol from isoprene photooxidation, *Environ. Sci. Technol.*, 48, 2253-2262, 10.1021/es404842g, 2014.

Zaytsev, A., Koss, A. R., Breitenlechner, M., Krechmer, J. E., Nihill, K. J., Lim, C. Y., Rowe, J. C., Cox, J. L., Moss, J., Roscioli, J. R., Canagaratna, M. R., Worsnop, D.,

390 Kroll, J. H., and Keutsch, F. N.: Mechanistic study of the formation of ring-retaining and ring-opening products from the oxidation of aromatic compounds under urban atmospheric conditions, *Atmos. Chem. Phys.*, 19, 15117-15129, 10.5194/acp-19-15117-2019, 2019.

Zhang, Y., Chen, Y., Lei, Z., Olson, N. E., Riva, M., Koss, A. R., Zhang, Z., Gold, A.,

395 Jayne, J. T., Worsnop, D. R., Onasch, T. B., Kroll, J. H., Turpin, B. J., Ault, A. P., and Surratt, J. D.: Joint Impacts of Acidity and Viscosity on the Formation of Secondary Organic Aerosol from Isoprene Epoxydiols (IEPOX) in Phase Separated Particles, *ACS Earth Space Chem.*, 3, 2646-2658, 10.1021/acsearthspacechem.9b00209, 2019.

Zou, Y., Deng, X. J., Zhu, D., Gong, D. C., Wang, H., Li, F., Tan, H. B., Deng, T., Mai,

400 B. R., Liu, X. T., and Wang, B. G.: Characteristics of 1 year of observational data of VOCs, NO_x and O₃ at a suburban site in Guangzhou, China, *Atmos. Chem. Phys.*, 15, 6625-6636, 10.5194/acp-15-6625-2015, 2015.

We sincerely thank the Referee for the valuable comments. Our manuscript has been revised according to the comments from the Referee and our responses to the comments are as follows. For clarity, the comments are reproduced in blue, authors' responses are in black and changes in the manuscript are in red.

5

Responses to Anonymous Referee #3

Overview:

10 The manuscript by Yang et al. examined the effect of SO₂ and NH₃ on the formation of SOA from 1,2,4-trimethylbenzene photooxidation. After the injection of SO₂ and/or NH₃, the apparent yield of the SOA increased after wall loss correction, which demonstrated the synergistic effect of SO₂ and NH₃ in facilitating SOA formation. The authors also used ATR-FTIR, IC, and UPLC-MS to systematically analyze the particle phase composition and identified various inorganic and organo-sulfates compounds.

15 My main comments are about the control experiment setup in this manuscript, which are discussed below. Other than the main comments, the manuscript is written clearly and comprehensive.

Major Comments:

20 The authors demonstrate that the addition of SO₂ and/or NH₃ during the photo-oxidation experiments can enhance the SOA formation and yield. However, part of the aerosol growth can arise from the formation of H₂SO₄ or (NH₄)₂SO₄ particles even without the presence of any SOA, which should be deducted from the enhancement effect of SO₂ and/or NH₃. I suggest the authors add in three control experiments (pure SO₂, pure NH₃, and SO₂+NH₃ mixtures but with similar levels of OH radicals and UV intensity using H₂O₂ or other OH generators) without any VOCs to rule out the formation of inorganic species contributing to the SOA.

25

Author Reply:

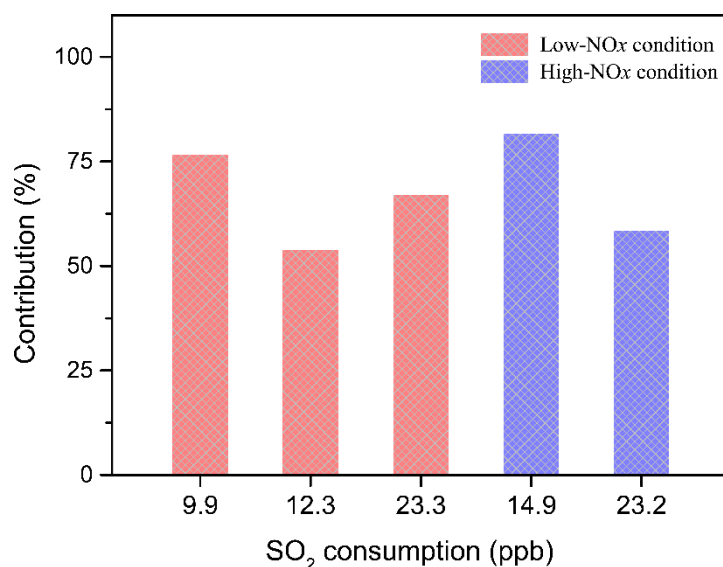
In the SO₂-added experiments, H₂SO₄ can be produced by OH oxidation of SO₂

30 upon photooxidation. With the coexistence of SO₂ and NH₃, the formed H₂SO₄ can be
neutralized by NH₃ to form (NH₄)₂SO₄ particles. Therefore, the addition of SO₂ and/or
NH₃ to the TMB/NO_x mixtures can lead to the increase in the volume concentration of
aerosol particles by the formation of inorganic species and/or the enhanced organic
products (Ye et al., 2018; Jaoui et al., 2008; Liu et al., 2019). In the present study, we
35 discussed the SO₂ dependence of the SOA yield as shown in Fig. 4, and we showed the
role of NH₃ in the total particle number and volume concentrations (as discussed in Sect.
3.2.1). We believe that the introduction of SO₂ can enhance SOA yield based on our
careful analysis as following:

(1) Some studies on the effects of SO₂ and/or NH₃ on SOA formation employed
40 aerosol mass spectrometer to measure in-situ the inorganic and organic components in
aerosol particles (Liu et al., 2016; Chen et al., 2019). For our online measurement of
aerosol particles, we solely used SMPS, whose data are insufficient to quantitatively
explain the contribution of organic aerosols to the increase in aerosol mass. Offline
measurement methods are also commonly adopted in chamber studies. Ion
45 chromatography (IC) is one of the most widely used instruments providing inorganic
aerosol information. Kleindienst et al. (2006) investigated the SO₂ effects on SOA
yields from the isoprene/NO_x/SO₂ photooxidation and used IC to determine the mass
concentrations of inorganic components. Jiang et al. (2020) revealed the influences of
SO₂ and NH₃ on furan SOA yield based on SMPS and IC measurements. In this work,
50 the concentrations of inorganic ions were measured through IC. To determine the net
SOA yield, the mass of inorganic components was subtracted from the total particle
mass based on IC and SMPS data as mentioned in Sect. 3.1.2 in the original manuscript
(Jiang et al., 2020). When SO₂ initial levels increased from 0 to 200 ppb, the net SOA
yield increased from 3.8% to 17.6% in the low-NO_x regime. Similarly, elevating SO₂
55 initial concentration to 228 ppb under high-NO_x condition enhanced the net SOA yield
by a factor of 3.49. The promoting effects of SO₂ on SOA yields were in line with
previous studies (Chen et al., 2019; Liu et al., 2019).

(2) We used an estimation method to explore the contribution of the generated

H₂SO₄ to the particle formation enhancement in TMB/NO_x/SO₂ photooxidation, where
60 we assumed the full conversion of the consumed SO₂ into H₂SO₄ aerosol particles (Ye
et al., 2018; Wyche et al., 2009). As shown in Fig. R1, the contribution of the formed
H₂SO₄ to the increase in particle volume concentration was less than 100%.
Furthermore, a previous study showed that half of the reacted SO₂ could transform into
65 sulfur-containing organic species during the photooxidation of 1,3,5-
trimethylbenzene/o-xylene/octane/toluene (Vivanco et al., 2011). HRMS
measurements reveal the OSs production in this work, which may result in the decrease
in the amount of H₂SO₄ in particle phase. Therefore, the enhanced SOA formation is
also responsible for the increased particle volume concentration in the presence of SO₂.



70

Figure R1. Contribution (%) of the formed H₂SO₄ to the increase in particle volume concentration during low-NO_x and high-NO_x experiments.

(3) We also performed different experiments without introducing TMB, which
could provide significant information about secondary inorganic aerosol formation as
75 suggested by the Referee. In TMB/NO_x/SO₂ photooxidation, the consumption of 9.9
and 23.3 ppb SO₂ can cause the particle volume concentration to increase by 32.9 and
89.2 μm³ cm⁻³, respectively. In pure SO₂ photooxidation, the volume concentrations of
the formed particles were only 25.3 and 43.2 μm³ cm⁻³ when the consumptions of SO₂

were 9.5 and 24.2 ppb, respectively. Comparison of the results of TMB/NO_x/SO₂ and
80 pure SO₂ oxidation experiments demonstrates that the enhancement in aerosol particles
by SO₂ introduction cannot be solely attributed to inorganic aerosol formation.

The yields shown in Table 1, obtained after ruling out the influences of inorganic
species, were net SOA yields. Now, the following note was included in Table 1 in the
revised manuscript. For SOA mass calculation, the inorganic mass concentration has
85 been subtracted from the particle mass concentration.

Besides, we have added the following text in the revised manuscript and supplement to
provide more evidence about SO₂ effects on the net SOA yield.

Manuscript, page 14, lines 400–404

90 We assumed full conversion of the consumed SO₂ into H₂SO₄ aerosol particles and
found that the contribution of the formed H₂SO₄ to the increase in particle volume
concentration was less than 100% (See Sect. S2). In addition, pure SO₂ oxidation
experiments without TMB addition also indicated that the enhancement in aerosol
particles by SO₂ introduction cannot be solely attributed to inorganic aerosol formation
95 (See Sect. S2).

Supplement

S2. The formed H₂SO₄ estimation and inorganic mixture experiments

In order to evaluate the SO₂ effects on SOA formation, we used the method of Ye
et al. (2018) to calculate the contribution of the generated H₂SO₄ to the particle
100 formation enhancement in TMB/NO_x/SO₂ photooxidation (Ye et al., 2018; Wyche et al.,
2009), where we assumed full conversion of the consumed SO₂ into H₂SO₄ aerosol
particles. The contribution of the formed H₂SO₄ to the increase in particle volume
concentration was less than 100% (Fig. S6), demonstrating that the enhanced SOA
formation is also responsible for the increased particle volume concentration.
105 Additionally, a previous study has shown that half of the reacted SO₂ can transform into
sulfur-containing organic species during the photooxidation of 1,3,5-
trimethylbenzene/o-xylene/octane/toluene (Vivanco et al., 2011). HRMS

measurements revealed the OSs production in this work, which may result in the decrease in the amount of H₂SO₄ in the particle phase. Therefore, the enhancement in aerosol particles by SO₂ introduction cannot be solely attributed to inorganic aerosol formation. Pure SO₂ oxidation experiments without introducing TMB were also carried out. In the TMB/NO_x/SO₂ regime, the consumption of 9.9 and 23.3 ppb SO₂ could cause the particle volume concentration to increase by 32.9 and 89.2 μm³ cm⁻³, respectively. However, in pure SO₂ oxidation experiments, the volume concentrations of the formed particles were only 25.3 and 43.2 μm³ cm⁻³ when the consumptions of SO₂ were 9.5 and 24.2 ppb, respectively. Comparison of the results of TMB/NO_x/SO₂ and pure SO₂ oxidation experiments also demonstrates that the enhancement in aerosol particles by SO₂ introduction cannot be solely attributed to inorganic aerosol formation.

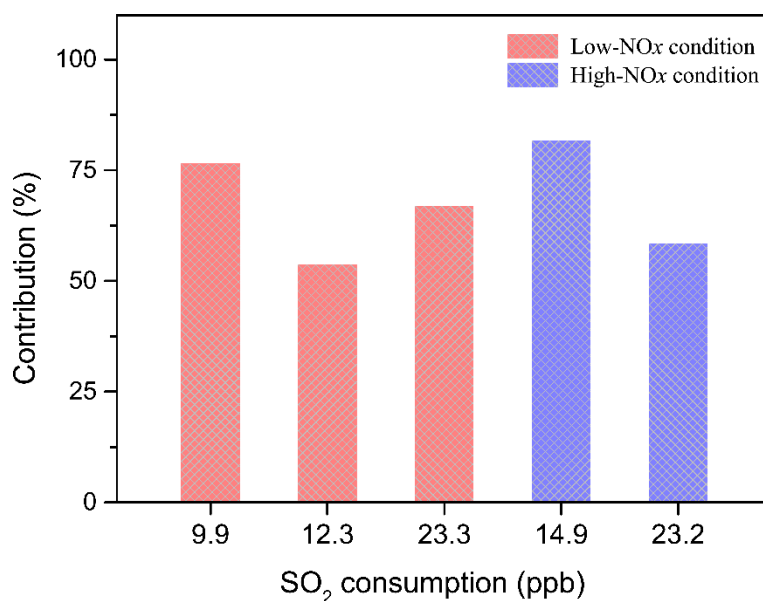


Figure S6. Contribution (%) of the formed H₂SO₄ to the increased particle volume concentration during low-NO_x and high-NO_x experiments.

Figure S7 shows the mass spectra with and without SO₂ and/or NH₃ are similar, suggesting that maybe inorganic species formed with OH are the likely source of enhancement. It would be important to understand that after ruling out this part of the inorganic aerosol formation, how much enhancement the SO₂ and/or NH₃ would add to

the yield of the SOA.

Author Reply:

130 It should be noted that Fig. S7 (now labeled as Fig. S10 in the revised supplement)
compared the mass spectra of aerosol particles from NH₃-free and NH₃-added
experiments. First, we carried out pure NH₃ oxidation experiments and found that
aerosol particles were not formed within 480 min of UV irradiation. In addition, the
promoting effect of NH₃ on SOA formation was not as strong as that of SO₂ with similar
135 level. Under SO₂-free condition, the net SOA yield increased slightly from 3.5% to 5.1%
as NH₃ initial level increased from 0 to 200 ppb. Our result is consistent with the finding
of Chen et al. (2020a), who showed that NH₃ did not significantly affect SOA formation
from toluene/NO_x photooxidation under dry condition. Therefore, the NH₃-induced
changes in the absolute concentrations of organic components might be small in SO₂-
140 free experiments, leading to similar mass spectra for Fig. S10(a) and Fig. S10(b). Under
SO₂-involved conditions, the introduction of NH₃ resulted in MS differences in the
range of m/z 200–400 as presented in Fig. S10(d). The sum of the ion signals in the
ranges of 50–199, 200–299, 300–399, and 400–750 were compared in Fig. S11, where
it can be seen that the abundance of organic compounds with $m/z > 200$ were enhanced
145 with the addition of NH₃ in TMB/NO_x/SO₂ photooxidation.

We have revised the text to explain why the mass spectra of aerosol particles from NH₃-
free and NH₃-added experiments are similar.

Page 22, lines 640–643

150 NH₃ could slightly enhance SOA formation in SO₂-free experiment as mentioned in
Sect. 3.2.1. Therefore, the NH₃-induced changes in the absolute concentrations of
organic components might be small in SO₂-free experiments, leading to similar mass
spectra for Fig. S10(a) and Fig. S10(b). In addition, the major products (Table S4) are
likely generated by similar chemical mechanisms (Fig. 8), which are not sensitive to
the change in initial NH₃ levels under current experimental conditions.

155 It is also necessary to show how much enhancement NH₃ would add to the net SOA
yield according to the Referee's suggestion. Hence, the discussions were revised in the

revised manuscript as following:

Page 20, lines 564–573

160 However, the effect of NH₃ on particle formation was not as pronounced as that of SO₂
with similar concentration (Fig. 7). In TMB/NO_x/NH₃ photooxidation, the net SOA
yield increased slightly from 3.5% to 5.1% as NH₃ initial level increased from 0 to 200
ppb (Table 1). Our result is consistent with the finding of Chen et al. (2020a), who
showed that NH₃ did not significantly affect SOA formation from toluene/NO_x
photooxidation under dry condition. Interestingly, SMPS measurements demonstrated
165 that the coexistence of SO₂ and NH₃ can considerably promote secondary aerosol
formation (Fig. 7). After subtracting the inorganic components, it was seen that the net
SOA yield could increase to 13.7% with the introduction of 200 ppb NH₃ and 234 ppb
SO₂, indicating the synergetic effects of NH₃ and SO₂ (Chu et al., 2016).

170 Another comment I have is that the enhancement of the SOA from the addition of SO₂
and/or NH₃ can also be attributed to the increase of the surface area from the formation
of inorganic species, which shifts the gas-particle equilibrium more to the particle side.
Can the authors discuss more about the effect of this shift of equilibrium? It seems
Figure 4 shows that the first three experiments after adding SO₂ seem to follow this rule.

175 **Author Reply:**

An important mechanism of SOA formation and growth is gas-particle partitioning
of semi-volatile compounds (SVOCs) generated from the atmospheric oxidation of
VOCs. The gas-particle partitioning of SVOCs have a great sensitivity to particle
surface areas in the batch-mode chamber experiments (Zhang et al., 2015; Han et al.,
180 2019). Increasing particle surface area can limit the gas-wall interactions of organic
vapors and is favorable for moving more SVOCs from the gas phase to the particle side
(Han et al., 2019). These additional SVOCs may undergo further particle chemistry to
strongly enhance aerosol particle formation (Apsokardu and Johnston, 2018).

Recently, the effects of the particle surface area concentration on organic aerosol
185 formation have been explored by Han et al. (2019), who found that increasing the

particle surface area concentrations can significantly increase organic aerosol mass yield due to greater partitioning of semi-volatility organic products to the particle-phase. In addition, some studies have confirmed that the SOA yields depend on the surface areas of inorganic aerosols when condensation of organic vapors onto particles is kinetically limited (McVay et al., 2014; Nah et al., 2016; Zhang et al., 2014). In the present work, the surface area concentrations of aerosol particles increased with increasing mixing ratios of SO₂ and/or NH₃ inside the chamber (Table 1), which may facilitate the gas-particle equilibrium shifting to the particle phase. The particle surface area concentrations have been included in Table 1. Based on the suggestion of the Referee, we have enriched the discussion in the revised manuscript as following:

3.1.2 SOA yield in SO₂-added photooxidation

Page 14, lines 421–437

In addition, the particle surface area concentrations significantly increased with increasing SO₂ initial concentrations in both low-NO_x and high-NO_x conditions (Table 1), which might also result in the enhancement in the SOA yield. Besides gas-particle partitioning of SVOCs, the fates of SVOCs in the chamber also include chemical reactions and chamber wall losses. Therefore, in the batch-mode chamber experiments, the gas-particle partitioning of SVOCs have a great sensitivity to particle surface areas (Zhang et al., 2015; Han et al., 2019). Recently, Zhao et al. (2018) examined the SO₂ effects on the SOA formation and suggested that providing additional particle surfaces by SO₂-induced new particle formation leads to the increase in SOA yield. The effects of the particle surface area concentration on organic aerosol formation were explored by Han et al. (2019), who also found that increasing the particle surface area concentrations can significantly increase the organic aerosol mass yield due to greater partitioning of semi-volatility organic products to the particle-phase. Increasing the particle surface area can limit the gas-wall interactions of organic vapors and is favorable for the movement of more SVOCs from the gas phase to the particle side (Han et al., 2019). These additional SVOCs can also undergo further particle chemistry such as acid-catalyzed heterogenous reactions to strongly enhance aerosol particle

215 formation in TMB/NO_x/SO₂ photooxidation (Apsokardu and Johnston, 2018).

3.2.1 Particle formation and growth in NH₃-involved photooxidation

Page 20, lines 573–577

The flux of the gas-phase products diffusing to a particle partly depends on the surface area of the particle. The coexistence of SO₂ and NH₃ promoted the increase in particle surface area concentrations (Table 1). The ability of particle formation originating from gas-to-particle conversion may be significantly stronger with SO₂ and NH₃ introduction, leading to the enhancement in particle formation.

3.2.2 Particle chemical composition in NH₃-involved photooxidation

Page 23, lines 662–665

225 The introduction of SO₂ and NH₃ lead to the formation of ammonium sulfate (Fig. S12), which is an attractive condensation sink for organic vapors. High particle surface area concentration in TMB/NO_x/SO₂/NH₃ experiments may increase the abundance of organic compounds in the bulk phase.

230 Minor Comment:

L217: Can the author make an additional plot in the SI or show how the size dependent wall loss factor is generated?

Author Reply:

The wall-loss of particles are commonly evaluated by seed-only experiments where inert ammonium sulfate (AS) particles are used (Chen et al., 2019; Charan et al., 2020). In the current work, the AS solution was added to a TSI atomizer (Model 3076) to produce droplets, which passed simultaneously through a silica gel diffusion dryer to inject dry AS particles into the chamber. AS particles were lost to the chamber walls due to diffusion, gravitational settling, and electrostatic forces during experiment and the mass size distributions of AS particles were measured by SMPS for 480 min.

240 The size-dependent particle wall-loss rate constants were determined based on the SMPS-measured particle size distribution. First-order loss rate constants (k_i) of particles in each size bin i across all measured sizes were firstly calculated as the slope of the

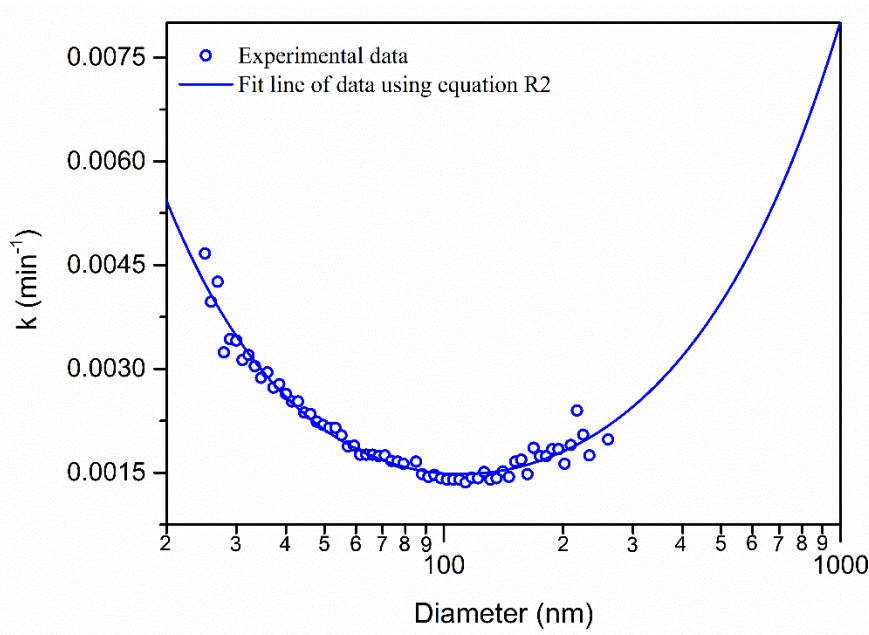
corresponding ln-linear fit line:

$$\ln[M_i(t)] = -k_i t + C \quad (\text{R1})$$

245 where M_i ($\mu\text{g m}^{-3}$) is the mass concentration of particles in the size bin i at time t (min) and C is an arbitrary constant. Then, the relationship between the k_i and the particle diameter ($d_{p,i}$) can be described as follows:

$$k_i(d_{p,i}) = ad_{p,i}^b + cd_{p,i}^{-d} \quad (\text{R2})$$

The optimized fitted line shown in Fig. R2 can express well our independent seed experimental results.



250

Figure R2. Wall loss rate constant of particles as a function of particle diameter.

The description about the wall loss experiments has been updated in the revised manuscript as follows:

255 In order to determine the particles wall loss rates, we carried out independent wall loss experiments using ammonium sulfate particles. An aqueous solution of ammonium sulfate was fed to a constant output atomizer (Model 3706, TSI, USA) to produce droplets, which passed simultaneously through a silica gel diffusion dryer to introduce dry particles into the chamber. The size distributions of ammonium sulfate particles
260 were measured by SMPS for 480 min. Almost identical humidity ($(25 \pm 1) \%$) condition

was achieved among each experiment. The wall losses of particles are size-dependent and, thus, we used a size-dependent particle wall-loss correction approach, which is described in detail in the Supplement.

265 Besides, the following text and Fig. R2 were added in the revised supplement to explain how the size dependent wall loss constant was obtained.

S1. Size-dependent wall loss correction method

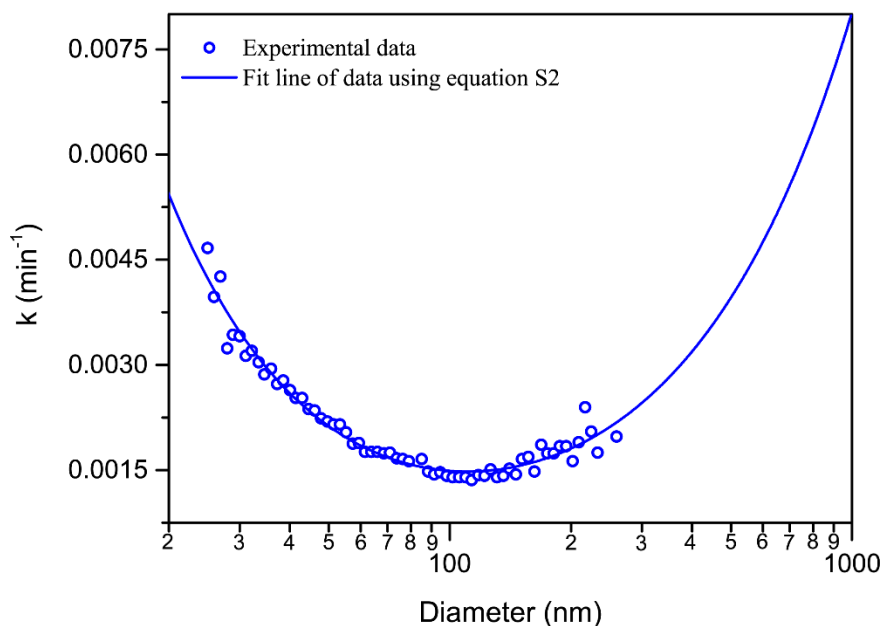
In the present work, the size-dependent particle wall-loss rate constants were determined based on the SMPS-measured particle size distribution. The first-order loss rate constants (k_i) of particles in each size bin i across all measured sizes were firstly
270 calculated as the slope of the corresponding ln-linear fit line:

$$\ln[M_i(t)] = -k_i t + C \quad (\text{S1})$$

where M_i ($\mu\text{g m}^{-3}$) is the mass concentration of particles in size bin i at time t (min) and C is an arbitrary constant. Then, the relationship between the k_i and the particle diameter ($d_{p,i}$) can be described as follows:

$$k_i(d_{p,i}) = a d_{p,i}^b + c d_{p,i}^{-d} \quad (\text{S2})$$

275 The optimized fitted line shown in Fig. S1 can express well our independent seed experimental results. Parameters a , b , c , and d in Eq. (S2) were determined to be 5.5×10^{-6} , 1.05, 0.18, 1.19, respectively. Therefore, the size-dependent loss rate (k) of ammonium sulfate particles can be expressed as $k = 5.5 \times 10^{-6} \times d_p^{1.05} + 0.18 \times d_p^{-1.19}$.



280 **Figure S1.** Wall loss rate constant of particles as a function of particle diameter.

Figure 1: It would be better to change the plots all in the same scale for easy comparison of different conditions.

Author Reply:

285 Figure 1 has been revised according to the comment of the Referee as follows:

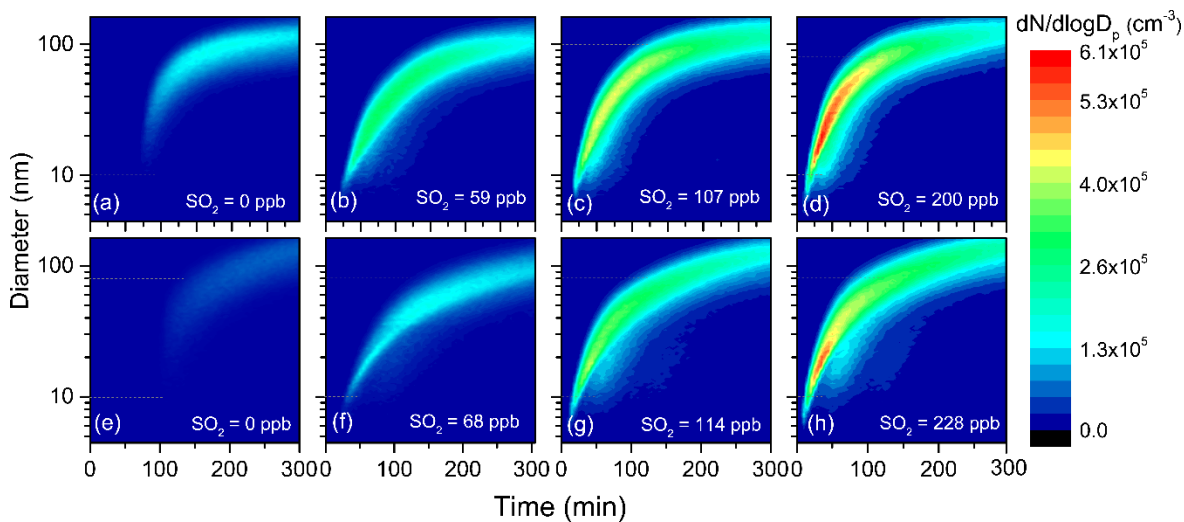


Figure 1. Evolutions of the number distributions of aerosol particles generated from TMB photooxidation in low-NO_x (Panels a–d) and high-NO_x (Panels e–h) experiments.

290

L305: an extra space before “to”

Author Reply:

The extra space has been deleted in the revised manuscript.

295 L367: Please add the recent paper by Chen et al. 2020 also demonstrate that OS-228 could be from isoprene-derived SOA.

Author Reply:

We have cited the study of Chen et al. (2020b) and added the related description. Please, refer to the last comment.

300

L389: The author should also consider adding Zhang et al. 2019 here, which discussed the effects of inorganic sulfates to organosulfates conversion in affecting aerosol growth, multiphase chemistry, and pH.

Author Reply:

305 The paper by Zhang et al. (2019) has now been cited and the original sentence was modified as follow:

The conversion of inorganic sulfates to organosulfates could cause changes in aerosol growth, multiphase chemistry, and acidity (Zhang et al., 2019; Riva et al., 2019).

310 L525: As mentioned, OS-228 was observed by Chen et al. 2020 from the aging of isoprene-SOA. Even though the source might be different from the OS-228 here, the author should mention it in the conclusion instead of defining OS-228 as from unknown source.

Author Reply:

315 We have carefully read the literature suggested by the Referee. Chen et al. (2020b) investigated the heterogeneous OH oxidation of 2-methyltetrol sulfate diastereomers and identified OS at m/z 227 as the oxidation product of 2-methyltetrol sulfate diastereomers. Methyltetrol sulfates are significant tracers for isoprene-derived SOA. Therefore, the OH aging of isoprene SOA is also a potential source of OS-228 in the

320 atmosphere. The inappropriate conclusion has been removed in the revised manuscript.
We have added the following text in Sect. 3.1.3 to describe the findings in the study by
Chen et al. (2020b).

Page 18, lines 504–509

325 More recently, Chen et al. (2020b) suggested that heterogeneous OH oxidation of
isoprene-derived SOA can contribute to the formation of an organosulfate with
molecular weight at 228. Our results show the detection of OS-226, OS-228, OS-240,
and OS-268 organosulfates, which are isomers of organosulfates derived from isoprene
(Cai et al., 2020), isoprene (Chen et al., 2020b), limonene (Cai et al., 2020), and
limonene (Boris et al., 2016), respectively.

330

References:

Chen, Y., et al. (2020). "Heterogeneous Hydroxyl Radical Oxidation of Isoprene-
Epoxydiol-Derived Methyltetrol Sulfates: Plausible Formation Mechanisms of
335 Previously Unexplained Organosulfates in Ambient Fine Aerosols." *Environmental
Science & Technology Letters* 7(7): 460-468.

Zhang, Y., et al. (2019). "Joint Impacts of Acidity and Viscosity on the Formation of
Secondary Organic Aerosol from Isoprene Epoxydiols (IEPOX) in Phase Separated
Particles." *ACS Earth and Space Chemistry* 3(12): 2646-2658.

340

References

- Apsokardu, M. J., and Johnston, M. V.: Nanoparticle growth by particle-phase chemistry, *Atmos. Chem. Phys.*, 18, 1895-1907, 10.5194/acp-18-1895-2018, 2018.
- 345 Boris, A. J., Lee, T., Park, T., Choi, J., Seo, S. J., and Collett Jr, J. L.: Fog composition at Baengnyeong Island in the eastern Yellow Sea: detecting markers of aqueous atmospheric oxidations, *Atmos. Chem. Phys.*, 16, 437-453, 10.5194/acp-16-437-2016, 2016.
- Cai, D., Wang, X., Chen, J., and Li, X.: Molecular characterization of organosulfates in
350 highly polluted atmosphere using ultra-high-resolution mass spectrometry, *J. Geophys. Res.-Atmos.*, 125, 10.1029/2019jd032253, 2020.
- Charan, S. M., Buenconsejo, R. S., and Seinfeld, J. H.: Secondary organic aerosol yields from the oxidation of benzyl alcohol, *Atmos. Chem. Phys.*, 20, 13167-13190, 10.5194/acp-20-13167-2020, 2020.
- 355 Chen, L., Bao, Z., Wu, X., Li, K., Han, L., Zhao, X., Zhang, X., Wang, Z., Azzi, M., and Cen, K.: The effects of humidity and ammonia on the chemical composition of secondary aerosols from toluene/NO_x photo-oxidation, *Sci. Total Environ.*, 728, 138671, 10.1016/j.scitotenv.2020.138671, 2020a.
- Chen, T., Liu, Y., Ma, Q., Chu, B., Zhang, P., Liu, C., Liu, J., and He, H.: Significant
360 source of secondary aerosol: formation from gasoline evaporative emissions in the presence of SO₂ and NH₃, *Atmos. Chem. Phys.*, 19, 8063-8081, 10.5194/acp-19-8063-2019, 2019.
- Chen, Y., Zhang, Y., Lambe, A. T., Xu, R., Lei, Z., Olson, N. E., Zhang, Z., Szalkowski, T., Cui, T., Vizuete, W., Gold, A., Turpin, B. J., Ault, A. P., Chan, M. N., and Surratt, J.
365 D.: Heterogeneous Hydroxyl Radical Oxidation of Isoprene-Epoxydiol-Derived Methyltetrol Sulfates: Plausible Formation Mechanisms of Previously Unexplained Organosulfates in Ambient Fine Aerosols, *Environ. Sci. Technol. Lett.*, 7, 460-468, 10.1021/acs.estlett.0c00276, 2020b.
- Chu, B., Zhang, X., Liu, Y., He, H., Sun, Y., Jiang, J., Li, J., and Hao, J.: Synergetic
370 formation of secondary inorganic and organic aerosol: effect of SO₂ and NH₃ on particle

- formation and growth, *Atmos. Chem. Phys.*, 16, 14219-14230, 2016.
- Han, Y., Gong, Z., Liu, P., de Sá, S. S., McKinney, K. A., and Martin, S. T.: Influence of Particle Surface Area Concentration on the Production of Organic Particulate Matter in a Continuously Mixed Flow Reactor, *Environ. Sci. Technol.*, 53, 4968-4976, 10.1021/acs.est.8b07302, 2019.
- 375 Jaoui, M., Edney, E. O., Kleindienst, T. E., Lewandowski, M., Offenberg, J. H., Surratt, J. D., and Seinfeld, J. H.: Formation of secondary organic aerosol from irradiated α -pinene/toluene/NO_x mixtures and the effect of isoprene and sulfur dioxide, *J. Geophys. Res.*, 113, 10.1029/2007jd009426, 2008.
- 380 Jiang, X., Chen, L., You, B., Liu, Z., Wang, X., and Du, L.: Joint impacts of atmospheric SO₂ and NH₃ on the formation of nanoparticles from photooxidation of a typical biomass burning compound, *Environmental Science: Nano*, 10.1039/d0en00520g, 2020.
- Kleindienst, T. E., Edney, E. O., Lewandowski, M., Offenberg, J. H., and Jaoui, M.: 385 Secondary organic carbon and aerosol yields from the irradiations of isoprene and α -pinene in the presence of NO_x and SO₂, *Environ. Sci. Technol.*, 40, 3807-3812, 10.1021/es052446r, 2006.
- Liu, C., Chen, T., Liu, Y., Liu, J., He, H., and Zhang, P.: Enhancement of secondary organic aerosol formation and its oxidation state by SO₂ during photooxidation of 2- 390 methoxyphenol, *Atmos. Chem. Phys.*, 19, 2687-2700, 10.5194/acp-19-2687-2019, 2019.
- Liu, T., Wang, X., Hu, Q., Deng, W., Zhang, Y., Ding, X., Fu, X., Bernard, F., Zhang, Z., Lu, S., He, Q., Bi, X., Chen, J., Sun, Y., Yu, J., Peng, P., Sheng, G., and Fu, J.: Formation of secondary aerosols from gasoline vehicle exhaust when mixing with SO₂, 395 *Atmos. Chem. Phys.*, 16, 675-689, 10.5194/acp-16-675-2016, 2016.
- McVay, R. C., Cappa, C. D., and Seinfeld, J. H.: Vapor–Wall Deposition in Chambers: Theoretical Considerations, *Environ. Sci. Technol.*, 48, 10251-10258, 10.1021/es502170j, 2014.
- Nah, T., McVay, R. C., Zhang, X., Boyd, C. M., Seinfeld, J. H., and Ng, N. L.: Influence

400 of seed aerosol surface area and oxidation rate on vapor wall deposition and SOA mass yields: a case study with α -pinene ozonolysis, *Atmos. Chem. Phys.*, 16, 9361-9379, 10.5194/acp-16-9361-2016, 2016.

Riva, M., Chen, Y., Zhang, Y., Lei, Z., Olson, N. E., Boyer, H. C., Narayan, S., Yee, L. D., Green, H. S., Cui, T., Zhang, Z., Baumann, K., Fort, M., Edgerton, E.,
405 Budisulistiorini, S. H., Rose, C. A., Ribeiro, I. O., RL, E. O., Dos Santos, E. O., Machado, C. M. D., Szopa, S., Zhao, Y., Alves, E. G., de Sa, S. S., Hu, W., Knipping, E. M., Shaw, S. L., Duvoisin Junior, S., de Souza, R. A. F., Palm, B. B., Jimenez, J. L., Glasius, M., Goldstein, A. H., Pye, H. O. T., Gold, A., Turpin, B. J., Vizuete, W., Martin, S. T., Thornton, J. A., Dutcher, C. S., Ault, A. P., and Surratt, J. D.: Increasing Isoprene
410 Epoxydiol-to-Inorganic Sulfate Aerosol Ratio Results in Extensive Conversion of Inorganic Sulfate to Organosulfur Forms: Implications for Aerosol Physicochemical Properties, *Environ. Sci. Technol.*, 53, 8682-8694, 10.1021/acs.est.9b01019, 2019.

Vivanco, M. G., Santiago, M., Martinez-Tarifa, A., Borrás, E., Rodenas, M., Garcia-Diego, C., and Sanchez, M.: SOA formation in a photoreactor from a mixture of organic
415 gases and HONO for different experimental conditions, *Atmos. Environ.*, 45, 708-715, 10.1016/j.atmosenv.2010.09.059, 2011.

Wyche, K. P., Monks, P. S., Ellis, A. M., Cordell, R. L., Parker, A. E., Whyte, C., Metzger, A., Dommen, J., Duplissy, J., Prevot, A. S. H., Baltensperger, U., Rickard, A. R., and Wulfert, F.: Gas phase precursors to anthropogenic secondary organic aerosol:
420 detailed observations of 1,3,5-trimethylbenzene photooxidation, *Atmos. Chem. Phys.*, 9, 635-665, 10.5194/acp-9-635-2009, 2009.

Ye, J., Abbatt, J. P. D., and Chan, A. W. H.: Novel pathway of SO₂ oxidation in the atmosphere: reactions with monoterpene ozonolysis intermediates and secondary organic aerosol, *Atmos. Chem. Phys.*, 18, 5549-5565, 10.5194/acp-18-5549-2018, 2018.

425 Zhang, R., Wang, G., Guo, S., Zamora, M. L., Ying, Q., Lin, Y., Wang, W., Hu, M., and Wang, Y.: Formation of urban fine particulate matter, *Chem. Rev.*, 115, 3803-3855, 10.1021/acs.chemrev.5b00067, 2015.

Zhang, X., Cappa, C. D., Jathar, S. H., McVay, R. C., Ensber, J. J., Kleeman, M. J., and

- Seinfeld, J. H.: Influence of vapor wall loss in laboratory chambers on yields of
430 secondary organic aerosol, *P. Natl. Acad. Sci. USA*, 111, 5802-5807, 2014.
- Zhang, Y., Chen, Y., Lei, Z., Olson, N. E., Riva, M., Koss, A. R., Zhang, Z., Gold, A.,
Jayne, J. T., Worsnop, D. R., Onasch, T. B., Kroll, J. H., Turpin, B. J., Ault, A. P., and
Surratt, J. D.: Joint Impacts of Acidity and Viscosity on the Formation of Secondary
Organic Aerosol from Isoprene Epoxydiols (IEPOX) in Phase Separated Particles, *ACS*
435 *Earth Space Chem.*, 3, 2646-2658, 10.1021/acsearthspacechem.9b00209, 2019.
- Zhao, D., Schmitt, S. H., Wang, M., Acir, I.-H., Tillmann, R., Tan, Z., Novelli, A., Fuchs,
H., Pullinen, I., Wegener, R., Rohrer, F., Wildt, J., Kiendler-Scharr, A., Wahner, A., and
Mentel, T. F.: Effects of NO_x and SO₂ on the secondary organic aerosol formation from
photooxidation of α -pinene and limonene, *Atmos. Chem. Phys.*, 18, 1611-1628,
440 10.5194/acp-18-1611-2018, 2018.

SO₂ and NH₃ emissions enhance organosulfur compounds and fine particles formation from the photooxidation of a typical aromatic hydrocarbon

5 Zhaomin Yang¹, Li Xu¹, Narcisse T. Tsona¹, Jianlong Li¹, Xin Luo², Lin Du¹

¹Environment Research Institute, Shandong University, Qingdao, 266237, China

²Technology Center of Qingdao Customs, Qingdao, 266003, China

Correspondence to: Lin Du (lindu@sdu.edu.cn)

10 **Abstract.** Aromatic hydrocarbons can dominate the volatile organic compounds budget in the urban atmosphere. Among them, 1,2,4-trimethylbenzene (TMB), mainly emitted from solvent use, is one of the most important secondary organic aerosols (SOA) precursors. Although atmospheric SO₂ and NH₃ levels can affect secondary aerosol formation, the influenced extent of their impact and their detailed driving mechanisms are not well understood. The focus of the present study is to examine the chemical compositions and formation mechanisms of SOA from TMB photooxidation
15 influenced by SO₂ and/or NH₃. Here, we showed that SO₂ emission could considerably enhance aerosol particle formation due to SO₂-induced sulfate generation and acid-catalyzed heterogeneous reaction. Orbitrap mass spectrometry (MS) measurements revealed the generation of not only typical TMB products but also hitherto unidentified organosulfates (OSs) in SO₂-added experiments.
20 The OSs designated as unknown origin in earlier field measurements were also detected in TMB SOA, indicating that atmospheric OSs might be also originated from TMB photooxidation. For NH₃-involved experiments, results demonstrated a positive correlation between NH₃ levels and particle volume as well as number concentrations. The effects of NH₃ on SOA composition was slight under SO₂-free conditions but stronger in the presence of SO₂. A series of multifunctional products with carbonyl, alcohols, and nitrate functional groups were tentatively characterized in
25 NH₃-involved experiments based on infrared spectra and MS analysis. Plausible formation pathways were proposed for detected products in the particle-phase. The volatility distributions of products, estimated using parameterization methods, suggested that the detected products gradually condense onto the nucleation particles to contribute to aerosol formation and growth. Our results suggest that strict control of SO₂ and NH₃ emissions might remarkably reduce organosulfates and secondary aerosol burden in the atmosphere. Updating the aromatic oxidation mechanism in models could result in more accurate treatment of particles formation for urban regions with considerable SO₂, NH₃, and aromatics emissions.
30

35 1 Introduction

Secondary organic and inorganic aerosols have been observed to account for a considerable fraction of fine particulate matter (aerosol particles $\leq 2.5 \mu\text{m}$ in aerodynamic diameter, $\text{PM}_{2.5}$) during $\text{PM}_{2.5}$ pollution events, which had frequently occurred and lasted for days or even weeks in China during the last decade (Huang et al., 2014; Guo et al., 2014). These particles can directly and indirectly
40 impact regional and global climate (Kanakidou et al., 2005), air quality (Zhang et al., 2015), and human health (Lelieveld et al., 2015).

Secondary organic aerosols (SOA) arise predominantly from the oxidation of volatile organic compounds (VOCs) in the atmosphere. Early atmospheric models underestimated the measured
45 SOA mass concentrations in field studies by 1–2 orders of magnitude (Volkamer et al., 2006; Heald et al., 2010). Although recent efforts such as updating missing SOA precursors, accounting unknown processes of gas-to-particle conversion, and improving emission inventories have narrowed the observed gap between the modeled and measured SOA mass, uncertainties still exist in organic aerosol estimates (Shrivastava et al., 2011; Cheng et al., 2021). Inorganic perturbations on SOA
50 formation (Shrivastava et al., 2017) are partly responsible for these uncertainties, and they include the addition of mineral particles (Yu and Jang, 2019), nitrogen oxide (NO_x) (Zhao et al., 2018), ammonia (NH_3) (Hao et al., 2020), and sulfur dioxide (SO_2) (Yang et al., 2020), which can engage in the gas- or particle-phase chemistry and subsequently influence SOA formation and growth (Friedman et al., 2016; Ng et al., 2007; Na et al., 2006). NO_x effects on particle formation are
55 generally known to be pronounced. High levels of SO_2 , NH_3 , and VOCs have been reported in certain regions such as Guangzhou (Zou et al., 2015), Beijing (Meng et al., 2020), Handan (Li et al., 2017) in China. During haze pollution episodes, Li et al. (2017) observed that SO_2 levels can be up to 200 ppb in Handan, China. A recent study also showed significant increasing NH_3 levels in the atmosphere over the United States and the European Union (Warner et al., 2017). However, less
60 focus has been placed on the SO_2 and NH_3 perturbations on SOA formation and chemical composition. Aerosol particles contain a multitude of compounds with different physicochemical properties. Previous laboratory studies examined the photooxidation of cyclohexene, fuel, and 1,3,5-trimethylbenzene in the presence of SO_2 and reported organosulfates (OSs) formation (Yang et al., 2020; Liu et al., 2017; Blair et al., 2017). The atmospheric oxidation of SO_2 can generate sulfuric acid that is critical for the increase of particle acidity. SO_2 -induced acidic sulfate plays an active role in the production of OSs, which have been recognized as significant SOA tracers describing the enhancement in SOA by SO_2 emission (Xu et al., 2015).

OSs are ubiquitous in ambient aerosol particles and they are estimated to account for 3–30% of the
70 organic mass in fine aerosol particles (Surratt et al., 2008; Tolocka and Turpin, 2012). The presence of OSs could alter aerosol morphology (Riva et al., 2019), viscosity (Riva et al., 2019; Zhang et al.,

2019), particle acidity (Riva et al., 2019), phase state (Zhang et al., 2019), hygroscopicity (Estillore et al., 2016; Hansen et al., 2015), and optical properties (Fleming et al., 2019), thereby resulting in large climate effects. A large number of OSs have previously been observed in field measurements but only a few biogenic VOCs can be clearly designated as OSs precursors (Wang et al., 2019b; Shalamzari et al., 2014). Recent field studies reported that some unidentified OSs with C₂–C₂₅ skeletons may not be originated from biogenic VOCs and suggested that anthropogenic VOCs may contribute to these OSs formation (Wang et al., 2016; Blair et al., 2017). In addition, Ma et al. (2014) demonstrated that OSs derived from aromatic hydrocarbons contribute to up to 67% of the total OSs mass in Shanghai, China, highlighting the potentially significant role of anthropogenic aromatics in organosulfate formation. While several studies have shown that SO₂ emissions have implications for the SOA burden and OSs formation, detailed characterizations of OSs formation from anthropogenic monocyclic aromatic photooxidation are poorly performed.

85 NH₃ is the most abundant form of reduced nitrogen and it is ubiquitous in the ambient environment. NH₃ levels increased substantially in recent years and are estimated to continue to increase in the future (Warner et al., 2017). It is established that the increased NH₃ emissions could reduce the effectiveness of PM_{2.5} control by controlling SO₂ and NO_x (Wu et al., 2016; Fu et al., 2017). However, the effects of NH₃ on the formation of aerosol particles have not been well understood.

90 NH₃ has a promoting effect on the formation of new particles (Wang et al., 2020a) where low volatile organic compounds could condense to form SOA in the atmosphere. A previous chamber study reported that the addition of NH₃ could lead to the enhancement in the volume and number concentrations of SOA from α -pinene ozone system (Na et al., 2007). Another study by Babar et al. (2017) utilized newly developed flow reactor and confirmed that the presence of NH₃ can enhance

95 SOA formation from both ozonolysis and photooxidation of α -pinene. Besides α -pinene, the promoting effects of NH₃ on particle formation were also discovered in the photooxidation of aromatics (Chu et al., 2016) and vehicle exhaust (Chen et al., 2019). In contrast, addition of NH₃ decreased aerosol particle formation from the reaction of styrene with ozone owing to the decomposition of products by NH₃ nucleophilic attack (Na et al., 2006). Laboratory evidence

100 suggests that NH₃ can influence SOA composition via the neutralization of organic acids (Hao et al., 2020) and via the NH₃ uptake by carbonyl-containing compounds (Flores et al., 2014). The reaction of organic compounds in particle-phase with NH₃ can decrease gaseous NH₃ concentrations and can enhance the formation of nitrogen-containing organic compounds (Liu et al., 2015b), which are a class of brown carbon and could modify SOA optical properties. The neglect of NH₃ effects on SOA

105 formation might increase the model-measurement disagreement in SOA mass and can lead to an overprediction of NH₃ concentration in the gas-phase, especially in a complex urban environment. Consequently, it is necessary to explicitly explore the influence of NH₃ on aerosol particles formation.

110 The complex mixture of ozone and fine particles is an emerging environmental problem affecting regional and urban air quality in China (Song et al., 2017), and investigating the chemistry of aromatic hydrocarbons has become greatly important for ozone and PM_{2.5} control because aromatics have high ozone- and SOA-forming potential (Chu et al., 2020). Aromatic hydrocarbons comprise a substantial fraction of the total VOCs at urban locations and even in rural areas (Guo et al., 2006; 115 Ran et al., 2009), and evidence shows that global SOA formation from aromatic hydrocarbons lies in the range of 2 to 12 Tg yr⁻¹ (Henze et al., 2008). 1,2,4-Trimethylbenzene (TMB) is a small monocyclic aromatic emitted primarily from industrial solvent evaporation (Mo et al., 2021). In the troposphere, TMB is mainly oxidized via hydroxyl radical (OH), producing multigenerational oxidized compounds that can contribute to SOA formation and growth (Zaytsev et al., 2019; Mehra et al., 2020). The OH oxidation of TMB can also generate small dicarbonyls glyoxal and methylglyoxal (Zaytsev et al., 2019), which are significant precursors for light-absorbing SOA formation. In addition, the Master Chemical Mechanism (MCM, <http://mcm.leeds.ac.uk/MCMv3.2/>, last access: 23 February 2021) is a near-explicit chemical mechanism that can describe, in detail, the tropospheric degradation of TMB. A recent study reported that identified autoxidation pathways 125 during OH oxidation of TMB are not included in the current MCM and the detected TMB products are more diverse than the products shown in MCM (Wang et al., 2020b). The updates for the OH-initiated oxidation mechanism of TMB can be achieved only when the rate constants, branching ratios and product distributions can be explicitly obtained. However, TMB photooxidation is highly complex and sensitive to environmental conditions. To better understand TMB SOA formation and 130 growth, investigating chemical processes of TMB photooxidation with inorganic perturbation is required.

The mechanisms leading to secondary aerosol formation in the urban environment remain highly elusive and controversial, particularly for the processes related to changes in secondary aerosol mass and chemical composition. Recent studies have suggested that inorganic pollution emissions could 135 perturb SOA formation, yet very little is known about the SO₂ and NH₃ effects on SOA formation. Given the ubiquity of SO₂, NH₃, and TMB in the atmosphere, a key goal of this work is to determine the detailed chemical compositions and formation mechanisms of secondary aerosol from TMB photooxidation with SO₂ and/or NH₃. We investigated the effects of SO₂ and NH₃ on the growth of 140 particles from TMB photooxidation for the first time and discussed the role of inorganic species in TMB chemistry. The chemical composition of TMB SOA was rigorously characterized based on laboratory measurements. We also revealed some hitherto unidentified organosulfates and tentatively proposed relevant formation pathways of products.

2 Experimental methods

145 2.1 Particle generation

Aerosol particles were produced from TMB photooxidation in the presence of NO_x in a new indoor smog chamber, which consists of a 1.1 m³ Teflon reactor (0.6 mm Teflon film) housed in a temperature-controlled room. For photooxidation, a panel of black light lamps (F40BLB, GE) were used to provide ultraviolet (UV) irradiation centered at 365 nm. Before each run, the chamber was
150 continually purged with dry and purified air prepared by zero air supply (Model 111, Thermo Scientific, USA) and simultaneously irradiated with UV lights until the concentrations of background contaminants (i.e., NO, NO₂, SO₂, and O₃) were lower than 1 ppb and the particle number concentration was below 5 cm⁻³.

155 The TMB photooxidation experiments were carried out by the following steps. First, a known volume of TMB liquid (98%, Aladdin) was transported into the chamber through a heated (80 °C) Teflon tube carried by a flow of zero air. Second, according to experimental design, different quantities of NO (504 ppm in N₂, Qingdao Yuyan Gas Company, China), SO₂ (1013 ppm in N₂, Qingdao Yuyan Gas Company, China), and NH₃ (497 ppm in N₂, Qingdao Yuyan Gas Company,
160 China) were introduced into the chamber from corresponding high-pressure cylinders using calibrated mass flow controllers (D07-7, Beijing Sevenstar Electronics Co., Ltd, China). Note that before the injection of NH₃, the inlet tubes were flushed with NH₃ flow for 30 min to minimize the adsorption losses of NH₃ in the tubes. After all species in the chamber were well mixed (initial concentrations of TMB, NO, and/or SO₂ were constant), black light lamps were turned on, marking
165 the beginning of photooxidation experiments. The chamber was operated in batch mode with a reaction time of approximately 300–360 min. **Seed particles were not introduced into the chamber over the course of particle formation experiments.** Temperature and relative humidity (RH) inside the chamber were (299 ± 4) K and (25 ± 1) %, respectively. Detailed experimental conditions and results for each experiment are provided in Table 1. Twelve experiments were conducted under four
170 different scenarios. In the first set of experiments (Exps. 1–4, Table1), SO₂ levels in the chamber varied from 0 to 200 ppb while the initial ratio of [TMB] to [NO_x] was kept higher than 10 ppbC ppb⁻¹ (low-NO_x condition). The second set of experiments (Exps. 5–8, Table1) were performed under high-NO_x condition ([TMB]₀/[NO_x]₀ < 10 ppbC ppb⁻¹) with SO₂ concentration being the only variable (ranged from 0 to 228 ppb). The third part of experiments (Exps. 9–10, Table1) consisted
175 of an irradiation of TMB, NO_x, and NH₃, while the subsequent part of experiments (Exps. 11–12, Table1) consisted of an irradiation of TMB, NO_x, SO₂, and NH₃.

Different physicochemical parameters were measured over the course of photooxidation experiments. A digital thermo-hydrometer (Model 645, Testo AG, Lenzkirch, Germany) was used
180 to measure temperature and RH inside the chamber. The concentrations of NO and NO_x were

measured with a NO-NO₂-NO_x analyzer (model 42i, Thermo scientific, USA), while a Thermo scientific model 43i-TLE pulsed fluorescence SO₂ analyzer was used to measure SO₂ levels throughout the experiments. The O₃ level was monitored with a Thermo scientific model 49i O₃ analyzer. The initial concentration of NH₃ was calculated based on the introduced amount of NH₃ and the reactor volume. The decay of TMB was measured by a gas chromatography (GC, 7890B, Agilent Technologies, USA) equipped with a DB-624 column (30 m × 0.32 mm, 1.8 μm film thickness, Agilent Technologies, USA) and a flame ionization detector (FID). The GC temperature was programmed to increase from 80 to 200 °C at 20 °C min⁻¹ rate. Particle size distributions and volume concentrations in all experiments were recorded in situ using a scanning mobility particle sizer (SMPS), which consists of a long differential mobility analyzer (long-DMA, Model 3082, TSI, USA) and a condensation particle counter (CPC, Model 3776, TSI, USA). The long-DMA was available for measuring the particle size distribution in the range of 13.8–723.4 nm while smaller particles between 4.5–162.5 nm were measured with a nano differential mobility analyzer (nano-DMA, Model 3085, TSI, USA). The measured volume concentration in each experiment was converted into particle mass concentration with an estimated particle density of 1.4 g cm⁻³.

Table 1. Experimental conditions and results for the TMB photooxidation experiments.

Exp.	[TMB] ₀ (ppb)	[TMB] consumed ($\mu\text{g m}^{-3}$)	[TMB] ₀ /[NO _x] ₀ (ppbC ppb ⁻¹)	[NO _x] ₀ (ppb)	[SO ₂] ₀ (ppb)	[NH ₃] ₀ (ppb)	[OH] $\times 10^{-6}$ (molecules cm ⁻³) ^a	RH (%)	T (K)	Surface area concentration $\times 10^{-3}$ ($\mu\text{m}^2 \text{cm}^{-3}$) ^b	N _{max} $\times 10^{-5}$ (cm ⁻³) ^c	SOA mass ($\mu\text{g m}^{-3}$) ^d	SOA yield (%) ^e
1	374	1404	18.9	178	-	-	2.52	25	295	1.08	0.27	52.6	3.8 ± 0.4
2	350	1385	17.3	182	59	-	2.33	24	296	2.33	1.12	97.8	8.2 ± 0.7
3	368	1303	17.3	191	107	-	2.29	25	296	2.82	1.13	164.8	12.6 ± 1.3
4	220	766	10.0	199	200	-	3.00	25	295	3.45	1.40	175.6	17.6 ± 2.0
5	393	1693	7.6	465	-	-	3.62	26	298	1.21	0.29	59.4	3.5 ± 0.4
6	346	1599	6.8	457	68	-	3.44	24	295	2.65	0.93	120.7	7.9 ± 0.7
7	260	1069	5.1	457	114	-	3.12	26	298	2.06	0.98	78.7	8.0 ± 0.7
8	379	1534	7.4	464	228	-	3.06	24	297	3.76	1.10	186.9	12.2 ± 1.2
9	454	1880	8.6	475	-	100	3.42	26	303	1.58	0.45	70.6	3.8 ± 0.4
10	464	1946	9.1	457	-	200	3.37	25	299	2.13	0.60	99.3	5.1 ± 0.5
11	425	1972	8.6	447	227	100	3.51	24	299	4.45	1.57	209.6	12.9 ± 1.3
12	450	1974	8.9	455	234	200	3.32	26	303	4.80	2.00	244.9	13.7 ± 1.4

^a The average OH concentration was determined from the measured TMB decay. ^b The particle surface area concentration measured by SMPS at 300 min of each experiment. ^c Aerosol particle maximum number concentration. ^d SOA mass concentrations have been wall-loss corrected. For SOA mass calculation, the inorganic mass concentration has been subtracted from the particle mass concentration. ^e Errors in SOA yield were calculated from error propagation using the sum of the uncertainties in TMB data and the systematic error of SMPS.

2.2 Particle collection and analysis

2.2.1 Attenuated total reflectance-Fourier transform infrared spectroscopy analysis

205 Following 300–360 min of reaction, aerosol samples were collected onto aluminum foils (25 mm, Jowin Technology Co. Ltd.) by a low-pressure impactor (DLPI+, DeKati Ltd, Finland) and were stored at -20 °C thereafter until analysis to reduce evaporative losses of aerosol. The chemical functional groups of aerosols were characterized by an attenuated total reflectance-Fourier transform infrared (ATR-FTIR) spectrophotometer (Vertex 70, Bruker, Germany) with mercury cadmium telluride detector. The ATR-FTIR spectra of aerosol particles in each run were recorded
210 by averaging 64 scans from 4000–600 cm^{-1} with a resolution of 4 cm^{-1} . Prior to each measurement with ATR-FTIR, the surface of the diamond crystal was thoroughly cleaned with ethanol and ultrapure water to rule out interferences of other sources of contamination. The ATR-FTIR spectra of blank aluminum foils were also acquired to confirm the absence of IR absorption by the aluminum
215 foil on which aerosols are collected.

2.2.2 Ion chromatography analysis

Following the ATR-FTIR measurements, aerosol samples were extracted in 3 mL of ultrapure water (Milli-Q water, 18.2 M Ω) under sonication in an ice bath for 30 min. The extracted samples were filtered through polyethersulfone syringe filters (0.22 μm pore size) and subsequently analyzed for
220 their ionic concentrations using an ion chromatography (Dionex ICS-600, Thermo Fisher Scientific, USA) with electrical conductivity detection. A Dionex IonPacTM AS19 column (4 \times 250 mm) connected with AG19 guard column (4 \times 50 mm, Dionex Ionpac) was used to separate anions. An aqueous solution of 20 mM potassium hydroxide (KOH) prepared by reagent-free controller (Dionex, Thermo Scientific, USA) was used as anion eluent. Cation analysis was carried out with
225 the pair of CG12A guard column (4 \times 50 mm, Dionex Ionpac) and analytical column (4 \times 250 mm, CS12A, Dionex IonPacTM) and an isocratic 20 mM methanesulfonic acid ($\text{CH}_4\text{O}_3\text{S}$). The same volume of extract was injected into the ion chromatograph by a six-way valve mounted with a loop of 250 μL . The elution flow rates of KOH and $\text{CH}_4\text{O}_3\text{S}$ were both set to 1 L min^{-1} .

2.2.3 Ultra-high-performance liquid chromatography high resolution mass spectrometry 230 analysis

Laboratory-generated aerosols were also collected on 47 mm polytetrafluoroethylene (PTFE) filters (0.22 μm pore size, Tianjin Jinteng Experimental Equipment, China) using a stainless steel inline filter holder (Sartorius 16254, Sartorius Stedim Biotech GmbH, Germany) with a flow rate of 10 L min^{-1} . The collected samples were wrapped in foil and stored in the freezer (-20 °C) until mass
235 spectrometry analysis. Filter samples were extracted twice with 5 mL of high-purity methanol

(Optima® LC-MS grade, Fisher Scientific) under sonication in ice for 30 min. The extracts were mixed, filtered with a 0.2 μm pore size PTFE syringe filter (Millipore), and concentrated to near dryness under a gentle stream of high-purity nitrogen. The concentrated samples were reconstituted with ultrapure water (Milli-Q water, 18.2 M Ω) and methanol (Optima® LC-MS grade, Fisher Scientific) with a volume ratio of 50:50. Control mass spectrometry measurements of solvent and extracts from blank PTFE filters were performed to remove the interferences of solvent and handling protocols. The chemical compositions of aerosols were characterized using an ultra-high-performance liquid chromatography (UPLC, Ultimate 3000, Thermo scientific, USA) coupled to a Q-Exactive Focus Hybrid Quadrupole-Orbitrap mass spectrometry (MS, Thermo Scientific, USA) with electrospray ionization (ESI). The ESI source was operated in both positive (+) and negative (-) ionization mode. Product molecules could be detected as $[\text{M} + \text{H}]^+$ in the positive ion mode while products could be ionized via deprotonation and were detected as $[\text{M} - \text{H}]^-$ in the negative ion mode. The following parameters were set for the optimal operation of LC/ESI-MS: spray voltage (+), 3.5 kV; spray voltage (-), -3.0 kV; S-lens RF level (+), 50 V; S-lens RF level (-), 50 V; capillary temperature, 320 °C; sheath gas (nitrogen) pressure, 2.76×10^5 Pa; auxiliary gas (nitrogen) flow, 3.33 L min⁻¹. MS spectra were recorded in the range of m/z 50 to 750 in full MS scan with a mass resolving power of 70000 (FWHM at m/z 200). The full MS scan was followed by data-dependent MS/MS (dd-MS²) scans using stepped collision energies of 20, 40, and 60 eV via high-energy collisional dissociation. The resolution was 17500 and an isolation width of 2 m/z units was applied for the dd-MS² scan. The other parameters for MS² experiments were as follow: AGC target, 2×10^5 ; maximum IT, 50 ms; loop count, 3; minimum AGC target, 1×10^5 ; apex trigger, 2–6 s; dynamic exclusion, 6 s. The MS instrument was calibrated every five days with standard calibration solutions provided by the manufacturer. The separation of analytes was carried out on an Atlantis T3 C18 column (100 Å, 3 mm particle size, 2.1 mm \times 150 mm, Waters, USA) at 35 °C. The mobile phases consisted of (A) 0.1% formic acid (Optima® LC-MS grade, Fisher Scientific) in ultra-pure water (Milli-Q water, 18.2 M Ω) and (B) 0.1% formic acid in methanol (Optima® LC-MS grade, Fisher Scientific). The injected volume of samples was 2 μL in this study. Samplers were eluted using a 60-min gradient elution program with a flow rate of 200 $\mu\text{L min}^{-1}$: initially set to 3% B over the first 3 min, the concentration of eluent B was increased linearly to 50% in 22 min, from 50% to 90% from 25 min to 43 min, then it was decreased from 90% to 3% from 43 to 48 min, and finally kept at 3% for 12 min. The chemical formulas of observed ions were proposed based on reaction pathways, chemical consideration, and measured m/z value with a mass tolerance of ± 5 ppm. All data were recorded and processed using Xcalibur V4.2.47 software package.

2.3 Wall losses of vapors and particles

The SOA yield, usually used to quantify the propensity of a parent hydrocarbon to form SOA, could be determined as the ratio of the generated particle mass to the amount of consumed parent hydrocarbon. The particle and vapor wall depositions in chambers can lead to the underestimation

of the SOA yield. In order to determine the particles wall loss rates, we carried out independent wall loss experiments using ammonium sulfate particles. An aqueous solution of ammonium sulfate was fed to a constant output atomizer (Model 3706, TSI, USA) to produce droplets, which passed simultaneously through a silica gel diffusion dryer to introduce dry particles into the chamber. The size distributions of ammonium sulfate particles were measured by SMPS for 480 min. Almost identical humidity ($(25 \pm 1) \%$) condition was achieved among each experiment. The wall losses of particles are size-dependent and, thus, we used a size-dependent particle wall-loss correction approach, which is described in detail in the Supplement. The size-dependent loss rate (k) of ammonium sulfate particles could be expressed as $k = 5.5 \times 10^{-6} \times d_p^{1.05} + 0.18 \times d_p^{-1.19}$ and was applied to correct the aerosol particle concentrations. The wall loss rates of NO, NO₂, SO₂, and TMB were determined to be 2.0×10^{-6} , 3.9×10^{-6} , 4.0×10^{-7} , and $2.3 \times 10^{-6} \text{ s}^{-1}$, respectively, indicating that the wall losses of these species were negligible over the course of the experiment. However, gas-phase species that could deposit to the chamber walls include not just the parent hydrocarbon, in this case TMB, but also the oxidation products, which in general are not all totally monitored and characterized. It is difficult to correct directly and accurately for the impact of vapor wall losses on the SOA yield. Therefore, the SOA yield in this work is only the lower limit. Here, the underestimation of SOA yields due to vapor wall losses was determined by the method in the study of Zhang et al. (2014). In brief, the effect of vapor wall losses on SOA yield significantly arose from the competition between vapors condensation onto aerosol particles versus vapor depositions to chamber walls. The extent to which vapor wall depositions influence the SOA yield could be estimated by the ratio of the average timescale of gas-particle partitioning during the photooxidation experiments to the timescale of vapor wall deposition. The evaluated results suggested that the SOA yield could be underestimated by a factor of 1.8 to 8.4 without accounting for vapor losses.

3 Results and discussion

3.1 Effects of SO₂

3.1.1 Particle formation and growth in SO₂-added photooxidation

To evaluate the impacts of SO₂ on aerosol formation and growth from TMB photooxidation, a series of experiments were conducted with various initial SO₂ levels under both low- and high-NO_x conditions. Evolutions of the number distributions of secondary aerosols with particle size within 4.5–162.5 nm are provided in Fig. 1. There was no new secondary aerosol formation in the beginning of photooxidation. After a period of time, particles were burst produced and the number concentration of particle increased rapidly. At the same time, the particles continuously grew via condensation and coagulation mechanisms, consistent with a previous study (Jorga et al., 2020). After 300 min UV irradiation without SO₂ introduction, the total maximum number concentration of aerosol particles was only $2.7 \times 10^4 \text{ cm}^{-3}$ and $2.9 \times 10^4 \text{ cm}^{-3}$ under low-NO_x (Exp. 1) and high-

NO_x (Exp. 5) experiments, respectively. Interestingly, the particle maximum number concentration considerably increased with increasing SO₂ levels, regardless of low- or high-NO_x conditions (Table 1). As shown in Fig. 1, although the unimodal particle size distribution in the presence of SO₂ was similar to that in its absence, particles with mobility diameter ranging from 10 to 80 nm, especially, dominated particle number concentrations with SO₂ addition. The time series of total ultrafine particles (diameter < 100 nm) number concentration are shown in Fig. S2, where it is seen that SO₂ considerably enhanced ultrafine particle formation. Ultrafine particles are more harmful to human than larger particles because they can more easily penetrate deep into the lungs and blood circulation (Terzano et al., 2010). Our results indicate that SO₂ concentration is a key parameter for ultrafine particle formation. It has been suggested that reducing the number concentration of ultrafine particles can decrease mortality, highlighting again the need to continue to implement strict SO₂ emission standards (Fuzzi et al., 2015).

320

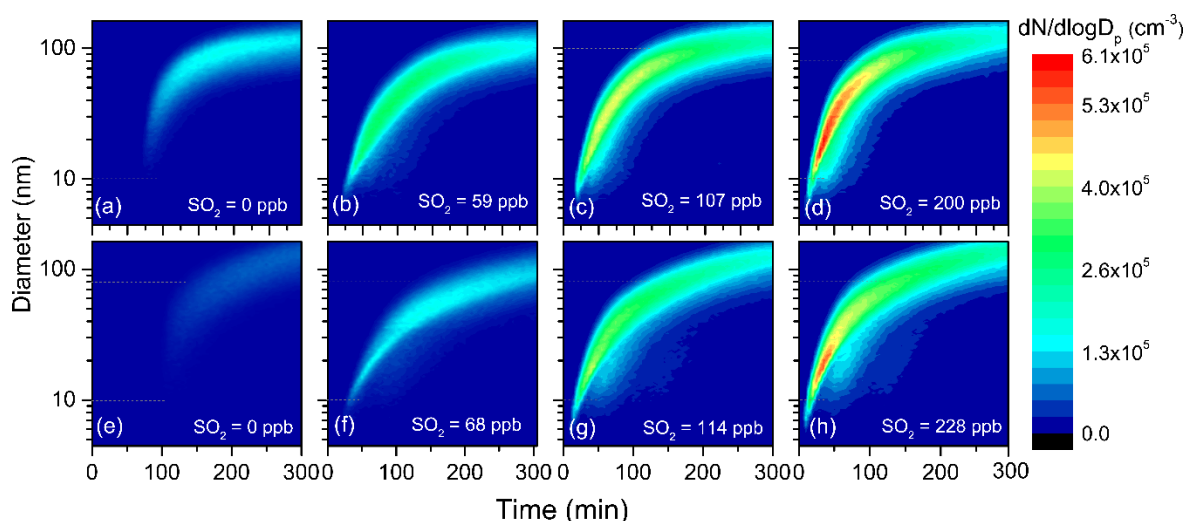


Figure 1. Evolutions of the number distributions of aerosol particles generated from TMB photooxidation in low-NO_x (Panels a–d) and high-NO_x (Panels e–h) experiments.

325 To fully give account for effects of changes in SO₂ emissions on aerosol formation, the key particle phase parameters (i.e., nucleation time, initial growth rate, and particle mean diameter) as a function of SO₂ levels are further compared in Fig. 2. In the present study, the SMPS instrument can measure particle larger than 4.5 nm and, therefore, the nucleation time here is defined as the time required for new secondary aerosols to grow to 4.5 nm after the lights have been turned on (Wyche et al., 2009). The particle size rapidly increased within 30 min after nucleation, and gradually reached a stable level within 300 min photooxidation (Fig. 1). Consequently, the initial growth rate (GR_{initial}), calculated based on the method of Kulmala et al. (2012), is defined as the particle growth rate within 30 min after nucleation (Li et al., 2018). The mean diameter reported in this work represents the particle mean diameter measured at 300 min in each experiment. From Fig. 2, a significant negative correlation was found between nucleation time and initial SO₂ level. Furthermore, when similar

330

335

amounts of SO₂ were introduced to the reaction mixture, the gap between the nucleation time of low-NO_x and high-NO_x would be reduced, which is in agreement with a previous study (Zhao et al., 2018). Under SO₂-free condition, new secondary aerosol could be generated by homogeneous nucleation involving key intermediate products of TMB oxidation. The delay time for particle formation largely corresponds to the time required for intermediate products to build to sufficient concentrations in such a way that their saturation vapor pressure relative to the particle phase is exceeded. New secondary aerosol consists of later stage oxidation products, which might be also responsible for the delayed occurrence. It was demonstrated that higher OH concentration in the chamber could result in faster particle formation (Sarrafzadeh et al., 2016). However, the average OH concentration in SO₂-free experiments is comparable with that in SO₂-added experiments (Table 1). There has been a gradual fall in the mixing ratio of SO₂ (Fig. S3) that could be oxidized to sulfuric acid (H₂SO₄) during TMB photooxidation. **The formed H₂SO₄ could induce nucleation and increase the nucleation rate (Zhao et al., 2018; Blair et al., 2017), and these processes are responsible for the short nucleation time observed in the TMB/NO_x/SO₂ regime (Wyche et al., 2009).** The mean diameter of secondary aerosol decreased by 4–10 nm when 60–70 ppb of SO₂ was included in the matrix (Fig. 2). In contrast, at high-SO₂ levels ([SO₂]₀ > 100 ppb), increase in the initial SO₂ concentration led to an increase in particle mean diameter, regardless of low- or high-NO_x. The initial growth rate also showed a similar dependence on the SO₂ level as presented in Fig. 2. **The nonlinear response of the particle mean diameter to SO₂ initial level is similar to the findings of Julin et al. (2018), who found the response of particle size distribution to NH₃ emissions to be also nonlinear. Aerosol particles can grow in different ways such as gas-particle partitioning of semi-volatility organic compounds (SVOCs). Since the evaporation of SVOCs is important after partitioning to the particle phase, the rate at which SVOCs participate in the particle growth is lower than their condensation rate. However, recent advances give an insight that the particle-phase chemistry such as heterogeneous reactions of SVOCs are substantially pronounced for the particle growth (Shiraiwa et al., 2013; Paasonen et al., 2018; Apsokardu and Johnston, 2018). Organosulfates can be produced by particle-phase reactions involving interactions between organics and inorganics. In this work, organosulfates were only detected in SO₂-involved photooxidation, indicating that additional particle-phase reactions can occur under SO₂-involved conditions.** Increasing the initial SO₂ level could induce the formation of more sulfate (Fig. S4) and the enhancement in the particle acidity during photooxidation (Liu et al., 2016; Kroll et al., 2006). The elevated particle acidity can promote more SVOCs to transform into low-volatile products such as organosulfates in the particle phase, thereby promoting the particle growth (Lin et al., 2014; Lal et al., 2012). Then, additional SVOCs could be further transferred from the gas phase to the particle phase to increase the particle size. However, the particle mean diameter in low-SO₂ ([SO₂]₀ < 100 ppb) experiments is smaller than that in SO₂-free experiments. Our result is in line with the study of Wyche et al. (2009), who attributed this phenomenon to the larger number of particles produced under SO₂-involved condition. The presence of 59 ppb SO₂ caused the maximum number

concentration of particles to increase by $8.5 \times 10^4 \text{ cm}^{-3}$ under low- NO_x condition. When the SO_2 level increased from 0 to 68 ppb in high- NO_x experiments, the corresponding particle number concentration increased from 2.9×10^4 to $9.3 \times 10^4 \text{ cm}^{-3}$. Therefore, the amounts of products that condensed onto each aerosol particles significantly decreased in low- SO_2 experiments, which could result in the decrease in particle diameter (Liu et al., 2015a). The promoting effect of particle-phase chemistry on the particle size growth may not offset the inhibiting effect of the emergence of large number of particles on the particle size growth, thereby leading to the low particle diameter in low- SO_2 experiments.

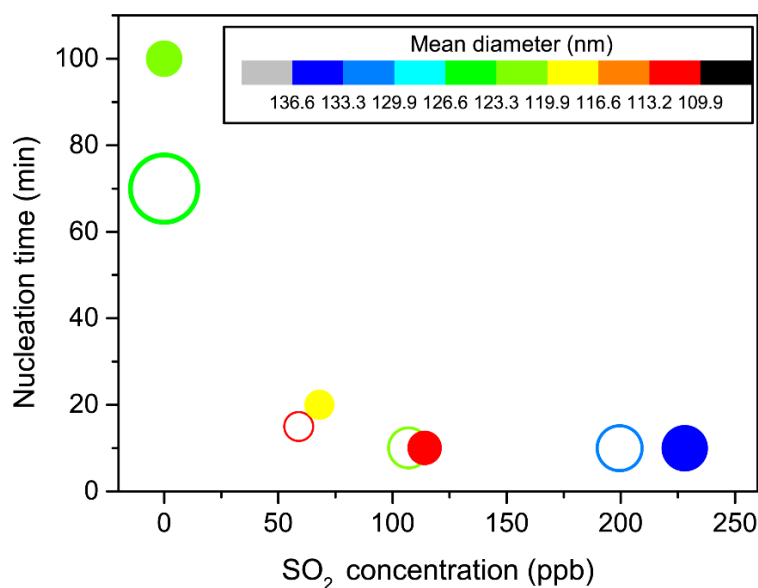


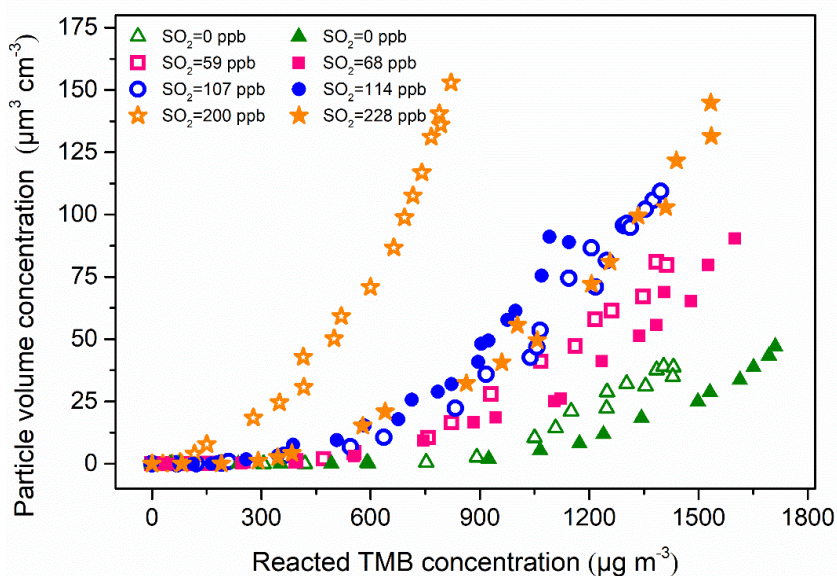
Figure 2. Particle nucleation time as a function of initial SO_2 concentration under low- NO_x (open circles) and high- NO_x (solid circles) conditions (Exps. 1–8). The symbol color indicates the particle mean diameter and symbol size represents the particle initial growth rate. Values of the particle parameters are listed in Table S1.

3.1.2 SOA yield in SO_2 -added photooxidation

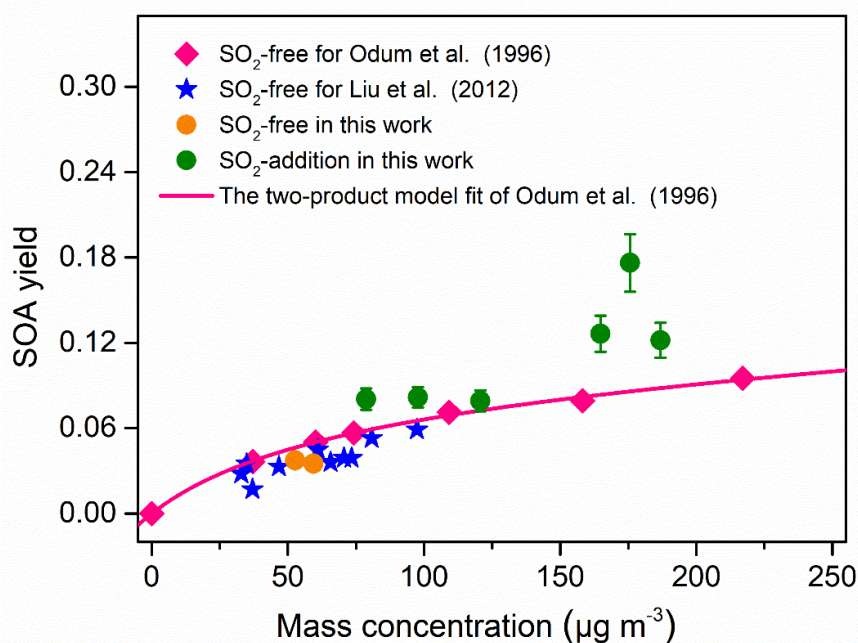
The particle volume concentration as a function of TMB consumption is presented in Fig. 3, where it can be observed that the particle formation increased with increasing initial SO_2 levels regardless of low- or high- NO_x conditions. The present result is consistent with a previous research, which found that limonene SOA formation is significantly promoted with SO_2 addition (Ye et al., 2018). SO_2 was found to perturb particle formation by inducing chemical reactions in the gas- and particle-phase (Wang et al., 2019a; Friedman et al., 2016). We are unable to fully rule out the SO_2 impacts on gas-phase chemistry. However, the decay of TMB was essentially unchanged when SO_2 was introduced into the chamber (Fig. S5), which suggests the unlikeliness of SO_2 addition to affect the gas-phase chemistry of TMB photooxidation (Kleindienst et al., 2006). Instead, it is more likely

attributed to the formation and condensation of H₂SO₄ and/or the enhancement of organic aerosols formation. We assumed full conversion of the consumed SO₂ into H₂SO₄ aerosol particles and found that the contribution of the formed H₂SO₄ to the increase in particle volume concentration was less than 100% (See Sect. S2). In addition, pure SO₂ oxidation experiments without TMB addition also indicated that the enhancement in aerosol particles by SO₂ introduction cannot be solely attributed to inorganic aerosol formation (See Sect. S2). To calculate the net SOA yield, the inorganic mass concentration was subtracted from the particle mass concentration based on IC measurements of generated particles. The influence of SO₂ initial level on SOA yield can be seen in Table 1 as high SO₂ levels contribute to produce somewhat high SOA yields. Figure 4 compares the SOA yields obtained from the present work with those found in previous studies with similar experimental conditions. The SOA yields from the two SO₂-free experiments are comparable to that reported from the study of Liu et al. (2012) and fit quite well with the yield curve of Odum et al. (1996). The SOA yields in our TMB/NO_x photooxidation experiments were 3.8% and 3.5%, which were closed to 3.9% and 4.2% derived from yield curve of Odum et al. (1996) under same mass concentration. In contrast, with similar mass concentration, the SOA yields in SO₂-added regimes were higher than those in previous studies (Odum et al., 1996; Liu et al., 2012). Here the neutralization degree of particle, which was calculated as the molar ratio of NH₄⁺ to the sum of SO₄²⁻ and NO₃⁻ (Lin et al., 2013), was used as a tool to roughly estimate the aerosol acidity of collected particle samples. The value of neutralization degree were lower than 1 in this work, indicating acidic aerosols (Lin et al., 2013). The increase in aerosol acidity could be largely responsible for the observed enhancements in SOA formation in SO₂-involved experiments. The OH oxidation of TMB can result in the formation of multifunctional carbonyl compounds (Liu et al., 2012; Zaytsev et al., 2019), which could promote SOA formation via acid-catalyzed heterogeneous reactions. In addition, the particle surface area concentrations significantly increased with increasing SO₂ initial concentrations in both low-NO_x and high-NO_x conditions (Table 1), which might also result in the enhancement in the SOA yield. Besides gas-particle partitioning of SVOCs, the fates of SVOCs in the chamber also include chemical reactions and chamber wall losses. Therefore, in the batch-mode chamber experiments, the gas-particle partitioning of SVOCs have a great sensitivity to particle surface areas (Zhang et al., 2015; Han et al., 2019). Recently, Zhao et al. (2018) examined the SO₂ effects on the SOA formation and suggested that providing additional particle surfaces by SO₂-induced new particle formation leads to the increase in SOA yield. The effects of the particle surface area concentration on organic aerosol formation were explored by Han et al. (2019), who also found that increasing the particle surface area concentrations can significantly increase the organic aerosol mass yield due to greater partitioning of semi-volatility organic products to the particle-phase. Increasing the particle surface area can limit the gas-wall interactions of organic vapors and is favorable for the movement of more SVOCs from the gas phase to the particle side (Han et al., 2019). These additional SVOCs can also undergo further particle chemistry such as acid-catalyzed heterogenous reactions to strongly enhance aerosol particle formation in TMB/NO_x/SO₂ photooxidation (Apsokardu and

Johnston, 2018).



440 **Figure 3.** Growth of particle volume concentrations from TMB photooxidation as a function of TMB consumption for eight experiments with different initial SO₂ concentrations (Exps. 1–8). The open symbols and solid symbols represent low- and high-NO_x experiments, respectively.



445 **Figure 4.** Comparison of SOA yields from TMB photooxidation as a function of SOA mass concentration with data reported from literature. The SOA density in the whole study was assumed to be 1.4 g cm⁻³. The error bars represent errors in the SOA yield results and the errors were calculated from error propagation using the sum of the uncertainties in TMB data and the systematic error of SMPS. The SOA yields for Liu et al. (2012) were extracted from Table 1 in the study. The pink line is the best fit two-product model for the SOA yields and was extracted from Figure 2 in the work of Odum et al. (1996).

450 3.1.3 Particle chemical composition in SO₂-added photooxidation

In order to investigate the effects of SO₂ on the chemical composition of aerosol particles, the particles were first characterized by ATR-FTIR. Figure 5 compares the characteristic ATR-FTIR spectra of particles formed from the photooxidation of TMB under different conditions and the detailed information on the assignment of absorption peaks are given in Table S2. For the samples collected from TMB/NO_x photooxidation, the particles exhibited an O-H stretch at 3600–3000 cm⁻¹ as shown in Fig. 5(a) and (b). The C=O stretch of carbonyl at 1720 cm⁻¹ suggests that aldehydes, ketones, and carboxylic acids are significant particle components, while the absorptions at 844 cm⁻¹ (NO symmetric stretch), 1284 cm⁻¹ (NO₂ symmetric stretch), and 1647 cm⁻¹ (NO₂ asymmetric stretch) are the characteristic peaks of organic nitrates. The slight absorbance at 941 cm⁻¹ indicates the presence of peroxides containing O-O groups. Interestingly, compared with the particles from TMB/NO_x experiments, there was a new peak at 615 cm⁻¹ for the particles generated from TMB/NO_x/SO₂ experiments, regardless of low- or high-NO_x conditions. The 615 cm⁻¹ peak is characteristic of inorganic sulfates, and further highlights that the presence of SO₂ promotes the formation of inorganic sulfates as pointed out in previous studies (Chen et al., 2019; Liu et al., 2016). The strong absorption at 1081 cm⁻¹ arises from the S=O bands in the particle components. Field and laboratory studies have reported that inorganic sulfate could convert into organosulfur compounds in the atmosphere (Riva et al., 2019; Nestorowicz et al., 2018). Therefore, the peak at 1081 cm⁻¹ may be mainly from the absorption of both inorganic sulfates and organosulfur compounds.

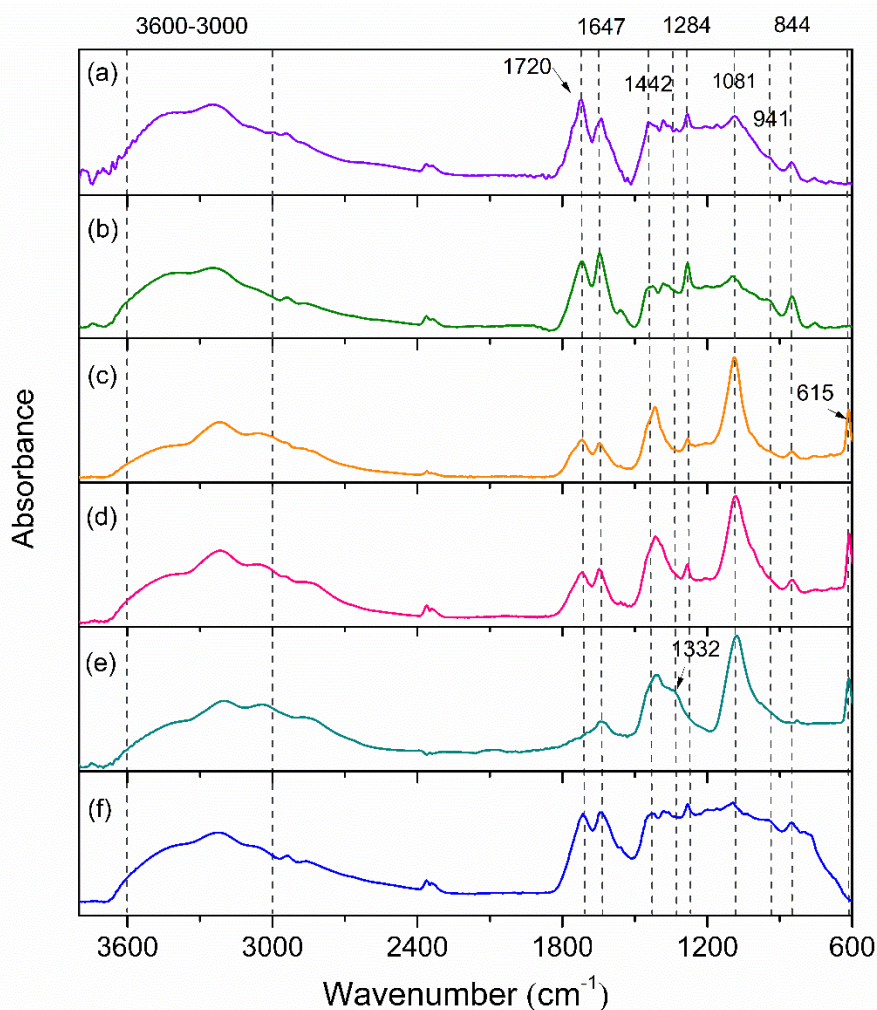


Figure 5. ATR-FTIR spectra of aerosol particles generated from TMB/NO_x (a, Exp. 1; b, Exp. 5), TMB/NO_x/SO₂ (c, Exp. 4; d, Exp. 8), TMB/NO_x/NH₃/SO₂ (e, Exp. 12), and TMB/NO_x/NH₃ (f, Exp. 10) photooxidation.

470

475 The chemical compositions of particles generated in TMB/NO_x and TMB/NO_x/SO₂ photooxidations were further measured with high-resolution mass spectrometry (HRMS), to determine whether organosulfur compounds were formed in SO₂-added experiments. The formation of organosulfur compounds was recognized by the oxidation mechanism and the loss of characteristic fragment ions at *m/z* 79.95 (SO₃⁻), 80.96 (HSO₃⁻), and 96.96 (HSO₄⁻) in MS/MS spectra (Figs. S7-S8). The list of compounds observed in this work along with molecular weights (MW), measured masses and proposed structures are presented in Table S3. In SO₂-free experiments, the major aerosol components were multifunctional alcohols, peroxides, organic nitrates, ketoaldehydes, and ketocarboxylic acids. With the same analytical methods, the same products were also observed in SO₂-added photooxidation. The most striking result to emerge from Table S3 is that ten organosulfates (OS-214, OS-226, OS-228, OS-240, OS-242, OS-244, OS-268, OS-300, OS-316, and OS-345) and two organic sulfonates were only detected in filter samples collected from the

480

485

TMB/NO_x/SO₂ photooxidation experiment, indicating that SO₂ emissions in the atmosphere can alter the aerosol formation chemistry and thus influence the aerosol chemical composition. To the best of our knowledge, this is the first time the ten organosulfates are identified in TMB/NO_x/SO₂ photooxidation experiments. Recently, some sulfur-containing compounds from field measurements were designated as compounds of unknown origin. For example, the MW 214 organosulfate has been detected in PM_{2.5} collected from the highly polluted megacity Shanghai (Cai et al., 2020). However, the VOC precursor for this organosulfate formation was not reported. The MW 242 organosulfate found in Baengnyeong Island was also classified as organosulfur of unknown origin (Boris et al., 2016). O'Brien et al. (2014) found the formation of MW 228 organosulfate in ambient aerosol particles but its specific source was not pointed out. Evidence from this study suggests that TMB photooxidation in the presence of SO₂ might contribute to the formation of these organosulfates (MW = 214, 228, and 242) in the ambient air. Importantly, an organosulfur compound with a formula of C₇H₁₂O₇S (MW = 240) was observed in ambient fine aerosols and was tentatively assigned to an oxidation product of anthropogenic 1,3,5-trimethylbenzene (Boris et al., 2016). The finding of the current study suggests that the organosulfur compound (MW = 240) may also be produced from the photooxidation of 1,2,4-trimethylbenzene in the presence of SO₂. In addition, the MW 226, 240, and 268 organosulfur compounds were designated as biogenic-derived organosulfates in previous field studies (Cai et al., 2020; Boris et al., 2016). **More recently, Chen et al. (2020b) suggested that heterogeneous OH oxidation of isoprene-derived SOA can contribute to the formation of an organosulfate with molecular weight at 228.** Our results show the detection of OS-226, OS-228, OS-240, and OS-268 organosulfates, which are isomers of organosulfates derived from isoprene (Cai et al., 2020), **isoprene (Chen et al., 2020b)**, limonene (Cai et al., 2020), and limonene (Boris et al., 2016), respectively. More studies need to be undertaken to differentiate various sources of organosulfates in the ambient aerosols through chemical synthesis of authentic organosulfates standards.

The mechanisms describing the formation of OS-226, OS-228, OS-240, OS-242, OS-244, OS-300, OS-316, and OS-345 are proposed in Fig. 6. Following analogous mechanisms for toluene photooxidation, the oxidation of TMB is dominantly initiated by OH addition to the benzene ring to form TMB-OH adduct, which can react with O₂ through recombination to produce bicyclic peroxy radical. It has been established that a series of ring-retaining (product A in Fig. 6) and ring-opening products (products B, C, and D in Fig. 6) can be generated by the further reaction of bicyclic peroxy radical in the presence of NO (Zaytsev et al., 2019; Li and Wang, 2014). Both ring-opening and ring-retaining compounds are expected to contribute significantly to organosulfate production. Here, we take unsaturated ketoaldehyde (product C in Fig. 6) as an example to describe the possible formation mechanism of organosulfate observed in the present study. The reaction of OH with compound C involves OH addition to unsaturated C=C bonds to form an alkyl radical, which can react subsequently with O₂ to yield organic peroxy radical. Further reactions of organic peroxy

525 radical can follow two different pathways. One pathway is that the organic peroxy radical undergoes
 a 1,5-H-shift isomerization to form a new acyl radical. Insight from a previous review suggested
 that acyl radical react with O₂ to yield acylperoxy radical, which could further react with HO₂ to
 form multifunctional hydroperoxide (Ziemann and Atkinson, 2012). The second channel is the
 530 reaction of organic peroxy radical with HO₂ to produce hydroperoxide, terminating directly the
 radical chain. Acid-driven heterogeneous chemistry of hydroperoxide has been previously adopted
 to explain the generation of certain OSs (Riva et al., 2016a; Riva et al., 2016b). With the presence
 of sulfuric acid formed by the oxidation of SO₂ by OH, TMB-derived hydroperoxides can be
 hydrolyzed by H⁺ and then react with inorganic SO₄²⁻ to form organosulfates. The conversion of
 inorganic sulfates to organosulfates could cause changes in aerosol growth, multiphase chemistry,
 535 and acidity (Zhang et al., 2019; Riva et al., 2019).

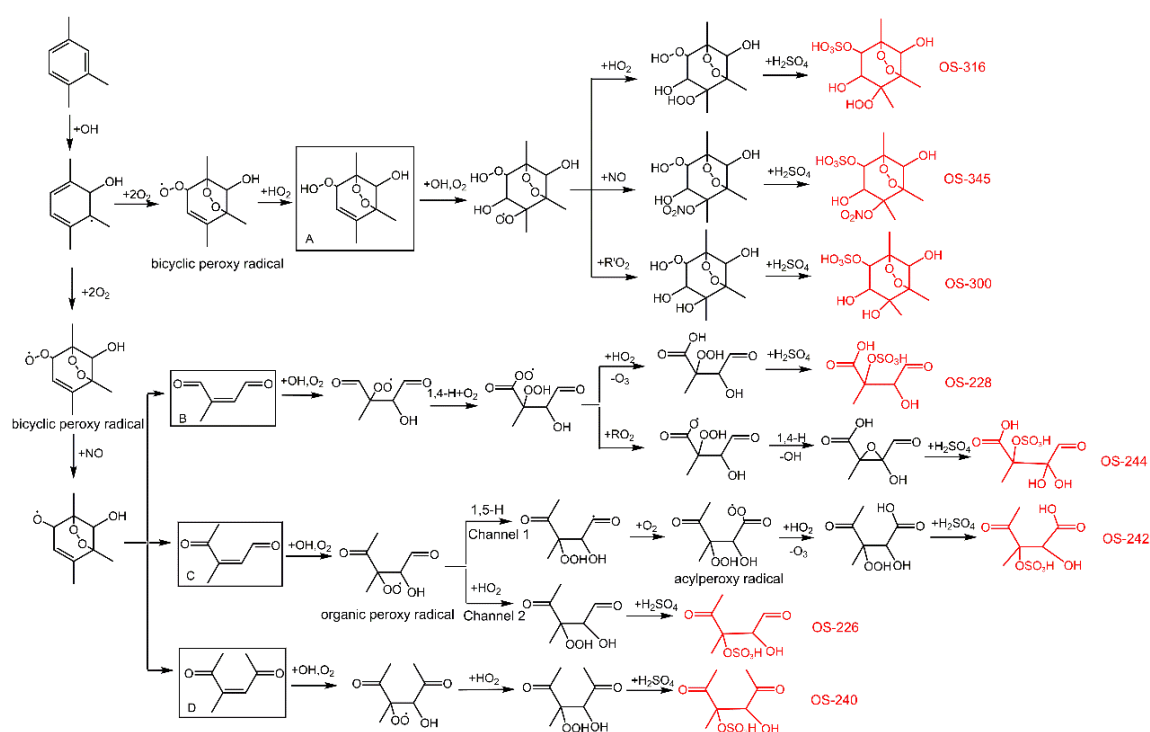


Figure 6. Proposed mechanisms for organosulfate formation from the photooxidation of TMB in the presence of SO₂. The black boxes mark the ring-opening and ring-retaining products suggested in previous studies (Li and Wang, 2014; Zaytsev et al., 2019). The compounds in red are organosulfates detected by UPLC-HRMS in this work.

The MW 228 and 230 organic sulfonates were assigned as sulfonates containing an aromatic ring based on accurate mass measurements and comparison of mass fragmentation patterns with other aromatic sulfonates (Riva et al., 2015a). MS/MS spectra and the proposed fragmentation schemes of sulfonates are reported in Fig. S8. For MW 228 sulfonate, the MS/MS spectra showed the fragment ions at *m/z* 79.95721 (SO₃⁻), 118.96625 (C₈H₇O⁺, M - SO₃⁻ - CO), and 163.04025 (C₉H₇O₃⁻, M - SO₂) as presented in Fig. S8. For the MW 230 sulfonate, the fragment of parent ion

at m/z 229.01706 could occur by the loss of 44 mass units to give the product ion at m/z 185.02777 (Fig. S8). The loss of 79.95747 mass units as sulfite radical is in accord with the MS/MS spectra of aromatic sulfonates generated from the photooxidation of polycyclic aromatic hydrocarbons (Riva et al., 2015b). A recent field measurement demonstrated that aromatic organosulfur compounds account for a substantial fraction of total organosulfur compounds in Shanghai, China, highlighting the importance of aromatic organosulfur compounds (Ma et al., 2014). Aromatic sulfonates formation from the photooxidation of TMB in the presence of SO₂ was unexpected and the exact formation pathway of the aromatic sulfonates warrants further investigation.

3.2 Effects of NH₃

3.2.1 Particle formation and growth in NH₃-involved photooxidation

High-NO_x photooxidation experiments were carried out in the presence/absence of NH₃. The average OH concentrations were similar for each experiment within 300 min of irradiation (Table 1). Figure 7 displays the volume and number concentrations of aerosols as a function of time in different photooxidations (Exps. 5, 8–12). TMB was oxidized to produce many secondary aerosols under continuous UV irradiation. The volume concentrations of aerosol particles have a clear positive correlation with NH₃ initial level for all conditions. However, the effect of NH₃ on particle formation was not as pronounced as that of SO₂ with similar concentration (Fig. 7). In TMB/NO_x/NH₃ photooxidation, the net SOA yield increased slightly from 3.5% to 5.1% as NH₃ initial level increased from 0 to 200 ppb (Table 1). Our result is consistent with the finding of Chen et al. (2020a), who showed that NH₃ did not significantly affect SOA formation from toluene/NO_x photooxidation under dry condition. Interestingly, SMPS measurements demonstrated that the coexistence of SO₂ and NH₃ can considerably promote secondary aerosol formation (Fig. 7). After subtracting the inorganic components, it was seen that the net SOA yield could increase to 13.7% with the introduction of 200 ppb NH₃ and 234 ppb SO₂, indicating the synergetic effects of NH₃ and SO₂ (Chu et al., 2016). The flux of the gas-phase products diffusing to a particle partly depends on the surface area of the particle. The coexistence of SO₂ and NH₃ promoted the increase in particle surface area concentrations (Table 1). The ability of particle formation originating from gas-to-particle conversion may be significantly stronger with SO₂ and NH₃ introduction, leading to the enhancement in particle formation. The total number concentrations of aerosol particles increased rapidly in all experiments after nucleation was initiated as shown in Fig. 7 (b). After reaching the maximum concentration, the number density of particles declined gradually because of particles coagulation and deposition to the chamber walls. Increasing the NH₃ level to 200 ppb enhanced the particle maximum number concentration by factors of 2.0 and 1.7 under SO₂-free and SO₂-involved conditions, respectively. Our results are valuable in terms of the potential of NH₃ emission reductions to improve air quality by decreasing total particle number concentrations.

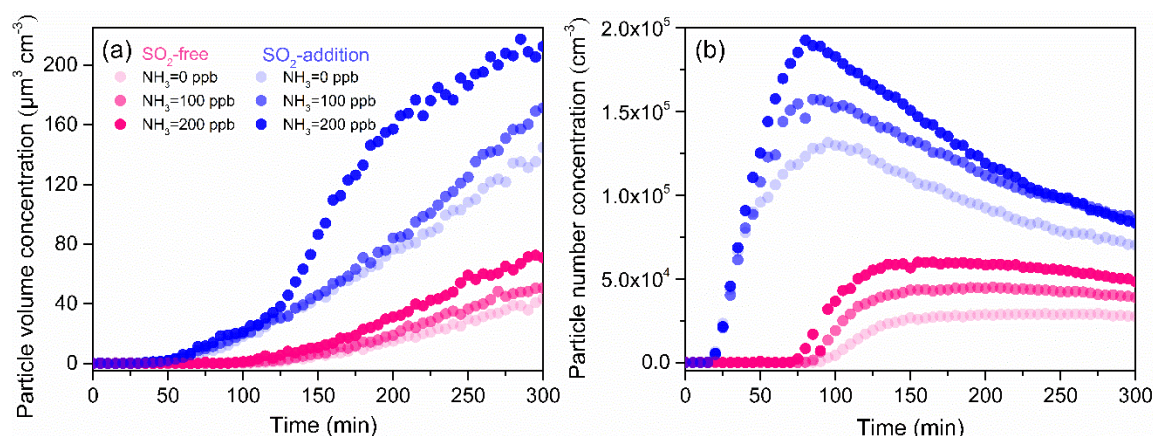


Figure 7. Time evolutions of the volume (a) and number (b) concentrations of aerosol particles from TMB photooxidation with different initial NH_3 levels under SO_2 -free and SO_2 -addition (~ 230 ppb) conditions.

590

Once generated, aerosol particles need to grow to a larger size ($> 50\text{--}100$ nm) before they exert significant impact on global climate and public health. To explore the effects of NH_3 on particle growth, the initial growth rate of aerosol particles from different experiments are also compared in Fig. S9. In SO_2 -free experiments, the increase in NH_3 initial concentrations led to remarkable increase of the initial growth rate of aerosol particles. High initial growth rates were also found in the photooxidation of other aromatics such as toluene and o/m/p-xylene with NH_3 addition (Li et al., 2018). This result may be explained by the fact that under SO_2 -free condition, NH_3 mainly reacts with acids to produce ammonium salts. Previous studies have reported that ammonium salts could partition into the initial growth process of new secondary aerosol particles and thus increase the particle initial growth rate (Li et al., 2018; Zhu et al., 2014). More interestingly, NH_3 level did not substantially affect the initial growth rate of particles in the presence of SO_2 (Fig. S9). The results in Fig. 7 have demonstrated that the synergetic effects of NH_3 and SO_2 can promote new particle formation (Lehtipalo et al., 2018). In SO_2 -involved experiments, NH_3 molecules tend to promote new particles formation rather than particles growth. Note that these effects of NH_3 on particle initial growth might be more complex in the ambient air with high levels of SO_2 , NH_3 , NO_x , VOCs than current smog chamber experiments.

595

600

605

3.2.2 Particle chemical composition in NH_3 -involved photooxidation

The ATR-FTIR spectra of aerosol particles from NH_3 -added experiment are also given in Fig. 5. A previous study suggested that the absorbances at $3310\text{--}3360$ cm^{-1} and $1550\text{--}1650$ cm^{-1} can be assigned to N-H stretch and C-N-H bend in secondary amine molecules, respectively (Babar et al., 2017). However, no evidence of secondary amine formation was detected and no clear FTIR spectra

610

differences between aerosols from TMB/NO_x experiment and aerosols from TMB/NO_x/NH₃ photooxidation were found in this work (Fig. 5). It has been recently discovered that the conversion of oxidized organics to nitrogen-containing compounds in the presence of NH₃ is more likely to occur in high RH condition (Zhang et al., 2020). NH₃ uptake by TMB-derived aerosol particles may be limited to the aerosol surface under low RH condition (RH < 20%) (Bell et al., 2017). The amounts of secondary amine compounds formed from the NH₃ uptake by aerosol may be small, resulting in no characteristic peaks of secondary amine in ATR-FTIR spectra. Surprisingly, the effects of NH₃ on aerosol chemical compositions were increasingly important under SO₂-rich condition. As displayed in Fig. 5(e), the strong C=O band at 1720 cm⁻¹ converted to a shoulder upon NH₃ addition to the TMB/NO_x/SO₂ reaction system. In addition, the C-N stretch at 1332 cm⁻¹ was observed in TMB/NO_x/SO₂/NH₃ photooxidation (Fig. 5). The particle-phase C-N stretch has been also characterized in m-xylene photooxidation experiments with NH₃ addition and was suggested to account for nitrogen-containing compounds (Liu et al., 2015b). A smog chamber study also found that the coexistence of SO₂ and NH₃ substantially enhanced the formation of nitrogen-containing compounds from the photooxidation of toluene (Chu et al., 2016). In the current work, the presence of SO₂ could promote the increase in particle acidity. Elevating particle acidity could facilitate the reaction of NH₃/NH₄⁺ with carbonyl-containing compounds, leading to the formation of nitrogen-containing organic compounds (Liu et al., 2015b).

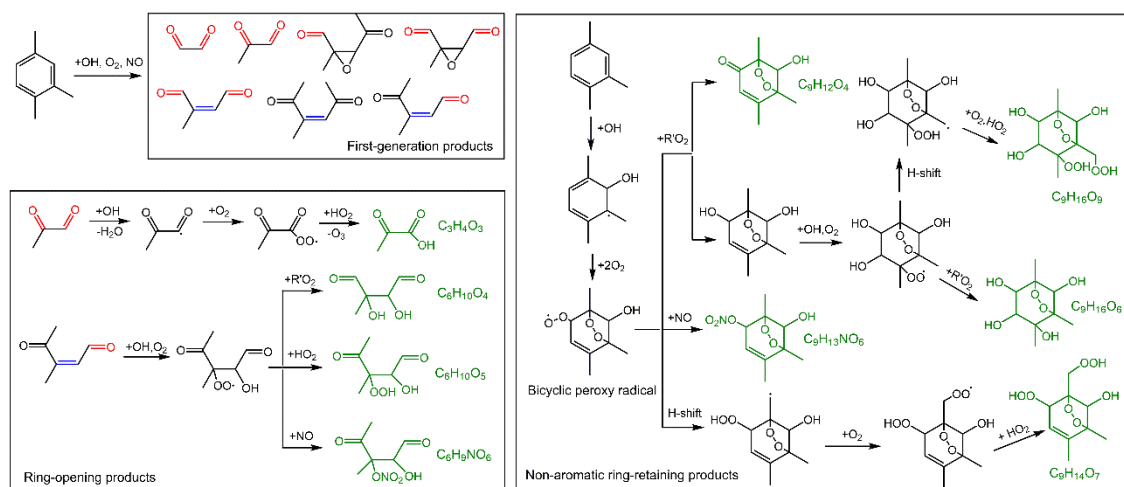


Figure 8. Simplified formation mechanism of the detected products in SOA formed from NH₃-involved photooxidation. Some observed products are produced through same chemical mechanism and for simplicity, only one product is drawn in this figure as an example.

The MS measurement results are consistent with FTIR analysis. As shown in the MS spectra of aerosol samples (Fig. S10), under SO₂-free condition, the presence of NH₃ did not result in considerable changes in peak numbers and abundance for both positive ion mode and negative ion mode. NH₃ could slightly enhance SOA formation in SO₂-free experiment as mentioned in Sect. 3.2.1. Therefore, the NH₃-induced changes in the absolute concentrations of organic components

might be small in SO₂-free experiments, leading to similar mass spectra for Fig. S10(a) and Fig. S10(b). In addition, the major products (Table S4) are likely generated by similar chemical mechanisms (Fig. 8), which are not sensitive to the change in initial NH₃ levels under current experimental conditions. First, the photooxidation of TMB in the presence of NO can result in the formation of bicyclic oxy radicals that could decompose to a series of ring-opening products including biacetyl, epoxy-dicarbonyl, and carbonylic products (Li and Wang, 2014). As depicted in Fig. 8, the first-generation products could be further oxidized by OH. For example, oxidation of methylglyoxal by OH can proceed through abstraction of the aldehydic hydrogen to form the CH₃C(O)C(O)• radical, which may react with O₂ and then with HO₂ to form pyruvic acid. Second, bicyclic peroxy radical (BPR) is a key intermediate for the formation of non-aromatic ring-retaining products. Reactions of BPR with R'O₂ can form either bicyclic carbonyl and bicyclic alcohol, which further undergoes OH oxidation to yield the C₉H₁₆O₆ and C₉H₁₆O₉ compounds. BPR can produce bicyclic organonitrates by reaction with NO, and can also undergo intramolecular H-shift followed by O₂ addition to form a new bicyclic peroxy radical. The new bicyclic peroxy radical reacts with HO₂ to generate highly oxygenated organic molecules, consistent with a recent study (Wang et al., 2020b). To our knowledge, NH₃ does not basically affect the reaction of free radicals in gas-phase during the photooxidation of TMB. Generally, NH₃ levels play a negligible role in the aerosol organic composition in TMB photooxidation without SO₂ addition. In contrast, under SO₂-rich condition, the increase in NH₃ level led to a significant increase in the abundance of organic compounds (especially for compounds with $m/z > 200$) in both positive and negative ion modes (Fig. S11). The introduction of SO₂ and NH₃ lead to the formation of ammonium sulfate (Fig. S12), which is an attractive condensation sink for organic vapors. High particle surface area concentration in TMB/NO_x/SO₂/NH₃ experiments may increase the abundance of organic compounds in the bulk phase. To better explain this effect, the saturation mass concentrations of detected products were predicted based on a previous method (Li et al., 2016) and the calculated results are shown in Fig. 9 and Table S4. During the photooxidation of TMB, the fates of organic compounds are mainly governed by the competition between fragmentation and functionalization. Losing carbon atoms increases product volatility, which could be partly compensated by functionalization. Among the compounds present in aerosol particles formed from NH₃-added systems, fourteen products were C₉ or smaller multifunctional oxidation products. From Fig.9, the range of product saturation mass concentration spanned approximately 8 orders of magnitude, indicating that the measured particle-phase products are considerably different regarding volatility. The products in the particle-phase are classified into three classes in Fig. 9: low-volatility organic compound, intermediate volatility organic compounds, and semi-volatility organic compounds. The measured products might not be responsible for homogenous nucleation but these compounds can gradually condense onto nucleation particles (i.e., ammonium sulfate) to contribute to aerosol formation and growth, which highlights the role of ammonium sulfate in this case.

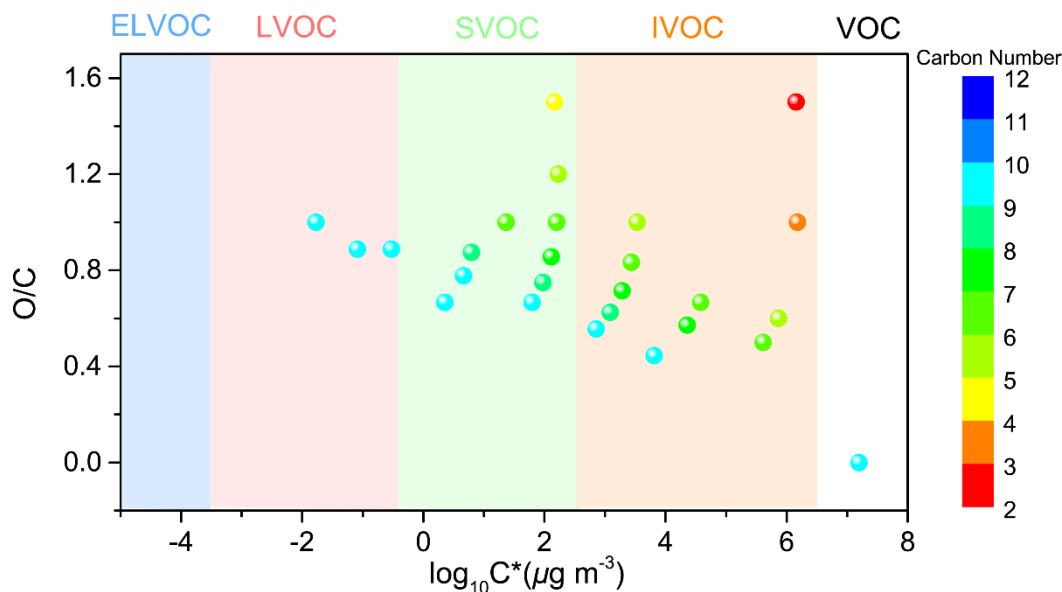


Figure 9. TMB and detected products (Table S4) displayed in the two-dimensional volatility-oxidation space. Based on the method of Li et al. (2016), we grouped the detected compounds in the classes of extremely low-volatility organic compound (ELVOC), low-volatility organic compound (LVOC), semi-volatility organic compound (SVOC), intermediate volatility organic compounds (IVOC), and volatility organic compound (VOC).

4 Conclusions

In summary, we explored the detailed effects of SO₂ and NH₃ on secondary aerosol formation from TMB photooxidation. Our results demonstrate a substantial increase in ultrafine particle (< 100 nm) number concentrations resulting from SO₂ addition. Significant increases in SOA yields were found in TMB/NO_x/SO₂ photooxidation, due to acid-driven heterogeneous reaction. The laboratory characterization of SOA composition confirmed the formation of new organosulfates at MW 214, 226, 228, 240, 242, 244, 268, 300, 316, and 345. The MS data give experimental evidence that the MW 214 and 242 organosulfates could account for organosulfates previously designated as unknown origin in ambient PM_{2.5}, while some of them that were observed in TMB/NO_x/SO₂ photooxidation are isomers of recognized biogenic organosulfates. This indicates that care must be taken in the identification of TMB-derived organosulfates in ambient aerosols. More laboratory and field studies with organosulfate authentic standard should be carried out to determine the accurate yield of the measured organosulfates and the contribution of TMB-derived organosulfate to total atmospheric organosulfate. In addition, the composition of secondary aerosol could determine the physicochemical properties of aerosol particles (e.g. viscosity and phase state). Changes in SO₂ emissions in different regions all over the world have great implications for the physicochemical properties of aromatics-derived SOA and, thus, highly influence the global climate.

705 The presence of NH_3 also increased the number and volume concentration of secondary aerosol particles, especially under SO_2 -rich condition. We characterized a series of multifunctional ring-retaining and ring-opening organic compounds containing one and even more carbonyl and alcohol. The predicted volatility distributions of products suggested that the measured later-generation products progressively condense onto nucleation particles to enhance particle formation in NH_3 -
710 added photooxidation. Current models that are used to assess aerosol-climate interactions should fully take into account the influence of NH_3 on secondary aerosol formation, which is especially significant in regions with strong NH_3 emissions.

715

Data availability. Experimental data are available upon request to the corresponding author.

Supplement. The supplement related to this article is available online at:

720 *Author contribution.* Zhaomin Yang: Conceptualization, Methodology, Investigation, Validation, Visualization, Writing – original draft preparation. Li Xu: Investigation. Narcisse T. Tsona: Visualization, Writing – review & editing. Jianlong Li: Visualization, Writing – review & editing. Xin Luo: Methodology, Resources. Lin Du: Conceptualization, Investigation, Funding acquisition, Project administration, Resources, Supervision, Visualization, Writing – review & editing.

Competing interests. The authors declare that they have no conflict of interest.

725 *Financial support.* This work was supported by National Natural Science Foundation of China (91644214), Youth Innovation Program of Universities in Shandong Province (2019KJD007), and Fundamental Research Fund of Shandong University (2020QNQT012).

References

- Apsokardu, M. J., and Johnston, M. V.: Nanoparticle growth by particle-phase chemistry, *Atmos. Chem. Phys.*, 18, 1895-1907, 10.5194/acp-18-1895-2018, 2018.
- 730 Babar, Z. B., Park, J.-H., and Lim, H.-J.: Influence of NH₃ on secondary organic aerosols from the ozonolysis and photooxidation of α -pinene in a flow reactor, *Atmos. Environ.*, 164, 71-84, 10.1016/j.atmosenv.2017.05.034, 2017.
- Bell, D. M., Imre, D., S, T. M., and Zelenyuk, A.: The properties and behavior of alpha-pinene secondary organic aerosol particles exposed to ammonia under dry conditions, *Phys. Chem. Chem. Phys.*, 19, 6497-735 6507, 10.1039/c6cp08839b, 2017.
- Blair, S. L., MacMillan, A. C., Drozd, G. T., Goldstein, A. H., Chu, R. K., Pasa-Tolic, L., Shaw, J. B., Tolic, N., Lin, P., Laskin, J., Laskin, A., and Nizkorodov, S. A.: Molecular characterization of organosulfur compounds in biodiesel and diesel fuel secondary organic aerosol, *Environ. Sci. Technol.*, 51, 119-127, 10.1021/acs.est.6b03304, 2017.
- 740 Boris, A. J., Lee, T., Park, T., Choi, J., Seo, S. J., and Collett Jr, J. L.: Fog composition at Baengnyeong Island in the eastern Yellow Sea: detecting markers of aqueous atmospheric oxidations, *Atmos. Chem. Phys.*, 16, 437-453, 10.5194/acp-16-437-2016, 2016.
- Cai, D., Wang, X., Chen, J., and Li, X.: Molecular characterization of organosulfates in highly polluted atmosphere using ultra-high-resolution mass spectrometry, *J. Geophys. Res.-Atmos.*, 125, 745 10.1029/2019jd032253, 2020.
- Chen, L., Bao, Z., Wu, X., Li, K., Han, L., Zhao, X., Zhang, X., Wang, Z., Azzi, M., and Cen, K.: The effects of humidity and ammonia on the chemical composition of secondary aerosols from toluene/NO_x photo-oxidation, *Sci. Total Environ.*, 728, 138671, 10.1016/j.scitotenv.2020.138671, 2020a.
- Chen, T., Liu, Y., Ma, Q., Chu, B., Zhang, P., Liu, C., Liu, J., and He, H.: Significant source of secondary aerosol: formation from gasoline evaporative emissions in the presence of SO₂ and NH₃, *Atmos. Chem. Phys.*, 19, 8063-8081, 10.5194/acp-19-8063-2019, 2019.
- 750 Chen, Y., Zhang, Y., Lambe, A. T., Xu, R., Lei, Z., Olson, N. E., Zhang, Z., Szalkowski, T., Cui, T., Vizuete, W., Gold, A., Turpin, B. J., Ault, A. P., Chan, M. N., and Surratt, J. D.: Heterogeneous Hydroxyl Radical Oxidation of Isoprene-Epoxydiol-Derived Methyltetrol Sulfates: Plausible Formation Mechanisms of Previously Unexplained Organosulfates in Ambient Fine Aerosols, *Environ. Sci. Technol. Lett.*, 7, 460-468, 10.1021/acs.estlett.0c00276, 2020b.
- 755 Cheng, Y., Yu, Q.-Q., Liu, J.-M., Zhu, S., Zhang, M., Zhang, H., Zheng, B., and He, K.-B.: Model vs. observation discrepancy in aerosol characteristics during a half-year long campaign in Northeast China: The role of biomass burning, *Environ. Pollut.*, 269, 116167-116167, 10.1016/j.envpol.2020.116167, 760 2021.
- Chu, B., Zhang, X., Liu, Y., He, H., Sun, Y., Jiang, J., Li, J., and Hao, J.: Synergetic formation of secondary inorganic and organic aerosol: effect of SO₂ and NH₃ on particle formation and growth, *Atmos. Chem. Phys.*, 16, 14219-14230, 2016.
- Chu, B., Ma, Q., Liu, J., Ma, J., Zhang, P., Chen, T., Feng, Q., Wang, C., Yang, N., Ma, H., Ma, J., Russell, 765 A. G., and He, H.: Air pollutant correlations in china: Secondary air pollutant responses to NO_x and SO₂

- control, *Environ. Sci. Technol. Lett.*, 7, 695-700, 10.1021/acs.estlett.0c00403, 2020.
- Estillore, A. D., Hettiyadura, A. P. S., Qin, Z., Leckrone, E., Wombacher, B., Humphry, T., Stone, E. A., and Grassian, V. H.: Water Uptake and Hygroscopic Growth of Organosulfate Aerosol, *Environ. Sci. Technol.*, 50, 4259-4268, 10.1021/acs.est.5b05014, 2016.
- 770 Fleming, L. T., Ali, N. N., Blair, S. L., Roveretto, M., George, C., and Nizkorodov, S. A.: Formation of Light-Absorbing Organosulfates during Evaporation of Secondary Organic Material Extracts in the Presence of Sulfuric Acid, *ACS Earth Space Chem.*, 3, 947-957, 10.1021/acsearthspacechem.9b00036, 2019.
- Flores, J. M., Washenfelder, R. A., Adler, G., Lee, H. J., Segev, L., Laskin, J., Laskin, A., Nizkorodov, S. A., Brown, S. S., and Rudich, Y.: Complex refractive indices in the near-ultraviolet spectral region of biogenic secondary organic aerosol aged with ammonia, *Phys. Chem. Chem. Phys.*, 16, 10629-10642, 10.1039/c4cp01009d, 2014.
- 775 Friedman, B., Brophy, P., Brune, W. H., and Farmer, D. K.: Anthropogenic Sulfur Perturbations on Biogenic Oxidation: SO₂ Additions Impact Gas-Phase OH Oxidation Products of α - and β -Pinene, *Environ. Sci. Technol.*, 50, 1269-1279, 10.1021/acs.est.5b05010, 2016.
- 780 Fu, X., Wang, S., Xing, J., Zhang, X., Wang, T., and Hao, J.: Increasing Ammonia Concentrations Reduce the Effectiveness of Particle Pollution Control Achieved via SO₂ and NO_x Emissions Reduction in East China, *Environ. Sci. Technol. Lett.*, 4, 221-227, 10.1021/acs.estlett.7b00143, 2017.
- Fuzzi, S., Baltensperger, U., Carslaw, K., Decesari, S., Denier van der Gon, H., Facchini, M. C., Fowler, D., Koren, I., Langford, B., Lohmann, U., Nemitz, E., Pandis, S., Riipinen, I., Rudich, Y., Schaap, M., Slowik, J. G., Spracklen, D. V., Vignati, E., Wild, M., Williams, M., and Gilardoni, S.: Particulate matter, air quality and climate: lessons learned and future needs, *Atmos. Chem. Phys.*, 15, 8217-8299, 10.5194/acp-15-8217-2015, 2015.
- 785 Guo, H., Wang, T., Blake, D., Simpson, I., Kwok, Y., and Li, Y.: Regional and local contributions to ambient non-methane volatile organic compounds at a polluted rural/coastal site in Pearl River Delta, China, *Atmos. Environ.*, 40, 2345-2359, 2006.
- 790 Guo, S., Hu, M., Zamora, M. L., Peng, J., Shang, D., Zheng, J., Du, Z., Wu, Z., Shao, M., Zeng, L., Molina, M. J., and Zhang, R.: Elucidating severe urban haze formation in China, *P. Natl. Acad. Sci. USA*, 111, 17373-17378, 10.1073/pnas.1419604111, 2014.
- 795 Han, Y., Gong, Z., Liu, P., de Sá, S. S., McKinney, K. A., and Martin, S. T.: Influence of Particle Surface Area Concentration on the Production of Organic Particulate Matter in a Continuously Mixed Flow Reactor, *Environ. Sci. Technol.*, 53, 4968-4976, 10.1021/acs.est.8b07302, 2019.
- Hansen, A. M. K., Hong, J., Raatikainen, T., Kristensen, K., Ylisirniö, A., Virtanen, A., Petäjä, T., Glasius, M., and Prisle, N. L.: Hygroscopic properties and cloud condensation nuclei activation of limonene-derived organosulfates and their mixtures with ammonium sulfate, *Atmos. Chem. Phys.*, 15, 14071-14089, 10.5194/acp-15-14071-2015, 2015.
- 800 Hao, L., Kari, E., Leskinen, A., Worsnop, D. R., and Virtanen, A.: Direct contribution of ammonia to α -pinene secondary organic aerosol formation, *Atmos. Chem. Phys.*, 20, 14393-14405, 10.5194/acp-20-14393-2020, 2020.
- 805 Heald, C. L., Kroll, J. H., Jimenez, J. L., Docherty, K. S., DeCarlo, P. F., Aiken, A. C., Chen, Q., Martin,

- S. T., Farmer, D. K., and Artaxo, P.: A simplified description of the evolution of organic aerosol composition in the atmosphere, *Geophys. Res. Lett.*, 37, 10.1029/2010gl042737, 2010.
- Henze, D. K., Seinfeld, J. H., Ng, N. L., Kroll, J. H., Fu, T. M., Jacob, D. J., and Heald, C. L.: Global modeling of secondary organic aerosol formation from aromatic hydrocarbons: high- vs. low-yield pathways, *Atmos. Chem. Phys.*, 8, 2405-2420, 10.5194/acp-8-2405-2008, 2008.
- 810 Huang, R.-J., Zhang, Y., Bozzetti, C., Ho, K.-F., Cao, J.-J., Han, Y., Daellenbach, K. R., Slowik, J. G., Platt, S. M., Canonaco, F., Zotter, P., Wolf, R., Pieber, S. M., Bruns, E. A., Crippa, M., Ciarelli, G., Piazzalunga, A., Schwikowski, M., Abbazade, G., Schnelle-Kreis, J., Zimmermann, R., An, Z., Szidat, S., Baltensperger, U., El Haddad, I., and Prevot, A. S. H.: High secondary aerosol contribution to particulate pollution during haze events in China, *Nature*, 514, 218-222, 10.1038/nature13774, 2014.
- 815 Jorga, S. D., Kaltsonoudis, C., Liangou, A., and Pandis, S. N.: Measurement of Formation Rates of Secondary Aerosol in the Ambient Urban Atmosphere Using a Dual Smog Chamber System, *Environ. Sci. Technol.*, 54, 1336-1343, 10.1021/acs.est.9b03479, 2020.
- Julin, J., Murphy, B. N., Patoulias, D., Fountoukis, C., Olenius, T., Pandis, S. N., and Riipinen, I.: Impacts of Future European Emission Reductions on Aerosol Particle Number Concentrations Accounting for Effects of Ammonia, Amines, and Organic Species, *Environ. Sci. Technol.*, 52, 692-700, 10.1021/acs.est.7b05122, 2018.
- 820 Kanakidou, M., Seinfeld, J. H., Pandis, S. N., Barnes, I., Dentener, F. J., Facchini, M. C., Van Dingenen, R., Ervens, B., Nenes, A., Nielsen, C. J., Swietlicki, E., Putaud, J. P., Balkanski, Y., Fuzzi, S., Horth, J., Moortgat, G. K., Winterhalter, R., Myhre, C. E. L., Tsigaridis, K., Vignati, E., Stephanou, E. G., and Wilson, J.: Organic aerosol and global climate modelling: a review, *Atmos. Chem. Phys.*, 5, 1053-1123, 10.5194/acp-5-1053-2005, 2005.
- 825 Kleindienst, T. E., Edney, E. O., Lewandowski, M., Offenber, J. H., and Jaoui, M.: Secondary organic carbon and aerosol yields from the irradiations of isoprene and α -pinene in the presence of NO_x and SO_2 , *Environ. Sci. Technol.*, 40, 3807-3812, 10.1021/es052446r, 2006.
- Kroll, J. H., Ng, N. L., Murphy, S. M., Flagan, R. C., and Seinfeld, J. H.: Secondary organic aerosol formation from isoprene photooxidation, *Environ. Sci. Technol.*, 40, 1869-1877, 10.1021/es0524301, 2006.
- 835 Kulmala, M., Petaja, T., Nieminen, T., Sipila, M., Manninen, H. E., Lehtipalo, K., Dal Maso, M., Aalto, P. P., Junninen, H., Paasonen, P., Riipinen, I., Lehtinen, K. E., Laaksonen, A., and Kerminen, V. M.: Measurement of the nucleation of atmospheric aerosol particles, *Nat. Protoc.*, 7, 1651-1667, 10.1038/nprot.2012.091, 2012.
- Lal, V., Khalizov, A. F., Lin, Y., Galvan, M. D., Connell, B. T., and Zhang, R.: Heterogeneous reactions of epoxides in acidic media, *J. Phys. Chem. A*, 116, 6078-6090, 10.1021/jp2112704, 2012.
- 840 Lehtipalo, K., Yan, C., Dada, L., Bianchi, F., Xiao, M., Wagner, R., Stolzenburg, D., Ahonen, L. R., Amorim, A., Baccarini, A., Bauer, P. S., Baumgartner, B., Bergen, A., Bernhammer, A. K., Breitenlechner, M., Brilke, S., Buchholz, A., Mazon, S. B., Chen, D. X., Chen, X. M., Dias, A., Dommen, J., Draper, D. C., Duplissy, J., Ehn, M., Finkenzeller, H., Fischer, L., Frege, C., Fuchs, C., Garmash, O., Gordon, H., Hakala, J., He, X. C., Heikkinen, L., Heinritzi, M., Helm, J. C., Hofbauer, V., Hoyle, C. R., Jokinen, T., 845 Kangasluoma, J., Kerminen, V. M., Kim, C., Kirkby, J., Kontkanen, J., Kurten, A., Lawler, M. J., Mai,

- H. J., Mathot, S., Mauldin, R. L., Molteni, U., Nichman, L., Nie, W., Nieminen, T., Ojdanic, A., Onnela, A., Passananti, M., Petaja, T., Piel, F., Pospisilova, V., Quelever, L. L. J., Rissanen, M. P., Rose, C., Sarnela, N., Schallhart, S., Schuchmann, S., Sengupta, K., Simon, M., Sipila, M., Tauber, C., Tome, A., Trostl, J., Vaisanen, O., Vogel, A. L., Volkamer, R., Wagner, A. C., Wang, M. Y., Weitz, L., Wimmer, D.,
850 Ye, P. L., Ylisirnio, A., Zha, Q. Z., Carslaw, K. S., Curtius, J., Donahue, N. M., Flagan, R. C., Hansel, A., Riipinen, I., Virtanen, A., Winkler, P. M., Baltensperger, U., Kulmala, M., and Worsnop, D. R.: Multicomponent new particle formation from sulfuric acid, ammonia, and biogenic vapors, *Sci. Adv.*, 4, 9, 10.1126/sciadv.aau5363, 2018.
- Lelieveld, J., Evans, J. S., Fnais, M., Giannadaki, D., and Pozzer, A.: The contribution of outdoor air
855 pollution sources to premature mortality on a global scale, *Nature*, 525, 367-371, 10.1038/nature15371, 2015.
- Li, H., Zhang, Q., Zhang, Q., Chen, C., Wang, L., Wei, Z., Zhou, S., Parworth, C., Zheng, B., Canonaco, F., Prevot, A. S. H., Chen, P., Zhang, H., Wallington, T. J., and He, K.: Wintertime aerosol chemistry and haze evolution in an extremely polluted city of the North China Plain: significant contribution from coal
860 and biomass combustion, *Atmos. Chem. Phys.*, 17, 4751-4768, 10.5194/acp-17-4751-2017, 2017.
- Li, K., Chen, L., White, S. J., Yu, H., Wu, X., Gao, X., Azzi, M., and Cen, K.: Smog chamber study of the role of NH₃ in new particle formation from photo-oxidation of aromatic hydrocarbons, *Sci. Total Environ.*, 619-620, 927-937, 10.1016/j.scitotenv.2017.11.180, 2018.
- Li, Y., and Wang, L.: The atmospheric oxidation mechanism of 1,2,4-trimethylbenzene initiated by OH radicals, *Phys. Chem. Chem. Phys.*, 16, 17908-17917, 10.1039/c4cp02027h, 2014.
- 865 Li, Y., Pöschl, U., and Shiraiwa, M.: Molecular corridors and parameterizations of volatility in the chemical evolution of organic aerosols, *Atmos. Chem. Phys.*, 16, 3327-3344, 10.5194/acp-16-3327-2016, 2016.
- Lin, Y. H., Knipping, E. M., Edgerton, E. S., Shaw, S. L., and Surratt, J. D.: Investigating the influences
870 of SO₂ and NH₃ levels on isoprene-derived secondary organic aerosol formation using conditional sampling approaches, *Atmos. Chem. Phys.*, 13, 8457-8470, 10.5194/acp-13-8457-2013, 2013.
- Lin, Y. H., Budisulistiorini, H., Chu, K., Siejack, R. A., Zhang, H. F., Riva, M., Zhang, Z. F., Gold, A., Kautzman, K. E., and Surratt, J. D.: Light-Absorbing Oligomer Formation in Secondary Organic Aerosol from Reactive Uptake of Isoprene Epoxydiols, *Environ. Sci. Technol.*, 48, 12012-12021,
875 10.1021/es503142b, 2014.
- Liu, C., Ma, Q., Chu, B., Liu, Y., He, H., Zhang, X., Li, J., and Hao, J.: Effect of aluminium dust on secondary organic aerosol formation in m-xylene/NO_x photo-oxidation, *Science China-Earth Sciences*, 58, 245-254, 10.1007/s11430-014-5023-0, 2015a.
- Liu, S., Shilling, J. E., Song, C., Hiranuma, N., Zaveri, R. A., and Russell, L. M.: Hydrolysis of
880 Organonitrate Functional Groups in Aerosol Particles, *Aerosol Sci. Technol.*, 46, 1359-1369, 10.1080/02786826.2012.716175, 2012.
- Liu, S., Jia, L., Xu, Y., Tsona, N. T., Ge, S., and Du, L.: Photooxidation of cyclohexene in the presence of SO₂: SOA yield and chemical composition, *Atmos. Chem. Phys.*, 17, 13329-13343, 10.5194/acp-17-13329-2017, 2017.
- 885 Liu, T., Wang, X., Hu, Q., Deng, W., Zhang, Y., Ding, X., Fu, X., Bernard, F., Zhang, Z., Lu, S., He, Q.,

- Bi, X., Chen, J., Sun, Y., Yu, J., Peng, P., Sheng, G., and Fu, J.: Formation of secondary aerosols from gasoline vehicle exhaust when mixing with SO₂, *Atmos. Chem. Phys.*, 16, 675-689, 10.5194/acp-16-675-2016, 2016.
- Liu, Y., Liggio, J., Staebler, R., and Li, S. M.: Reactive uptake of ammonia to secondary organic aerosols: kinetics of organonitrogen formation, *Atmos. Chem. Phys.*, 15, 13569-13584, 10.5194/acp-15-13569-2015, 2015b.
- 890 Ma, Y., Xu, X., Song, W., Geng, F., and Wang, L.: Seasonal and diurnal variations of particulate organosulfates in urban Shanghai, China, *Atmos. Environ.*, 85, 152-160, 10.1016/j.atmosenv.2013.12.017, 2014.
- 895 Mehra, A., Wang, Y., Krechmer, J. E., Lambe, A., Majluf, F., Morris, M. A., Priestley, M., Bannan, T. J., Bryant, D. J., Pereira, K. L., Hamilton, J. F., Rickard, A. R., Newland, M. J., Stark, H., Croteau, P., Jayne, J. T., Worsnop, D. R., Canagaratna, M. R., Wang, L., and Coe, H.: Evaluation of the chemical composition of gas- and particle-phase products of aromatic oxidation, *Atmos. Chem. Phys.*, 20, 9783-9803, 10.5194/acp-20-9783-2020, 2020.
- 900 Meng, Z., Wu, L., Xu, X., Xu, W., Zhang, R., Jia, X., Liang, L., Miao, Y., Cheng, H., Xie, Y., He, J., and Zhong, J.: Changes in ammonia and its effects on PM_{2.5} chemical property in three winter seasons in Beijing, China, *Sci. Total Environ.*, 749, 142208, 10.1016/j.scitotenv.2020.142208, 2020.
- Mo, Z., Lu, S., and Shao, M.: Volatile organic compound (VOC) emissions and health risk assessment in paint and coatings industry in the Yangtze River Delta, China, *Environ. Pollut.*, 269, 115740, 10.1016/j.envpol.2020.115740, 2021.
- 905 Na, K., Song, C., and Cockeriii, D.: Formation of secondary organic aerosol from the reaction of styrene with ozone in the presence and absence of ammonia and water, *Atmos. Environ.*, 40, 1889-1900, 10.1016/j.atmosenv.2005.10.063, 2006.
- Na, K., Song, C., Switzer, C., and Cocker, D. R., III: Effect of ammonia on secondary organic aerosol formation from alpha-Pinene ozonolysis in dry and humid conditions, *Environ. Sci. Technol.*, 41, 6096-6102, 10.1021/es061956y, 2007.
- Nestorowicz, K., Jaoui, M., Rudzinski, K. J., Lewandowski, M., Kleindienst, T. E., Spolnik, G., Danikiewicz, W., and Szmigielski, R.: Chemical composition of isoprene SOA under acidic and non-acidic conditions: effect of relative humidity, *Atmos. Chem. Phys.*, 18, 18101-18121, 10.5194/acp-18-18101-2018, 2018.
- 915 Ng, N. L., Kroll, J. H., Chan, A. W. H., Chhabra, P. S., Flagan, R. C., and Seinfeld, J. H.: Secondary organic aerosol formation from m-xylene, toluene, and benzene, *Atmos. Chem. Phys.*, 7, 3909-3922, 10.5194/acp-7-3909-2007, 2007.
- O'Brien, R. E., Laskin, A., Laskin, J., Rubitschun, C. L., Surratt, J. D., and Goldstein, A. H.: Molecular characterization of S- and N-containing organic constituents in ambient aerosols by negative ion mode high-resolution Nanospray Desorption Electrospray Ionization Mass Spectrometry: CalNex 2010 field study, *J. Geophys. Res. Atmos.*, 119, 12706-12720, 10.1002/2014jd021955, 2014.
- 920 Odum, J. R., Hoffmann, T., Bowman, F., Collins, D., Flagan, R. C., and Seinfeld, J. H.: Gas/particle partitioning and secondary organic aerosol yields, *Environ. Sci. Technol.*, 30, 2580-2585, 10.1021/es950943+, 1996.
- 925

- Paasonen, P., Peltola, M., Kontkanen, J., Junninen, H., Kerminen, V.-M., and Kulmala, M.: Comprehensive analysis of particle growth rates from nucleation mode to cloud condensation nuclei in boreal forest, *Atmos. Chem. Phys.*, 18, 12085-12103, 10.5194/acp-18-12085-2018, 2018.
- Ran, L., Zhao, C., Geng, F., Tie, X., Tang, X., Peng, L., Zhou, G., Yu, Q., Xu, J., and Guenther, A.: Ozone photochemical production in urban Shanghai, China: Analysis based on ground level observations, *J. Geophys. Res. Atmos.*, 114, 10.1029/2008jd010752, 2009.
- 930 Riva, M., Tomaz, S., Cui, T., Lin, Y.-H., Perraudin, E., Gold, A., Stone, E. A., Villenave, E., and Surratt, J. D.: Evidence for an Unrecognized Secondary Anthropogenic Source of Organosulfates and Sulfonates: Gas-Phase Oxidation of Polycyclic Aromatic Hydrocarbons in the Presence of Sulfate Aerosol, *Environ. Sci. Technol.*, 49, 6654-6664, 10.1021/acs.est.5b00836, 2015a.
- 935 Riva, M., Tomaz, S., Cui, T. Q., Lin, Y. H., Perraudin, E., Gold, A., Stone, E. A., Villenave, E., and Surratt, J. D.: Evidence for an unrecognized secondary anthropogenic source of organosulfates and sulfonates: gas-phase oxidation of polycyclic aromatic hydrocarbons in the presence of sulfate aerosol, *Environ. Sci. Technol.*, 49, 6654-6664, 10.1021/acs.est.5b00836, 2015b.
- 940 Riva, M., Barbosa, T. D. S., Lin, Y.-H., Stone, E. A., Gold, A., and Surratt, J. D.: Chemical characterization of organosulfates in secondary organic aerosol derived from the photooxidation of alkanes, *Atmos. Chem. Phys.*, 16, 11001-11018, 10.5194/acp-16-11001-2016, 2016a.
- Riva, M., Budisulistiorini, S. H., Chen, Y., Zhang, Z., D'Ambro, E. L., Zhang, X., Gold, A., Turpin, B. J., Thornton, J. A., Canagaratna, M. R., and Surratt, J. D.: Chemical Characterization of Secondary Organic Aerosol from Oxidation of Isoprene Hydroxyhydroperoxides, *Environ. Sci. Technol.*, 50, 9889-9899, 10.1021/acs.est.6b02511, 2016b.
- 945 Riva, M., Chen, Y., Zhang, Y., Lei, Z., Olson, N. E., Boyer, H. C., Narayan, S., Yee, L. D., Green, H. S., Cui, T., Zhang, Z., Baumann, K., Fort, M., Edgerton, E., Budisulistiorini, S. H., Rose, C. A., Ribeiro, I. O., RL, E. O., Dos Santos, E. O., Machado, C. M. D., Szopa, S., Zhao, Y., Alves, E. G., de Sa, S. S., Hu, W., Knipping, E. M., Shaw, S. L., Duvoisin Junior, S., de Souza, R. A. F., Palm, B. B., Jimenez, J. L., Glasius, M., Goldstein, A. H., Pye, H. O. T., Gold, A., Turpin, B. J., Vizuete, W., Martin, S. T., Thornton, J. A., Dutcher, C. S., Ault, A. P., and Surratt, J. D.: Increasing Isoprene Epoxydiol-to-Inorganic Sulfate Aerosol Ratio Results in Extensive Conversion of Inorganic Sulfate to Organosulfur Forms: Implications for Aerosol Physicochemical Properties, *Environ. Sci. Technol.*, 53, 8682-8694, 10.1021/acs.est.9b01019, 2019.
- 955 Sarrafzadeh, M., Wildt, J., Pullinen, I., Springer, M., Kleist, E., Tillmann, R., Schmitt, S. H., Wu, C., Mentel, T. F., Zhao, D., Hastie, D. R., and Kiendler-Scharr, A.: Impact of NO_x and OH on secondary organic aerosol formation from β-pinene photooxidation, *Atmos. Chem. Phys.*, 16, 11237-11248, 10.5194/acp-16-11237-2016, 2016.
- 960 Shalamzari, M. S., Kahnt, A., Vermeylen, R., Kleindienst, T. E., Lewandowski, M., Cuyckens, F., Maenhaut, W., and Claeys, M.: Characterization of polar organosulfates in secondary organic aerosol from the green leaf volatile 3-Z-hexenal, *Environ. Sci. Technol.*, 48, 12671-12678, 10.1021/es503226b, 2014.
- 965 Shiraiwa, M., Yee, L. D., Schilling, K. A., Loza, C. L., Craven, J. S., Zuend, A., Ziemann, P. J., and Seinfeld, J. H.: Size distribution dynamics reveal particle-phase chemistry in organic aerosol formation,

P. Natl Acad. Sci. U. S. A., 110, 11746-11750, 10.1073/pnas.1307501110, 2013.

Shrivastava, M., Fast, J., Easter, R., Gustafson, W. I., Zaveri, R. A., Jimenez, J. L., Saide, P., and Hodzic, A.: Modeling organic aerosols in a megacity: comparison of simple and complex representations of the volatility basis set approach, *Atmos. Chem. Phys.*, 11, 6639-6662, 10.5194/acp-11-6639-2011, 2011.

970 Shrivastava, M., Cappa, C. D., Fan, J., Goldstein, A. H., Guenther, A. B., Jimenez, J. L., Kuang, C., Laskin, A., Martin, S. T., Ng, N. L., Petaja, T., Pierce, J. R., Rasch, P. J., Roldin, P., Seinfeld, J. H., Shilling, J., Smith, J. N., Thornton, J. A., Volkamer, R., Wang, J., Worsnop, D. R., Zaveri, R. A., Zelenyuk, A., and Zhang, Q.: Recent advances in understanding secondary organic aerosol: Implications for global climate forcing, *Rev. Geophys.*, 55, 509-559, 10.1002/2016rg000540, 2017.

975 Song, C., Wu, L., Xie, Y., He, J., Chen, X., Wang, T., Lin, Y., Jin, T., Wang, A., Liu, Y., Dai, Q., Liu, B., Wang, Y. N., and Mao, H.: Air pollution in China: Status and spatiotemporal variations, *Environ. Pollut.*, 227, 334-347, 10.1016/j.envpol.2017.04.075, 2017.

Surratt, J. D., Gomez-Gonzalez, Y., Chan, A. W. H., Vermeylen, R., Shahgholi, M., Kleindienst, T. E., Edney, E. O., Offenberg, J. H., Lewandowski, M., Jaoui, M., Maenhaut, W., Claeys, M., Flagan, R. C.,
980 and Seinfeld, J. H.: Organosulfate formation in biogenic secondary organic aerosol, *J. Phys. Chem. A*, 112, 8345-8378, 10.1021/jp802310p, 2008.

Terzano, C., Di Stefano, F., Conti, V., Graziani, E., and Petroianni, A.: Air pollution ultrafine particles: toxicity beyond the lung, *Eur. Rev. Med. Pharmacol. Sci.*, 14, 809-821, 2010.

Tolocka, M. P., and Turpin, B.: Contribution of organosulfur compounds to organic aerosol mass, *Environ. Sci. Technol.*, 46, 7978-7983, 10.1021/es300651v, 2012.

Volkamer, R., Jimenez, J. L., San Martini, F., Dzepina, K., Zhang, Q., Salcedo, D., Molina, L. T., Worsnop, D. R., and Molina, M. J.: Secondary organic aerosol formation from anthropogenic air pollution: Rapid and higher than expected, *Geophys. Res. Lett.*, 33, 10.1029/2006gl026899, 2006.

990 Wang, M., Kong, W., Marten, R., He, X. C., Chen, D., Pfeifer, J., Heitto, A., Kontkanen, J., Dada, L., Kurten, A., Yli-Juuti, T., Manninen, H. E., Amanatidis, S., Amorim, A., Baalbaki, R., Baccarini, A., Bell, D. M., Bertozzi, B., Brakling, S., Brilke, S., Murillo, L. C., Chiu, R., Chu, B., De Menezes, L. P., Duplissy, J., Finkenzeller, H., Carracedo, L. G., Granzin, M., Guida, R., Hansel, A., Hofbauer, V., Krechmer, J., Lehtipalo, K., Lamkaddam, H., Lampimaki, M., Lee, C. P., Makhmutov, V., Marie, G., Mathot, S., Mauldin, R. L., Mentler, B., Muller, T., Onnela, A., Partoll, E., Petaja, T., Philippov, M., Pospisilova, V.,
995 Ranjithkumar, A., Rissanen, M., Rorup, B., Scholz, W., Shen, J., Simon, M., Sipila, M., Steiner, G., Stolzenburg, D., Tham, Y. J., Tome, A., Wagner, A. C., Wang, D. S., Wang, Y., Weber, S. K., Winkler, P. M., Wlasits, P. J., Wu, Y., Xiao, M., Ye, Q., Zauner-Wieczorek, M., Zhou, X., Volkamer, R., Riipinen, I., Dommen, J., Curtius, J., Baltensperger, U., Kulmala, M., Worsnop, D. R., Kirkby, J., Seinfeld, J. H., El-Haddad, I., Flagan, R. C., and Donahue, N. M.: Rapid growth of new atmospheric particles by nitric acid and ammonia condensation, *Nature*, 581, 184-189, 10.1038/s41586-020-2270-4, 2020a.

Wang, S., Zhou, S., Tao, Y., Tsui, W. G., Ye, J., Yu, J. Z., Murphy, J. G., McNeill, V. F., Abbatt, J. P. D., and Chan, A. W. H.: Organic Peroxides and Sulfur Dioxide in Aerosol: Source of Particulate Sulfate, *Environ. Sci. Technol.*, 53, 10695-10704, 10.1021/acs.est.9b02591, 2019a.

1005 Wang, X. K., Rossignol, S., Ma, Y., Yao, L., Wang, M. Y., Chen, J. M., George, C., and Wang, L.: Molecular characterization of atmospheric particulate organosulfates in three megacities at the middle

- and lower reaches of the Yangtze River, *Atmos. Chem. Phys.*, 16, 2285-2298, 10.5194/acp-16-2285-2016, 2016.
- Wang, Y., Ma, Y., Li, X., Kuang, B. Y., Huang, C., Tong, R., and Yu, J. Z.: Monoterpene and Sesquiterpene alpha-Hydroxy Organosulfates: Synthesis, MS/MS Characteristics, and Ambient Presence, *Environ. Sci. Technol.*, 53, 12278-12290, 10.1021/acs.est.9b04703, 2019b.
- 1010 Wang, Y., Mehra, A., Krechmer, J. E., Yang, G., Hu, X., Lu, Y., Lambe, A., Canagaratna, M., Chen, J., Worsnop, D., Coe, H., and Wang, L.: Oxygenated products formed from OH-initiated reactions of trimethylbenzene: autoxidation and accretion, *Atmos. Chem. Phys.*, 20, 9563-9579, 10.5194/acp-20-9563-2020, 2020b.
- 1015 Warner, J. X., Dickerson, R. R., Wei, Z., Strow, L. L., Wang, Y., and Liang, Q.: Increased atmospheric ammonia over the world's major agricultural areas detected from space, *Geophys. Res. Lett.*, 44, 2875-2884, 10.1002/2016gl072305, 2017.
- Wu, Y., Gu, B., Erisman, J. W., Reis, S., Fang, Y., Lu, X., and Zhang, X.: PM_{2.5} pollution is substantially affected by ammonia emissions in China, *Environ. Pollut.*, 218, 86-94, 10.1016/j.envpol.2016.08.027, 1020 2016.
- Wyche, K. P., Monks, P. S., Ellis, A. M., Cordell, R. L., Parker, A. E., Whyte, C., Metzger, A., Dommen, J., Duplissy, J., Prevot, A. S. H., Baltensperger, U., Rickard, A. R., and Wulfert, F.: Gas phase precursors to anthropogenic secondary organic aerosol: detailed observations of 1,3,5-trimethylbenzene photooxidation, *Atmos. Chem. Phys.*, 9, 635-665, 10.5194/acp-9-635-2009, 2009.
- 1025 Xu, L., Guo, H., Boyd, C. M., Klein, M., Bougiatioti, A., Cerully, K. M., Hite, J. R., Isaacman-VanWertz, G., Kreisberg, N. M., Knote, C., Olson, K., Koss, A., Goldstein, A. H., Hering, S. V., de Gouw, J., Baumann, K., Lee, S.-H., Nenes, A., Weber, R. J., and Ng, N. L.: Effects of anthropogenic emissions on aerosol formation from isoprene and monoterpenes in the southeastern United States, *P. Natl Acad. Sci. U. S. A.*, 112, 37-42, 10.1073/pnas.1417609112, 2015.
- 1030 Yang, Z., Tsona, N. T., Li, J., Wang, S., Xu, L., You, B., and Du, L.: Effects of NO_x and SO₂ on the secondary organic aerosol formation from the photooxidation of 1,3,5-trimethylbenzene: A new source of organosulfates, *Environ. Pollut.*, 264, 114742, 10.1016/j.envpol.2020.114742, 2020.
- Ye, J., Abbatt, J. P. D., and Chan, A. W. H.: Novel pathway of SO₂ oxidation in the atmosphere: reactions with monoterpene ozonolysis intermediates and secondary organic aerosol, *Atmos. Chem. Phys.*, 18, 1035 5549-5565, 10.5194/acp-18-5549-2018, 2018.
- Yu, Z., and Jang, M.: Atmospheric Processes of Aromatic Hydrocarbons in the Presence of Mineral Dust Particles in an Urban Environment, *ACS Earth Space Chem.*, 3, 2404-2414, 10.1021/acsearthspacechem.9b00195, 2019.
- Zaytsev, A., Koss, A. R., Breitenlechner, M., Krechmer, J. E., Nihill, K. J., Lim, C. Y., Rowe, J. C., Cox, 1040 J. L., Moss, J., Roscioli, J. R., Canagaratna, M. R., Worsnop, D., Kroll, J. H., and Keutsch, F. N.: Mechanistic study of the formation of ring-retaining and ring-opening products from the oxidation of aromatic compounds under urban atmospheric conditions, *Atmos. Chem. Phys.*, 19, 15117-15129, 10.5194/acp-19-15117-2019, 2019.
- Zhang, G., Lian, X., Fu, Y., Lin, Q., Li, L., Song, W., Wang, Z., Tang, M., Chen, D., Bi, X., Wang, X., 1045 and Sheng, G.: High secondary formation of nitrogen-containing organics (NOCs) and its possible link

- to oxidized organics and ammonium, *Atmos. Chem. Phys.*, 20, 1469-1481, 10.5194/acp-20-1469-2020, 2020.
- Zhang, R., Wang, G., Guo, S., Zamora, M. L., Ying, Q., Lin, Y., Wang, W., Hu, M., and Wang, Y.: Formation of urban fine particulate matter, *Chem. Rev.*, 115, 3803-3855, 10.1021/acs.chemrev.5b00067, 1050 2015.
- Zhang, X., Cappa, C. D., Jathar, S. H., McVay, R. C., Ensber, J. J., Kleeman, M. J., and Seinfeld, J. H.: Influence of vapor wall loss in laboratory chambers on yields of secondary organic aerosol, *P. Natl. Acad. Sci. USA*, 111, 5802-5807, 2014.
- Zhang, Y., Chen, Y., Lei, Z., Olson, N. E., Riva, M., Koss, A. R., Zhang, Z., Gold, A., Jayne, J. T., 1055 Worsnop, D. R., Onasch, T. B., Kroll, J. H., Turpin, B. J., Ault, A. P., and Surratt, J. D.: Joint Impacts of Acidity and Viscosity on the Formation of Secondary Organic Aerosol from Isoprene Epoxydiols (IEPOX) in Phase Separated Particles, *ACS Earth Space Chem.*, 3, 2646-2658, 10.1021/acsearthspacechem.9b00209, 2019.
- Zhao, D., Schmitt, S. H., Wang, M., Acir, I.-H., Tillmann, R., Tan, Z., Novelli, A., Fuchs, H., Pullinen, I., 1060 Wegener, R., Rohrer, F., Wildt, J., Kiendler-Scharr, A., Wahner, A., and Mentel, T. F.: Effects of NO_x and SO₂ on the secondary organic aerosol formation from photooxidation of α -pinene and limonene, *Atmos. Chem. Phys.*, 18, 1611-1628, 10.5194/acp-18-1611-2018, 2018.
- Zhu, Y., Sabaliauskas, K., Liu, X., Meng, H., Gao, H., Jeong, C.-H., Evans, G. J., and Yao, X.: Comparative analysis of new particle formation events in less and severely polluted urban atmosphere, 1065 *Atmos. Environ.*, 98, 655-664, 10.1016/j.atmosenv.2014.09.043, 2014.
- Ziemann, P. J., and Atkinson, R.: Kinetics, products, and mechanisms of secondary organic aerosol formation, *Chem. Soc. Rev.*, 41, 6582-6605, 10.1039/c2cs35122f, 2012.
- Zou, Y., Deng, X. J., Zhu, D., Gong, D. C., Wang, H., Li, F., Tan, H. B., Deng, T., Mai, B. R., Liu, X. T., 1070 and Wang, B. G.: Characteristics of 1 year of observational data of VOCs, NO_x and O₃ at a suburban site in Guangzhou, China, *Atmos. Chem. Phys.*, 15, 6625-6636, 10.5194/acp-15-6625-2015, 2015.